

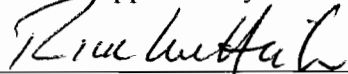
HYDRODYNAMIC BEHAVIOR OF THE CAPE FEAR RIVER ESTUARINE  
SYSTEM, NORTH CAROLINA

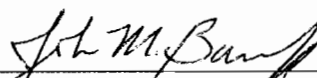
May Ling Becker

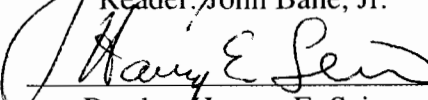
A dissertation submitted to the faculty of the University of North Carolina at Chapel Hill  
in partial fulfillment of the requirements for the degree of Doctor of Philosophy in the  
Department of Marine Sciences (Physical Oceanography).

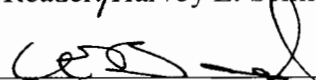
Chapel Hill  
2006


Approved by

  
\_\_\_\_\_  
Advisor: Richard A. Luetlich Jr.

  
\_\_\_\_\_  
Reader: John Barfe, Jr.

  
\_\_\_\_\_  
Reader: Harvey E. Seim

  
\_\_\_\_\_  
Reader: Lawrence Band

  
\_\_\_\_\_  
Reader: Michael A. Mallin

Copyright 2006  
May Ling Becker  
ALL RIGHTS RESERVED

## **ABSTRACT**

May Ling Becker: Hydrodynamic Behavior of the Cape Fear River Estuarine System,  
North Carolina  
(Under the direction of Richard A. Luetlich, Jr.)

Transport in estuaries depends on the relative strengths of dominant forcing mechanisms, which may include tides (which generate turbulence), river input (which adds buoyancy), and wind (which may act as a remote forcing in the coastal ocean or a local forcing over the estuary). In this study, we investigate the major physical mechanisms that influence circulation in the Cape Fear River Estuary (CRFE), a partially mixed estuary that is representative of other estuaries along the southeast Atlantic coast from southern North Carolina through northern Florida. First, we describe differences in velocity and stratification at along-channel sections of the estuary for relatively low-flow conditions based on historical data. Then, we discuss the influence of river inflow on the salinity intrusion using different methods of determining discharge in order to investigate the appropriate means of incorporating flow history into the discharge value. Finally, we discuss the role of tidal forcing based on findings of a field data study designed to characterize estuarine behavior during differing tidal conditions. Specifically, velocity, salinity, and tidal-height data were collected for an along-channel segment of the CFRE during two separate periods representing high versus low ranges, and mechanisms influencing observed differences are described.

Results indicate the salinity structure and circulation are impacted by tidal-range differences that vary over an approximately 29-day period, intra-tidal variations, and sub-tidal variations in freshwater input. For low-flow conditions, the system exhibits characteristics of a two-layer estuarine system in which density driven-circulation enhances inflow near the bottom while fresher, less dense water flows out near the surface. Specifically, 1) over 90 percent of the variability in the length of the salinity intrusion over a five-year period can be explained based on peaks in river discharge using the “hydrologic flood” exponential decay model, 2) intra-tidal and tidal-range variations significantly influence stratification, 3) these variations impact circulation including the along-channel velocity structure, and 4) salinity characteristics are critically linked to turbulent mixing characteristics and the strength of stratification within the water column.

## **ACKNOWLEDGEMENTS**

I thank my advisor, Dr. Rick Luettich, for his insightful contributions and support of this work. His helpful feedback and suggestions improved many areas of the research. I also thank Drs. John Bane, Harvey Seim, Larry Band, and Mike Mallin for their input on this project. Their many contributions have expanded the realm of the research and strengthened details of the work. Thanks also to Tony Whipple, Crystal Fulcher, Sara Haines, and David Meaux for their technical assistance. Further, I express appreciation to Dr. Narayan Rajbhandari, Dr. Jim Bowen, Dianne Reid, Jim Fisher, Harold Quidley, Captain Joe Purifoy, Matthew McIver, and Mark Ciccarello for assistance with the field study as well as to the members of the Aquatic Ecology Research Laboratory (University of North Carolina Wilmington Center for Marine Science) for their help in obtaining monitoring data.

Funding for this work was provided by an Environmental Protection Agency (EPA) STAR Grant and by the University of North Carolina at Chapel Hill. Field data collection was conducted in collaboration with the North Carolina State Division of Water Quality.

## TABLE OF CONTENTS

LIST OF TABLES .....	ix
----------------------	----

LIST OF FIGURES .....	x
-----------------------	---

### Chapter

I. INTRODUCTION .....	1
-----------------------	---

II. OBSERVATIONAL SYNTHESIS OF THE CAPE FEAR RIVER ESTUARY.....	4
--	---

Abstract.....	4
---------------	---

Introduction.....	5
-------------------	---

Background.....	7
-----------------	---

Study Area.....	7
-----------------	---

Tidal and River Environment.....	9
----------------------------------	---

Methods.....	11
--------------	----

Tidal Analysis.....	11
---------------------	----

Vertical Salinity Sections.....	12
---------------------------------	----

Salinity Intrusion.....	12
-------------------------	----

Relationship between Discharge and Salinity Intrusion.....	13
--	----

Results.....	15
--------------	----

Tidal Elevations.....	15
-----------------------	----

Tidal Velocities.....	16
-----------------------	----

Salinity Structure.....	17
-------------------------	----

Relationship between Discharge and Salinity Intrusion.....	18
Discussion.....	19
Stratification: Tidal Range Differences and Intra-tidal Variations .....	20
Relationship between Discharge and Salinity Intrusion.....	23
“Hydrologic Flood” Hypothesis .....	24
Exponential Decay Representation.....	27
Classic Estuarine Formulations.....	30
Summary and Conclusions .....	32
Literature Cited.....	35
<b>III. TIDAL INFLUENCES ON CIRCULATION AND SALINITY STRUCTURE IN THE CAPE FEAR RIVER ESTUARY.....</b>	<b>57</b>
Abstract.....	57
Introduction .....	58
Background.....	60
Study Area and Hydrodynamic Environment.....	60
Related Research: Parameterization of Mixing, Stratification, and Circulation.....	62
Methods: Experimental Design.....	65
Setting and Physical Conditions.....	65
Data Collection: Water Level, Velocity, and Salinity Measurements.....	66
Results.....	68
Tidal Elevations and Velocity Transects.....	68
Salinity and Density Distributions.....	69
Salt Balance and Mixing Coefficients.....	71

Discussion.....	73
Shear Structure.....	76
Gradient Richardson Number.....	76
Horizontal Richardson Number.....	77
Salt Balance and Mixing Coefficients.....	78
Salinity and Stratification Structure: A Descriptive Characterization.....	81
Conclusions.....	82
Literature Cited.....	86
IV. SYNTHESIS OF CONCLUSIONS .....	107



## LIST OF TABLES

### Table

2.1. Comparison of phase lags between Southport and Navassa... ..	39
2.2. Maximum spring-tide velocities at lower, middle, and upper sections of the estuary .....	40
2.3. Excursion distances at (a) mid-depth and (b) near-bottom for the lower, middle, and upper reaches of the estuary .....	41
2.4. Regression equations for the salinity intrusion position versus discharge.....	42
3.1. Calculated horizontal Richardson numbers around maximum flood and maximum ebb tide for low and higher tidal-range conditions.....	88

## LIST OF FIGURES

### Figure

2.1. Cape Fear River Watershed.....	43
2.2. Cape Fear River Estuary (CFRE) study area including locations of observational stations.....	44
2.3. Freshwater input in the CFRE: a) Mean daily discharge (1999-2003) on the Cape Fear River and the 35-year average of mean daily discharge; b) Mean daily discharge (1999-2003) on the Black and Northeast Cape Fear Rivers.....	45
2.4. Vertical salinity sections for the CFRE.....	46
2.5. Relationship between the observed salinity intrusion location and mean daily discharge.....	47
2.6. Correlation coefficients for iterations of the Complete Hydrologic Flood Method (CHFM), the Hydrologic Flood Method (HFM), and Complete Value Method (CVM).....	48
2.7. Water-level record at Wilmington Tide Gauge.....	49
2.8. Growth of the $M_4$ and $M_6$ tidal constituents.....	50
2.9. Relationship between tidal height, near-bottom speed, and stratification at mid-estuary (S3.9 and S4.0) during a) spring tide and b) neap tide.....	51
2.10. Tidal heights and near- surface, mid-depth, and bottom salinities for a) lower, b) middle, and c) upper estuary during a spring tidal cycle.....	52
2.11. Relationship between a) tidal range and bottom salinity and b) tidal range and stratification for a well-stratified section of the upper estuary (S6.9 and S7.0).....	53
2.12. Linear regression analysis for 1999 to 2000 based on the a) Hydrologic Flood Method (HFM), b) Complete Hydrologic Flood Method (CHFM) and c) Variable Travel-time Method (VTM).....	55
2.13. Comparison of a) power-law and b) exponential regression analysis for CHFM.....	56

3.1.	Cape Fear River Estuary field study area including field survey stations and charted channel .....	89
3.2.	Mean daily discharge from the Cape Fear River during the summer 2005 sampling period.....	90
3.3.	Measured tidal heights at a) Wilmington tide gauge and b) field data station S4.0.....	91
3.4.	Tidal height at S4.0 and depth-averaged along-channel velocity for a) July 12 and b) July 26, 2005.....	92
3.5.	Along-channel velocities on a) July 12 and b) July 26.....	93
3.6.	Tidally averaged (residual) velocity on July 12 and July 26.....	94
3.7.	Tidal velocity on a) July 12 and b) July 26.....	95
3.8.	Salinity stratification and tidal height at M44 on a) July 12 and b) July 26.....	96
3.9.	Transect- and depth-averaged along-channel velocities and depth-averaged buoyancy frequencies at M44 on a) July 12 and b) July 26.....	97
3.10.	Salinity profiles at M44 on a) July 12, b) July 26, and c) near slack tide on July 12 and July 26.....	98
3.11.	Along-channel vertical salinity sections on a) July 12 and b) July 26.....	99
3.12.	Buoyancy frequency squared ( $N^2$ ) and salinity contours at M44 on a) July 12 and b) July 26.....	100
3.13.	Transect-averaged shear magnitude and salinity contours at M44 on a) July 12 and b) July 26.....	101
3.14.	Transect-averaged $\text{Log}_{10}(4Ri_g)$ together with contours of shear magnitude (solid lines) on a) July 12 and b) July 26.....	102
3.15.	$\text{Log}_{10}(K_z)$ using Munk and Anderson's (1948) eddy diffusivity coefficient formulation ( $C_d = 0.001$ ) and salinity contours at M44 on a) July 12 and b) July 26.....	103
3.16.	Terms of simplified salt budget equation (Eq. 5) averaged from near-bottom to 5 m below surface on a) July 12 and b) July 26.....	104

3.17. Estimated vertical turbulent salt flux ( $w's'$ ) calculated from a simplified salt budget equation together with salinity contours at M44 on a) July 12 and b) July 26.....	105
3.18. $\text{Log}_{10}(K_z)$ together with contours of estimated vertical turbulent salt fluxes ( $w's'$ ) calculated from a simplified salt budget equation on a) July 12 and b) July 26.....	106

# **CHAPTER 1**

## **INTRODUCTION**

In estuarine systems, the transport of constituents such as pollutants, nutrients or salt depends strongly on the water body's hydrodynamic characteristics, which can be influenced by factors such as tides, river discharge, atmospheric forcing, and local geomorphology. In partially mixed estuaries in which river inflow and tidal forcing are the main physical influences, the observed salinity, density and circulation structures may change depending on how factors such precipitation events or periodic variations in the strength of tidal mixing impact the system.

The input of fresh river water and saltier ocean water induces a horizontal density gradient and associated density-driven (baroclinic) circulation. Buoyancy inputs associated with increased freshwater discharge can act to inhibit turbulence, while at the same time barotropic forcing, associated with the increased sea-surface slope, may push the salinity intrusion (representative of the boundary between fresh and salty water) seaward, increase the horizontal salinity gradient, and, accordingly, influence the strength of density-driven flow. Tidal currents, in contrast, may advect saline water along the estuary and act to break down stratification. The estuarine circulation and salinity structure, therefore, may change depending on the relative strengths of competing forces that influence the momentum and salt balances.

In order to understand how constituents are transported in an estuary and assess the impact on environmental and water-quality characteristics, the dominant forcing mechanisms and the time scales during which they act should first be identified and understood. In this study, we investigate the major physical mechanisms that influence circulation in the Cape Fear River Estuary (CFRE), a partially mixed estuary along the southeast United States. The CFRE is representative of the type of estuary that dominates the coast from southern North Carolina through northern Florida, a region comprised of estuaries in which tides and river inflow are typically the dominant physical drivers (Dame et al., 2000; Orlando et al. 1994). As parts of the CFRE fall below minimum standards for dissolved oxygen and the estuary is an important recreational and commercial fishery, the water quality of the area has significant human and environmental impacts. Specifically, results of this dissertation research provide insight that may guide the development of a North Carolina State Division of Water Quality Total Maximum Daily Load (TMDL) Environmental Management Plan for the CFRE and may provide a physical foundation for further study of biological, chemical, and environmental processes.

The aim of this research is to determine the main physical influences on mixing, stratification, and circulation in the CFRE. This is accomplished through 1) analysis of historical, hydrodynamic data sets, 2) design and implementation of a field study of varying tidal conditions, and 3) comparison and analysis of the field data (collected in collaboration with the North Carolina State Division of Water Quality) for the differing tidal conditions. In Chapter 2, we examine historical observational data in order to determine how the salinity and circulation structure is influenced by variability in tidal forcing (high versus low tidal ranges and flood versus ebb conditions) and by changes in river inflow (for example, high

freshwater input associated with storm events versus base-flow or “dry-weather” conditions). More specifically, the influence of tidal forcing is explored by examining an intensive United States Army Corps of Engineers (USACOE) data set that was collected during a low river-inflow period (summer 1993). Aspects that are studied include the differences in the velocity and stratification structure at along-channel sections of the estuary, the impact of intra-tidal (flood-ebb) and tidal-range variability on the circulation and salinity characteristics, and the mechanisms that may explain the observed differences. The role of river inflow on the salinity structure is then investigated in consideration of the relationship between discharge and the salinity intrusion location. This is based on analysis of monitoring data collected monthly (1999-2003) as part of the Lower Cape Fear River Program (LCFRP) and United States Geological Survey (USGS) streamflow measurements.

Based on findings from the historical data-set analyses, the influence of tidal-range variability during low river-inflow conditions is explored in more detail in Chapter 3. This was accomplished through the design and implementation of a field data study (summer 2005) and analysis of the collected data. Velocity, salinity, and tidal-height measurements were made for an along-channel section of the estuary during two different sampling periods, representing high- and low-tidal-range conditions in which river inflow was low and nearly constant. Analysis of the field data include characterization of observed differences in the salinity structure and circulation during low versus high tidal-range conditions. Mechanisms influencing the observed differences are discussed.

Finally, Chapter 4 provides a synthesis of conclusions that characterize temporal influences on the hydrodynamic environment.

## **CHAPTER 2**

### **OBSERVATIONAL SYNTHESIS OF THE CAPE FEAR RIVER ESTUARY**

#### **Abstract**

Transport of constituents in partially mixed estuaries depends on the relative strength of dominant forcing mechanisms, which may include tides (which generate turbulence), river input (which adds buoyancy), and wind. In this study, we investigated the major physical mechanisms that influence circulation in the Cape Fear River Estuary (CRFE), a partially mixed estuary that is representative of other estuaries along the southeast Atlantic coast (from southern North Carolina through northern Florida). Based on analysis of observed hydrographic and hydrodynamic data, we describe differences in velocity and stratification at along-channel sections of the estuary for relatively low-flow conditions. We then discuss the influence of river inflow on the salinity intrusion based on four methods of determining discharge (in order to investigate the appropriate means of incorporating flow history into the discharge value).

Our analyses indicate: 1) 92 percent of the variability in the length of salinity intrusion over a five-year period can be explained based on peaks in river discharge using an exponential decay function, 2) the salinity intrusion depends more weakly on discharge than predicted by classic analytical formulations in which the intrusion would vary with discharge to the power of  $(-1/3)$  in exchange-dominated systems, 3) intra-tidal and neap-spring variations have a significant influence on the salinity stratification and 4) these variations



impact baroclinic circulation and the along-channel velocity structure (in particular, on the neap, ebb tide).

Our results suggest that the salinity intrusion location is dependent upon the hydrologic “flood,” defined by a peak in the river discharge hydrograph. In river-estuary systems in which hydrologic flood peaks are large relative to base flow (and in which differences in bathymetry and width between the estuarine head and mouth may be significant), we hypothesize the hydrologic flood exponential decay model may offer a more direct means of predicting the estuarine salinity response compared to the classical power-law relations.

## **Introduction**

Transport in estuaries depends strongly on their physical hydrodynamic characteristics. Factors including tides, river discharge, atmospheric forcing, and local geomorphology determine the transport of salt, nutrients, dissolved oxygen, and other constituents and contribute to their impacts on environmental conditions. Along the North Carolina shoreline (Fig. 2.1, inset) differences in morphological and hydrodynamic features of estuaries may explain certain environmental characteristics of these water bodies. For example, the Neuse River Estuary is almost completely surrounded by barrier islands and represents a nearly enclosed, restricted environment in which water-level variations and circulation patterns are primarily determined by winds at short time scales and river discharge at longer time scales (Luettich et al., 2002). These factors largely determine the degree of stratification and many ecologically important quantities such as dissolved-oxygen distributions (including areas of hypoxia and anoxia) (Reynolds-Fleming, et al. 2004).

The Cape Fear River Estuary (CFRE), in contrast, exhibits notably different morphological and hydrodynamic features (Fig. 2.1). This estuary receives freshwater from the largest and most industrialized watershed in North Carolina via a major piedmont river (the Cape Fear River) and two “blackwater” streams (the Black and Northeast Cape Fear Rivers) that originate in swamps high in organic material. The CFRE has a relatively open mouth that allows tidal currents to propagate well into the system. The result is a partially mixed to well mixed estuary (Welch and Parker, 1979). While the system is generally considered non-eutrophic as a result of sufficient flushing (Ensign et al., 2004), its water quality has degraded with agricultural, industrial, and metropolitan development (Mallin, 2000; Mallin et. al., 2000). Dissolved oxygen levels in the CFRE system have frequently fallen below the state standard (5mg/L), in particular, during warm, low-streamflow summer conditions and after severe storms (Mallin, 2000; Mallin et. al., 2003). Research suggests dissolved oxygen patterns in the estuary may be strongly influenced by hydrodynamic factors including the strength of density driven flow and river inputs (Lin et al., 2006).

In order to assess the impact of anthropogenic and natural changes in a river-estuarine system, the dominant forcing mechanisms and the time scales during which they act must first be identified and understood. The purpose of this research is to provide a synthesis of the dominant physical influences on the lower CFRE through analysis of observed hydrographic and hydrodynamic data.

Physical forces include tides (whose associated currents advect saline water along the estuary and enhance mixing), river flow (which is a source of buoyancy, enhances stratification, and imposes a barotropic longitudinal pressure gradient along the estuary and a baroclinic pressure gradient due to density differences between salt and fresh water) and

wind stress (which may act as a remote forcing in the coastal ocean or a local forcing over the estuary). Because the coastal region is characterized by estuaries in which tides and river flow are important physical mechanisms (Dame et al., 2000; Orlando et al., 1994) and preliminary data analysis supports this characterization, this research focuses on the influence of these two physical mechanisms on the estuarine salinity and circulation structure.

First, we characterize the tidal environment (when river inflow is reasonably low, i.e., mean daily discharge does not exceed  $65 \text{ m}^3\text{sec}^{-1}$  on the main-stem Cape Fear River). In particular, differences in tidal excursions and salinity characteristics at along-channel sections of the estuary and variations in salinity characteristics for different temporal scales (ebb- versus flood-tide and low versus high tidal ranges) are discussed. Next, we consider how differences in river flow impact the salinity structure. More specifically, the influence of sub-tidal variations in discharge on the location of the salinity intrusion is investigated including consideration of the most appropriate means of incorporating the flow history into the discharge value based on regression and hydrograph analysis. Finally, we compare observed salinity-intrusion-discharge relationships to theoretically predicted values derived from momentum and salt equations (Chatwin, 1976; Hetland and Geyer, 2004; MacCready, 2005) and introduce alternate relationships which emerged from analysis of the observed data and hydrograph characteristics in the river-estuarine system.

## **Background**

### *Study Area*

The CFRE is representative of the type of estuary that dominates the Atlantic coast of the southeastern United States from southern North Carolina through northern Florida (Mallin et.

al 2000; Dame et al. 2000). This coastal region is typically comprised of estuaries in which tides and river inflow are dominant physical drivers (Dame et al., 2000; Orlando et al. 1994). Piedmont rivers that originate in upland areas or blackwater (coastal plain) rivers that drain smaller watersheds within the coastal plain typically feed estuaries in this region. Several estuarine complexes in this area, including the CFRE, are fed by both piedmont and coastal plain rivers (Dame et al., 2000).

The main-stem Cape Fear River originates in the North Carolina Piedmont and is fed by the Haw River and the Deep River. Jordan Dam and Lake, a reservoir built by the Army Corps of Engineers (USACOE), is located approximately 278 km upstream of Wilmington (USACOE, 2004a). In addition, three lock and dam structures modify flow in parts of the lower and middle river basin (Figs. 2.1, 2.2).

The Cape Fear Estuary receives most of its freshwater from the Cape Fear River. The entire Cape Fear River basin extends from near Greensboro, NC, to the coastal waters south of Wilmington (Figs. 2.1, 2.2) and encompasses approximately 23,600 km<sup>2</sup> (McAdory, 2000). Industry and agriculture are significant land uses. Approximately 24% of land in the basin is cropland or pasture, and more than 600 licensed point source dischargers are located within the watershed (Mallin et al., 2000, from NC DWQ, 1996). Contaminants from non-point sources include pesticides, fertilizers, and herbicides (Mallin et. al, 2000). In addition, waste from industrialized animal operations contributes to low-oxygen conditions and fish kills during intense storm events (Mallin, 2000).

The estuarine and lower river region considered in this study stretches from Lock and Dam 1 (Fig. 2.2) to the mouth of the estuary, approximately three kilometers south of Southport, N.C. In addition to the 6<sup>th</sup> order main-stem Cape Fear River, the estuarine system

receives freshwater inflow from two 5<sup>th</sup> order black-water tributaries--the Black River and the Northeast Cape Fear River (Benke and Cushing, 2005). The Northeast Cape Fear River discharges into the estuary near Wilmington; the Black River meets the main-stem Cape Fear River northwest of Wilmington.

The estuary is about 1800 m wide at the mouth and generally converges in a funnel shape to a width of approximately 700 m near S6.0 (Fig. 2.2). It then narrows to a width of about 160 m near Wilmington. A navigation channel, maintained by the Army Corps of Engineers, stretches from the Atlantic Ocean through the estuary and into the Cape Fear River near Navassa and into the Northeast Cape Fear River about 4 km north of Wilmington. Channel depths are typically 11.6 m in the estuary and Cape Fear River and 8.2 m in the Northeast Cape Fear River (McAdory, 2000). Outside of the main channel, several islands, spoil areas, and tidal flats occupy parts of the estuary (Welch and Parker, 1979).

#### *Tidal and River Environment*

The Cape Fear Estuary is characterized by semi-diurnal tides with a mean tidal range of approximately 1.3 m (McAdory, 2000). Results of an early hydrodynamic field (and one-dimensional model) study conducted by the National Oceanic and Atmospheric Administration (Welch and Parker, 1979) indicate the dominant tidal constituent is the  $M_2$  (main lunar semi-diurnal) component followed by the  $N_2$  (semidiurnal lunar elliptic),  $S_2$  (principal semidiurnal solar),  $K_1$  (luni solar) and  $O_1$  (principal lunar) components. The estuary is described as varying from partially mixed to well mixed. An  $M_2$ -phase lag of approximately 1.9 h was found between the mouth of the estuary near Southport and the Wilmington Tide Gauge (Welch and Parker, 1979). Results of more recent harmonic and

observational analyses indicate a lag of approximately 3.0 h in the riverine section between the Wilmington tide gauge and S11.0 near Lock and Dam 1 (Tetra-Tech, 2001).

The tidal prism across the mouth of the estuary was determined to be on the order of  $3 \times 10^8 \text{ m}^3$  based on ADCP current transects from a 13-hour spring tide survey (McNinch, 2002).

Freshwater inflow for the main-stem Cape Fear River based on USGS gauge data at Lock and Dam 1 (Fig. 2.2) for the five-year study period from 1999 to 2003 ranges from about  $14 \text{ m}^3 \text{ s}^{-1}$  during very low-flow summer conditions to about  $600 \text{ m}^3 \text{ s}^{-1}$  during peak (non-hurricane) flow months (Fig. 2.3). This range is punctuated by very high flow events ( $>1100 \text{ m}^3 \text{ s}^{-1}$ ; e.g. Hurricane Floyd in 1999) with a recurrence interval (based on a 32-year peak flow record) of about 4 years. Discharge on the Northeast and Black Rivers, based on USGS gauge data for locations shown in Fig. 2.2, ranges from about  $0.5 \text{ m}^3 \text{ s}^{-1}$  during low flow months to about  $130 \text{ m}^3 \text{ s}^{-1}$  during higher (non-hurricane) flows. Hydrographs for each river (based on USGS mean daily streamflow data) and a 35-year average daily discharge on the Cape Fear River are shown in Fig. 2.3. Flushing-time values for the CFRE, calculated from the fraction of freshwater method (Dyer, 1997), range from 1 to 22 d (median 6.7 d) with shorter flushing times occurring during higher flow winter months and longer times during more sluggish summer flows (Ensign et. al, 2004).

Several model studies have been conducted to simulate flow within the estuary and predict the effects of particular anthropogenic changes including deepening and widening at certain sections (McAdory, 2000; Hackney et al., 2002), channel realignment (Becker et al., 2001), and increased treatment-plant discharge into the water body (Tetra Tech, 2001). Ongoing field surveys in the estuary are currently being conducted to monitor changes

associated with channel deepening and realignment (USACOE, 2004b) and as part of a state-certified water-quality monitoring effort (LCFRP, 2004).

## **Methods**

### *Tidal Analysis*

We analyzed an intensive USACOE data set collected from mid-August through mid-October 1993 that included tidal height, velocity, salinity, and temperature measurements. Locations and instrumentation at observational stations used for the analysis are shown in Fig. 2.2. The observation period considered was August 17 through October 7, 1993.

Velocity data were available, in general, at mid-depth (referenced at low water) and near-bottom (~1.5 m above bottom). Salinity and temperature were measured at near-surface (corresponding to tide-gauge locations), mid-depth, and near-bottom locations (with the latter two corresponding to velocity-meter locations). The time-interval between measurements was 15 min. Initial data analysis for lower, middle, and upper along-channel regions of the estuary and sections of the Cape Fear, Black, and Northeast Cape Fear River included: (1) least squares analysis of tidal elevations using T\_TIDE (Pawlowicz et al., 2002) including the generation of M4 and M6 components; (2) calculation of tidal excursions using mid-depth and near-bottom velocities for spring and neap tides; and (3) comparison of strength of stratification.

The tidal excursion is defined as the distance a water parcel travels during a flood or ebb cycle. The excursion distance is formally based on a Lagrangian velocity and may be

calculated as:  $X = \int_0^T u dt$  where  $X$  = tidal excursion distance (m),  $u$  = along-channel velocity

(m s<sup>-1</sup>), and  $T$  = half a tidal period (s). If we assume the tidal velocity is nearly constant with

distance for a particular section of the estuary, the excursion distance may be approximated using an Eulerian velocity. A finite-difference integration with a time interval of 900 s was performed using velocity data at S1.2 (lower estuary), S3.9 (mid-estuary), and S6.9 (upper estuary) during spring-tide (Aug. 18-20, 1993) and neap-tide (Aug. 25-26, 1993) periods.

### *Vertical Salinity Sections*

Vertical sections of salinity (Fig. 2.4a) were constructed for the along-channel extent of the Cape Fear Estuary and river section using surface, mid-depth and bottom salinity data that were collected monthly from January 1999 to December 2003 as part of the Lower Cape Fear River Program (LCFRP). Data-collection stations are shown in Fig 2.2. In the estuary, data were collected from a vessel traveling upstream beginning at station M18 near the mouth of the estuary and terminating at Navassa (Fig. 2.2). The time period between the first and last sampling location was approximately 3.5 h, and data were typically collected during the ebb tide. River data were collected one day prior to or one day after the collection of the estuarine data. River samples were collected beginning at NC11 and ending at IC (Fig. 2.2); the time span between collection of the first and last river samples was typically 2 h.

### *Salinity Intrusion*

The along-channel, salinity intrusion during different seasons and flow events (Fig. 2.5) was determined from the vertical sections. The extent of the salinity intrusion into the estuary was defined by the location of the 1 ppt bottom-salinity contour (BSC1). Projections were made of the location of the BSC1 at slack after flood and slack after ebb tide based on the



time in the tidal cycle and the along-estuary position where the data were collected and the previously calculated average near-bottom ebb-tide and flood-tide excursions.

#### *Relationship between Discharge and Salinity Intrusion*

Relationships between the extent of the salinity intrusion and river discharge were examined using BSC1 and four measures of discharge, in order to determine the appropriate means of incorporating flow history into the discharge value. The first is based on peak discharge from the Cape Fear River alone (“Hydrologic Flood Method” or HFM), the second on peak discharge from Cape Fear River, the Northeast Cape Fear River, and the Black River combined (“Complete Hydrologic Flood Method” or CHFM where “Complete” refers to the inclusion of the three rivers), the third on mean daily discharge value on the three rivers (“Complete Value Method” or CVM), and the last on the estimated time it takes for freshwater to travel from the gauging station at Lock and Dam 1 to the BSC1 (“Variable Travel-time Method” or VTM). The Cape Fear River (gauged at Lock and Dam 1, Fig. 2.2) drains about 60% of the total watershed area and is the single-largest source of river flow into the CFRE.

For the HFM, fifteen different measures of discharge on the main-stem Cape Fear River (at Lock and Dam 1) were computed corresponding to the peak daily discharge that occurred *within* time intervals varying in length from one day prior to sampling to fifteen days prior to sampling. The upper limit of 15 days was based on an estimate of the maximum time a flow event would be expected to impact the location of the salinity intrusion and because regression coefficients (Fig 2.6, discussed below) dropped off systematically for longer intervals. Regressions of the BSC1 versus these discharge

measures were compared using the  $R^2$  regression statistics as a skill metric. Linear, exponential and power law regressions were considered to determine the optimal relationship between BSC1 and discharge.

For CHFM, a similar analysis was performed using peak daily discharge (including gauged inflow and a prorated amount for ungauged areas) from the main-stem Cape Fear River, Black River, and Northeast Cape Fear River. At times when BSC1 was located upstream of HB (Fig. 2.2), the Northeast Cape Fear River discharge was not included in the calculation shown in the results section (however, because discharge on the Northeast Cape Fear River was typically low when the BSC1 occupied a relatively far upstream position, the inclusion of this discharge had a little effect on regression results).

The CVM model was investigated to determine whether using the maximum (peak) discharge, as opposed to a mean daily discharge, affected the relationship between BSC1 and river discharge. In this case the mean daily discharge occurring *at* a specified number of days prior to sampling was used.

For the VTM, the discharge value for the (discharge-BSC1-) regression analysis was chosen based on the computed freshwater travel time from Lock and Dam 1 to the location of the BSC1. The freshwater travel time was computed using the along channel freshwater velocity (discharge divided by cross sectional area) and the distance between Lock and Dam 1 and the BSC1.

## Results

### *Tidal Elevations*

The CFRE is characterized by semidiurnal tides (Fig. 2.7) with a range that decreases upstream from a daily average (over the summer 1993 study period) of 1.5 m near the mouth (S1.3) to 1.3 m at the upper extent (S7.0). Mean high or low water precedes slack tide by approximately 1.5 h. Major astronomical constituents, in order of decreasing amplitude based on results of least squares analysis (Table 2.1), are the  $M_2$ ,  $N_2$ ,  $S_2$ ,  $K_1$  and  $O_1$ . Evidence of spring-neap cycles is evidence in the elevation record (e.g. relatively large tidal range observed around August 18 and lower ranges around August 25). In addition, a 27.6-day modulation between the  $M_2$  and  $N_2$  tides and 14.8-day modulation between  $M_2$  and  $S_2$  constituents (spring-neap cycles) may explain the occurrence of particularly large spring tides approximately every 29 days (e.g., August 18-20 and September 16-18). The relationship of this 29-day variation to the salinity structure will be discussed in the sections that follow.

Differences between our computed tidal amplitudes at Southport and phase lags between Southport and Navassa and those reported in an earlier harmonic analysis study (with a 29-day record) (Welch and Parker, 1979) are shown in Table 2.1. Our values for the dominant constituents are in reasonably close agreement with findings from the previous study.

The amplitude of the  $M_4$  and  $M_6$  constituents, which represent the non-linear growth of harmonics of the dominant  $M_2$  astronomical tide, generally increases upstream (Fig. 2.8). At all stations except S11.0, the  $O_1$  amplitude exceeds that of the  $M_4$ .

### *Tidal Velocities*

Maximum spring tide (Aug. 18-20) along-channel velocities at mid-depth and near-bottom are listed in Table 2.2. In general, greater velocities were observed near the mouth of the estuary and at mid-depth.

Observed velocities over the 52-day record at S1.2 near the mouth of the estuary were consistently greater during the ebb tide than during the flood tide and contributed to larger ebb than flood excursion values both at mid-depth and near-bottom. Around mid-estuary (S3.9), flood velocities were consistently greater than ebb velocities. At the upper end of the estuary (S6.9) near-bottom velocities were in general greater during the flood tide than ebb, while at mid-depth a clear trend was not discernable.

Tidal-excursion distances for mid-depth and near-bottom locations for the lower, middle and upper sections of the estuary (as well as averages of the three sections) are given in Table 2.3a. Excursion distances computed for large spring (Aug. 18-20) and following neap (Aug. 25-26) periods are shown in Table 2.3b.

Results indicate that for a relatively large spring tide, estuary-wide ebb-excursion distances (~14 km) exceeded flood distances (~11 km) at mid-depth, but the two were about equal near the bottom (8.8 km versus 8.7 km). During neap tide, the averaged ebb excursion distances exceeded the flood distances (10.5 km versus 9.4 km) at mid-depth, however the flood dominated near the bottom (7.3 km versus 6.0 km). Particularly low near-bottom, ebb-tide velocities at S3.9 and S6.9, for example  $\sim 0.05\text{--}0.1 \text{ m s}^{-1}$  versus  $\sim 0.5 \text{ m s}^{-1}$  during the flood at S3.9 (Fig. 2. 9), contributed to the reduction in ebb-excursion distances during the neap tide. During the large spring tide, in contrast, near-bottom velocities reach  $\sim 0.3$  to  $0.5 \text{ m s}^{-1}$  during the ebb versus  $\sim 0.6 \text{ m s}^{-1}$  to  $0.7 \text{ m s}^{-1}$  during the flood. As we discuss in the

sections that follow, the lower ebb velocities observed during the neap tide may be due to a near-bottom, up-estuary, density-driven flow that is strong during periods of greater stratification

A 14-day average (Aug. 17-Aug. 30) of along-estuary velocities suggests there is net outflow near the mouth (S1.2) at mid-depth ( $-0.12 \text{ m s}^{-1}$ ) and near-bottom ( $-0.10 \text{ m s}^{-1}$ ) locations. Around mid-estuary (S3.9), data indicate net flow is up-estuary at and below mid-depth; observed inflow is greater near the bottom ( $0.11 \text{ m s}^{-1}$ ) than at mid-depth ( $0.05 \text{ m s}^{-1}$ ). At the upper end of the estuary (S6.9), net flow at mid-depth is essentially zero ( $-0.003 \text{ m s}^{-1}$ ), while data suggest inflow occurs near the bottom ( $0.08 \text{ m s}^{-1}$ ). In these reasonably well-stratified parts of the estuary (S3.9 and S6.9), the net bottom inflow further supports the hypothesis that baroclinic density gradients are an important functional mechanism retarding outflow during the ebb tide and enhancing inflow during the flood.

### *Salinity Structure*

For the low-flow 1993-summer period, the estuary was well mixed near the mouth and reasonably stratified near mid-estuary (S4.0) and upstream. Along-channel salinities during a large spring tide are shown in Fig. 2.10. Values vary throughout the tidal cycle from about 30 ppt to 35 ppt at the mouth (S1.3); from 16 to 26 around mid-estuary (S4.0); and from 0 to 10 ppt near Navassa (S7.0), although salinity values as high as 17 ppt were observed over the 52-day record at S7.0.

Analysis of the monthly salinity profiles of the Cape Fear River and the continuous 52-day (Aug. 17-Oct 7, 1993) salinity measurements indicate salinity at IC and S11.0 (near NC11) is low (typically 0 to 0.1ppt at each station). On the Northeast Cape Fear, salinity at

S8.0 varies between about 8 ppt to 12 ppt but reaches only 0.2 ppt near St. 9.0. On the Black River (S10.0), salinity reaches only about 0.1 ppt.

Intra-tidal variations in stratification (e.g. increases during the ebb and decreases during the flood) near mid-estuary (S3.9) during a large spring tide and the following neap tide are shown in Fig. 2.9. Variations in average daily near-bottom salinity and average daily stratification during high and low tidal ranges, including the effect of the 29-day modulation discussed in the “Tidal Elevations” section above, are depicted in Fig. 2.11. Results indicate average daily bottom salinity and average vertical stratification decrease as the daily tidal range increases.

#### *Relationship between Discharge and Salinity Intrusion*

Analysis of the discharge time interval during which the salinity intrusion length is best correlated with discharge is shown in Fig. 2.6. The maximal regression correlation coefficient ( $R^2=0.92$ ) occurs using an exponential regression between BSC1 and the peak discharge computed from all three rivers (CHFM) during the 11-days prior to sampling. Linear regressions for the CHFM and HFM models show a similar trend in which correlation coefficients are maximal ( $R^2 = 0.89, 82$ ) for 11-day and 12-day discharge time intervals, respectively (as indicated by square and circle on Fig. 2.6). Power-law regressions correlation coefficients for the CHFM range from values of 0.72 to 0.75 and show relatively little variability for different values of discharge interval. Power-law regression coefficients for the HFM range from 0.65 to 0.67.

Correlation coefficients for the CVM did not indicate an optimal discharge time interval and remained below that of the exponential CHFM.

Linear regression plots for 1999-2003 for the HFM (discharge time interval of 12 days) and CHFM (discharge time interval of 11 days) are shown in Fig. 2.12a and 2.12b. The relationship between peak discharge and BCS1 using the travel-time-based discharge value (VTM) is shown in Fig. 2.12c. Comparisons of exponential and power-law relationships for the CHFM using an 11-day discharge time interval are given in Fig. 2.13.

## **Discussion**

In a partially mixed estuary like the CFRE, the relative strength of river flow, which adds buoyancy inputs, and tidal currents, which act to break down stratification, are important mechanisms that help determine the salinity structure and consequent transport of constituents. The horizontal salinity gradient resulting from the input of freshwater from the river and saltier water from the ocean induces a horizontal density gradient and associated density-driven (baroclinic) circulation. Baroclinic circulation can enhance stratification as a result of differential advection of lighter (fresher) water at the surface flowing seaward and heavier (saltier) water near the bottom flowing up-estuary. The estuarine circulation and salinity structure may then, or at the same time, change depending on the relative strength of competing forces that determine the momentum balance. Friction associated with tidal currents may act to inhibit density-driven circulation. A reduction in friction during periods of increased stratification, in contrast, may allow for stronger density-driven flow and greater up-estuary transport (Stacey et al., 2001).

Classic analyses of estuarine dynamics (Pritchard, 1956; Hansen and Rattray, 1965) suggests that tidally averaged circulation is largely controlled by the balance between the barotropic pressure gradient due to the along-estuary sea-surface slope, the baroclinic

pressure gradient due to the along-estuary density gradient, and friction. More recent research indicates that, in addition, differences in the turbulence and stratification during flood versus ebb tide may be important in controlling estuarine dynamics (Geyer et al., 2000; Monismith et al., 1996; Jay 1991; Simpson et al., 1990). Tidal straining, which describes the differential displacement of lighter, less dense water closer to the surface over saltier water below, has been observed to be an important mechanism for controlling stratification, mixing, and circulation in estuaries such as the Liverpool Bay region (Simpson et al., 1990), the Hudson River estuary (Nepf and Geyer, 1996), and San Francisco Bay (Monismith et al., 1996). Differences in the structure of flow can be further influenced by differences in the shear generated during the flood or ebb tide (Jay, 1991).

In our analysis of the CFRE, we discuss the dominant timescales that influence flow. Our analysis indicate the salinity structure and circulation are impacted by (1) tidal-range differences based on an approximately 29-day periodicity, (2) intra-tidal variations associated with tidal straining, and (3) sub-tidal scale variations in freshwater input which influence the location of the salinity intrusion.

#### *Stratification: Tidal Range Differences and Intra-tidal Variations*

Flow characteristics in a partially mixed estuary are linked to stratification. For strongly stratified conditions, buoyancy inputs (e.g. through freshwater discharge) act to suppress turbulence and deter vertical mixing. The action of tidal currents, which tends to break down stratification and generate turbulence in the bottom layer, may contribute to increased frictional influence.



The density distribution within an estuary can influence the strength of vertical mixing and vertical transport of salt, nutrients, and contaminants as well as the degree to which baroclinic conditions can enhance flow into or impede flow out of the water body. Our analysis of the CFRE shows the density distribution for relatively short time scales (e.g. tidal timescales) is largely determined by salinity, as data (from temperature sections and 52-day USACOE measurements) indicate the temperature remains nearly constant, typically less than 1 degree C variation, throughout a tidal cycle. In order to characterize the tidal influence on the stratification structure, we observed variations during low versus high tidal ranges and differences during ebb and flood tidal cycles when river inflow was minimal ( $<65 \text{ m}^3 \text{ sec}^{-1}$ ).

In consideration of how the salinity structure is affected by tidal range, a relationship between the approximately 29-day modulation discussed in the “Tidal Elevation” part of the “Results” section (i.e. the occurrence of particularly large spring tides approximately every 29-days) and salinity is notable. In the stratified upper estuary at S6.9, for example (Fig. 2.11), average daily bottom salinity and average vertical stratification decrease as the daily tidal range increases (in particular, in the absence of increased winds toward the north). Both bottom salinity and stratification generally reach low points during large spring-tide events. Similar relationships also exist between tidal range, bottom salinity, and stratification in the other stratified sections of the estuary (S3.9 and S5.9)

An explanation for the increased salinity during low tidal ranges is that a reduction in friction allows for greater stratification, stronger density-driven flow and, as a result, greater transport of salt up-estuary. During these periods when tidal range is at a minimum and stratification is high, the effects of baroclinic circulation likely become significant; data

suggest baroclinic circulation becomes important as velocities and excursion distances are low during the ebb neap tidal cycle (Fig. 2.9b). Near-bottom tidal excursions around mid-estuary reach only 1.5 km during the neap ebb tide (Table 2.3b), compared to 6.1 km during the neap flood. (Excursions of 4.7 km and 9.4 km occur during the large spring ebb and flood, respectively). Turbulent mixing of freshwater during strong spring-tide events may also contribute to lower observed salinities during the spring tide.

The influence of intra-tidal variations is evident in the middle (S3.9) to upper estuary (S5.9). During the ebb tide, stratification tends to increase, whereas during the flood tide, stratification is reduced. The stratification periodicity (the period between the occurrences of maximum or minimum stratification) corresponds to approximately a tidal period (Fig. 2.9). The consistent, periodic pattern of stratification variability in the mid to upper estuary may be attributed to tidal straining. During the ebb tide, fresher surface water moves faster than denser seawater, and stratification tends to increase (resulting in tilted isohalines that represent a stable density structure). During the flood tide, the differential displacement of water will tend to reduce stratification and could, if not for the mixing process, lead to an unstable density structure (Dyer, 1997; Simpson et al, 1990). Ebb-flood asymmetry in the development of shear may further influence mixing and circulation characteristics (Jay, 1991).

Evidence of the combined effects of flood-ebb and tidal range variability on circulation appears in the velocity structure. During the neap ebb tide, a correlation between particularly low near-bottom velocities (Fig. 2.9b) and stratification exists. These lower ebb velocities may be due to the along channel density gradient acting against outflow during the ebb tide and enhancing inflow during the flood. The near-bottom, up-estuary, density-driven

flow created by this gradient may increase in strength during periods of high stratification, as friction is inhibited. At the same time, during these periods of increased stratification and weaker friction, turbulent mixing of fresh and salt water may diminish (and further contribute to the observed variability in near-bottom salinities). As residual circulation is critically linked to time-dependent variability in shear, mixing, and stratification, we leave more detailed analysis of these interactions (e.g. development of the bottom boundary layer; characterization of the density, shear, and mixing structure during varying tidal conditions) for future investigation.

#### *Relationship between Discharge and Salinity Intrusion*

Characterization of the response of the estuarine salinity structure to changes in freshwater flow is fundamental to understanding estuarine circulation. As estuarine salinity characteristics may change depending on the time period during which the salinity structure is observed and depending on how different forcing mechanisms influence the transport of salt, temporal changes such as neap-spring variations, storm events, and ebb-flood differences can cause significant changes in the salt balance. How estuaries respond to such temporal changes, however, is not clear, as our knowledge of how estuaries adjust to changes in river discharge is relatively limited (Blanton, 2004). In particular, little research has been conducted to determine how changes in the discharge hydrograph affect the transport of salt in estuaries along the southeastern coast of the United States.

In order to gain insight into discharge-salinity intrusion relationships in the CFRE, we explored linear, exponential, and power-law regression relationships. We initially hypothesized the estuarine salinity response to freshwater input is largely dependent upon

the size of the hydrologic “flood” or peak in river discharge relative to base (“dry-weather”) flow. Findings are first discussed in this context, including year-to-year variations and the influence of the three rivers. Results of the observed data are then compared to theoretical predictions from classic estuarine formulations (Hansen and Rattray, 1965; Chatwin, 1976; MacCready, 2004).

### *“Hydrologic Flood” Hypothesis*

In estuaries in which river inflow may fluctuate significantly between low-flow and high-flow conditions and in which the location of the salinity intrusion changes accordingly (Fig. 2.5), a distinction between the mechanisms that determine the salinity intrusion during low-flow versus higher discharge may be considered. In order to analyze how discharge influences the extent of the salinity intrusion for the HFM and CHFM, we considered the relationship between the salinity intrusion and the hydrologic “flood”, defined as a peak in river discharge following rain or snowmelt. These floods may be represented as waves that move downstream; the study of their propagation characteristics (including peak height and speed) is an important part of understanding river responses to precipitation (Hornberger et al., 1998). Although research related to flood routing (the downstream river response given an upstream hydrograph) occupies a significant part of the hydrologic literature (Rutschmann and Hager, 1996; Lamberti and Pilati, 1996; Sivapalan et al., 1997; Hornberger et al., 1998), the estuarine response to peaks in river discharge is not well understood.

In order to distinguish between the flood described above and the flood tide (incoming tide), we refer to the former as the “hydrologic flood.” In our analysis of the CFRE, we hypothesized that the location of the salinity intrusion depends on the size of the

hydrologic flood. Following a peak in river discharge, the volume of freshwater associated with the peak would enter the estuary and, after adjusting for tidal fluctuations, be directly linked to the location of the salinity intrusion (assuming the time period of observation was within a period in which dispersion had not yet significantly mixed incoming freshwater). If a significant peak did not occur prior to the observed position of the BSC1 [i.e. the hydrograph represented base flow or “background discharge between floods” (Hornberger et al., 1998)], the salinity intrusion would remain in a position corresponding to low-flow conditions (for the CFRE, this position would be upstream of NAV for both the expected location after the ebb and flood tides). In other words, we hypothesized that the location of the salinity intrusion varies with discharge, and that this location can, to large a degree, be attributed to a particular flow event (quantifiable by finding the appropriate peak in the discharge hydrograph). In our research, we sought to test this hypothesis through interpretation of results of the regression formulations. Further consideration of the estuarine impacts of flood-versus base-flow conditions (e.g. how quickly the salinity intrusion responds to a hydrologic flood event, how the response differs depending on whether discharge is increasing or decreasing, or how long the intrusion holds its position following a flood event) are beyond the scope of this research and will be remain open topics for more detailed future research.

A comparison of linear regression curves (Fig. 2.12) indicates the greatest correlation results when the discharge value is based on a value associated with the hydrologic flood and when flow from the three rivers (CHFM) is accounted for. In the aggregate (1999-2003), 89% of the variation is captured for both slack after flood and slack after ebb using the simple linear CHFM representation (compared to 82% using the HFM or 78% to 79% using

the VTM). Inspection of plots shows points are less scattered for the CHFM than for the VTM or HFM, in particular when the calculated position at slack after ebb is downstream of mid-estuary about 18 to 22 km upstream of the origin at M18.

Extension of the CHFM to an exponential regression (Fig. 2.13b) shows trends similar to the linear representation; however, correlation values are greater in the aggregate (1999-2003,  $R^2=0.92$ ) and for individual years (Table 2.4). Analysis suggests the extension of the salinity intrusion in the area relatively far downstream may be more accurately predicted when discharge from all three rivers is included (CHFM, linear and exponential) than when discharge is represented by the Cape Fear River alone (CHM). Regression coefficients generally increased with the inclusion of the three rivers, especially when relatively large peaks were represented in the sampling year (e.g. 1999 and 2003). The analysis suggests that inflow from the Black River and Northeast Cape Fear River flow can become important in explaining the low salinities observed in the lower section of the estuary.

Lowest correlation coefficients occur for 2002, when sampling represented relatively low-flow events ( $38 - 469 \text{ m}^3 \text{ sec}^{-1}$ ) and when the salinity intrusion remained relatively far upstream. A relatively small variation in the migration of the BSC1, 12 km, was observed then, compared to 35 km-variation in 1999 and 2003. Correlation coefficients showed only slight differences between the HFM and CHFM (linear and exponential). Greatest correlation coefficients exist for 1999 and 2001 ( $R^2= 0.96$  for the CHFM exponential), when sampling generally included higher flow conditions (from less than 40 to greater than  $1000 \text{ m}^3 \text{ sec}^{-1}$ ).

In general, the salinity intrusion migrated farthest into the river sections during low-flow conditions, often occurring during sluggish summer months. Based on the CHFM, when total peak discharge prior to sampling was less than about  $140 \text{ m}^3 \text{ sec}^{-1}$ , the extents of BSC1 on both the flood and ebb tides generally remained upstream of Navassa (NAV). During higher-flow periods (e.g. total peak discharge  $> 500 \text{ m}^3 \text{ sec}^{-1}$ ), the BSC1 on flood tide was generally downstream of M61 (~24 km downstream of a typical location during low-flow conditions). Approximately 2.5 weeks after the passing of Hurricane Floyd on September 16, 1999, the intrusion at slack after flood-tide extended into the vicinity of M42, a distance of about 30 km from its typical upstream location during low-flow conditions (Fig. 2.4). Intrusion-migration distances within a tidal cycle (based on near-bottom excursion values), in contrast, were on the order of 6 km to 9 km.

The mean location of the BSC1 (based on the 1999-2003 samples) for the expected extent of the flood and ebb was 45.5 km and 37.3 km, respectively, upstream of the origin at M18. This places the average extent of the salinity intrusion a few km upstream of NAV at slack after flood and between M61 and HB at slack after ebb (Fig. 2.2). Peak discharge associated with these mean conditions (based on the HFM and CHFM) was about  $230 \text{ m}^3 \text{ sec}^{-1}$  for the Cape Fear River and  $350 \text{ m}^3 \text{ sec}^{-1}$  when including all three rivers.

#### *Exponential Decay Representation*

Observational data suggest the strongest correlation occurred using the exponential decay relation (CHFM) between peaks in river discharge ( $Q_p$ ) measured 11 days prior to sampling and the salinity-intrusion location. The regression equation for slack after flood-tide ( $R^2=0.92$ ) is:

$$Y = 54.6 e^{-0.0005Q_p}$$

where  $Y$  = salinity intrusion location relative to M18 near the mouth,

$Q_p$  = peak discharge =  $\text{Max } [Q(t_0-1):Q(t_0+1)]$ ,

$t_0$  = day of salinity intrusion sampling,  $Q$  = mean daily discharge ( $\text{m}^3\text{sec}^{-1}$ )

We hypothesize that the salinity intrusion location is dependent upon the relative size of the hydrologic “flood,” defined as a peak in river discharge associated with “quickflow,” the flow of water associated with the runoff contribution from storm events.

For base-flow conditions (during which discharge is small and approaches a value close to  $Q_p = 0$ ), the salinity intrusion approaches a position close to  $Y_0$  or 54.6 km upstream of the origin near the mouth of the CFRE. This corresponds to a location upstream of NAV (Fig. 2.2). With the introduction of freshwater and the associated increased barotropic pressure gradient, the location of the salinity intrusion decreases (decays) at a rate proportional to its location,  $Y$ , at any  $Q_p$ , where the rate constant is defined by the exponent ( $-5 \times 10^{-4}$  for the CFRE). For example, if the salinity intrusion is originally close to its base-flow position (for example at  $Y_0 = 54.6$  at slack after flood for the CHFM), the rate of decay is 0.05 percent of its position or  $2.7 \times 10^{-2}$  km per unit peak discharge ( $Q_p$ ). If the salinity intrusion were at a position downstream of that low-flow location due to an increase in  $Q_p$ , (for example at  $Y = 20.1$ , a location corresponding to  $e^{-1}$  times its base-flow position and a location close to the 1999 post-hurricane Floyd position), the salinity intrusion location would decay more slowly ( $1.0 \times 10^{-2}$  km per unit peak discharge). As discharge continues to increase, the salinity intrusion moves closer to the origin at M18 near the mouth.

A consequence of the exponential form of the regression equation is that it never actually reaches this position (M18). Given the position of the salinity intrusion following



Hurricane Floyd in 1999, however, this may not be a significant practical consideration. Furthermore, because one would expect the salinity at the mouth to be close to a constant value (of  $\sim 34$  ppt as one approaches ocean salinity), one would also expect the location of the BSC1 to be able to approach, but not reach, 0 (as the salinity of the BSC1 or 1 ppt will not equal the expected salinity at the mouth of  $\sim 34$  ppt). The exponential decay function depicts this expected behavior as the function (salinity intrusion distance) asymptotes toward zero as one approaches the mouth.

The CHFM linear regression model, in comparison, defines the rate of decrease of the salinity intrusion with peak discharge by the slope of the regression line, a value of approximately  $2.0 \times 10^{-2}$  km per unit peak discharge in the CFRE. The y-intercept (53.4 km at slack after flood) may be interpreted as the near base-flow location of the salinity intrusion. In this model the salinity intrusion may migrate downstream of M18. Although differences in regression coefficients between the linear and exponential models are slight and may not be statistically significant ( $R^2 = 0.89$  versus 0.92, respectively), the linear model does not asymptote toward zero near the mouth and may not predict the expected behavior of the salinity intrusion very close to the ocean boundary.

When the decay of a quantity is proportional to its present amount, one can anticipate an exponential solution. The exponential decay of the salinity intrusion location due to river forcing may be explained based on how the intrusion length is expected to respond to the introduction of freshwater. As a result of the increase in estuarine width as one approaches the mouth, one may predict a smaller change in salinity intrusion location per unit discharge (i.e. slower decrease). In addition, because a salinity intrusion location closer to the estuarine mouth is expected to be associated with increases in freshwater flow, the associated increase

in the longitudinal salinity gradient and stratification may create conditions in which density-driven flow and the upstream salt flux increase. As a result of the strengthening of this (baroclinic) force acting against the freshwater-induced barotropic pressure gradient, the decrease in the position of the salinity intrusion may be slower.

### *Classic Estuarine Formulations*

Techniques that have been used in other studies to investigate or characterize salinity-discharge relationships include the development of analytic formulations based on simplified momentum and salt budget equations for rectangular estuarine systems (Hansen and Rattray, 1965; Chatwin, 1976; MacCready, 2004), the construction and utilization of hydrodynamic models of such idealized systems to further investigate classic representations (Hetland and Geyer, 2004), and the analysis of observational/empirical data (MacCready, 2004; Monismith et al., 2002). Hansen and Rattray's (1965) classic work considers the balance between river flow, density-driven ("exchange") flow, and horizontal diffusion. Chatwin (1976) derives a relationship for a system in which the up-estuary flux of salt is dominated by constant river flow and exchange flow, conditions for which the horizontal diffusive flux of salt is zero. MacCready (2004) developed more general solutions to equations for salinity and circulation and was able to reproduce both the Hansen and Rattray (1965) and Chatwin (1976) analytic solutions.

The theoretical solutions described above result in relationships in which the salinity intrusion length ( $L$ ) varies with a fractional power of river discharge ( $Q$ ); i.e.  $L \propto Q^{-1/3}$  for exchange dominated systems and  $L \propto Q^{-1}$  for diffusion dominated conditions. Analysis of empirical data and numerical model investigations suggest, however, that variations in

mixing rates and bathymetry may influence differences between theory and observations (MacCready, 2004; Monismith et al., 2002). Monismith et al. (2002), for example, found that for Northern San Francisco Bay, salinity-intrusion versus discharge relationships based on power-law relations were more closely represented by  $L \propto Q^{-1/7}$ .

Deviations from predicted values may be attributed to variations in bathymetry, the influence of flow-induced variations in stratification on vertical mixing rates, and the consequent impact on density-driven circulation (Monismith et al., 2002). With increases in river flow (and associated increases in stratification and longitudinal salinity gradients), density-driven flow may strengthen, and the upstream transport of salt may be larger than theory prescribes. We expect variability in mixing, frictional characteristics, the intensity of baroclinic circulation, and along-channel cross-sectional area may account for differences between our observed and theoretical values based on the power-law formulations.

Our alternative approach, based on the hydrologic flood exponential decay model, suggests the system's dominant response is to sub-tidal events that are transient in nature (i.e. the salinity intrusion migrates downstream in response to the introduction of a hydrologic flood). We hypothesize the estuarine salinity response depends on the way in which these waves propagate with time (e.g. how the size and shape of the rising and falling limbs of the hydrograph change due to different frictional and bathymetric characteristics) as well as the degree to which up-estuary baroclinic forcing opposes the downstream barotropic push. In river-estuary systems in which hydrologic flood peaks are large relative to base flow (and in which the width or bathymetry of the estuary may vary significantly between the estuarine head and mouth), we hypothesize the hydrologic flood exponential decay model may offer a more accurate means of predicting the estuarine salinity response (compared to the classical

power-law relations). More detailed comparisons between methods (e.g. investigation of deviations of observed values from theoretical power-law formulations through parameterization of temporally and spatially varying mixing rates, exploration of differences in baroclinic circulation due to varying discharge and tidal conditions, consideration of the influence of frictional/bathymetric variations on flood wave propagation, and extension to other river-estuarine systems) are intriguing problems for future analysis.

### **Summary and Conclusions**

The salinity and circulation structure of the CFRE depends on the relative strength of main forcing mechanisms including river input (that induces a barotropic response and baroclinic circulation) and tidal currents (that generate turbulence). A mixture of freshwater from the Cape Fear River (a major piedmont river) as well as the Black and Northeast Cape Fear Rivers (coastal plain rivers) discharges into the estuary and influences the location of the boundary between fresh and salty water. The salinity intrusion distance varies from about 29 km upstream (referenced to M18 near the mouth) following high (non-hurricane) flow to about 53 km upstream following low flow based on the computed extent at slack after the flood tide. Tidal excursion distances, in comparison, are on the order of 8 km near the bottom.

Our analyses indicate the salinity and circulation structure are impacted by tidal-range differences based on an approximately 29-day periodicity, intra-tidal variations associated with tidal straining, and sub-tidal scale variations in freshwater input which influence the location of the salinity intrusion.

More specifically,

1. Tidally driven flow is dominated by the  $M_2$ ,  $N_2$ , and  $S_2$  constituents with significant  $M_4$  and  $M_6$  components in the upper estuary (upstream of S6.0). The combination of the dominant tidal constituents ( $M_2$ ,  $N_2$ , and  $S_2$ ) leads to an approximately 29-day periodicity in the elevation record (i.e. particularly large spring tides are observed about every 29 days).
2. Average daily bottom salinity and average daily stratification vary according to the 29-day modulation in the elevation record. The analysis suggests that during low tidal ranges, a reduction in friction may allow for weaker mixing, greater stratification, and increased up-estuary transport.
3. Analysis of observational hydrodynamic data supports the paradigm that asymmetry (e.g. tidal straining and differences in mixing) during the flood and ebb tide are significant in explaining estuarine circulation. An increase in stratification during the ebb and a decrease during the flood is observable in the mid to upper estuary. On the neap ebb tide, a correlation between notably low near-bottom velocities and stratification is evident. The analysis suggests stratification and baroclinic circulation are significantly impacted by intra-tidal variations.
4. The location of the salinity intrusion varies as a result of discharge and migrates approximately 30 km between drought- and extreme-flow periods. Tidal-cycle differences (based on near-bottom excursions) are on the order of 8 km.

Following sluggish river-flow periods the salinity intrusion (extent after a flood

tide) is typically located upstream of Navassa, whereas after higher flow events the intrusion is closer to mid-estuary.

5. Classical estuarine theory predicts the salinity intrusion would vary with discharge to the power of  $(-1/3)$  in exchange-dominated systems and to the power of  $(-1)$  in diffusion-dominated systems (MacCready, 2004, Chatwin, 1976). Our analysis suggests a weaker dependence on discharge than the  $(-1/3)$  exponent predicted by theory and an exponent close to the  $(-1/7)$  observed by Monismith et al. (2002), although in general our data were not well fit by a power-law relationship, but rather by an exponential function.
6. We hypothesize that the salinity intrusion location is dependent upon the relative size of the hydrologic “flood,” defined as a peak in river discharge associated with “quickflow” (e.g. the runoff contribution from storm events). Our results indicate 92% of the variability of the salinity intrusion location can be attributed to peaks in flow from the three rivers during the 11 days prior to sampling in the estuary using an exponential relationship between the peak discharge and the location of the salinity intrusion.
7. We hypothesize that in river-estuary systems in which hydrologic flood peaks are large relative to base flow (and in which variations in width and bathymetry between the estuarine head and mouth may be significant), the hydrologic flood exponential decay model may be a more accurate method of predicting the estuarine salinity response than classical power-law relationships.

## Literature Cited

- Becker, M.L., Luettich, R.A., and Westerink, J., 2001, "A Reconnaissance Modeling Study of Two-dimensional Tidal Circulation and Sediment Bed Change in the Vicinity of the Cape Fear River Navigation Channel, NC," Institute of Marine Sciences, University of North Carolina at Chapel Hill, 15 p.
- Benke, A.C. and Cushing, C.I., 2005, *Rivers of North America*, 1144 p.
- Blanton, J.O., 2004, "LU-CES State of Knowledge Report on Physical Oceanography," (<http://www.luces.org/documents/SOKreports/physicaloceanography.pdf>), 42 p.
- Chatwin, P.C., 1976, "Some remarks on the maintenance of the salinity distribution in estuaries, *Estuarine Coastal Marine Science*, 4, p. 555-566.
- Dame, R., Alber, M., Allen, D., Mallin, M., Montague, C., Lewitus, A., Chalmers, A., Gardner, R., Gilman, C., Kjerfve, Bjorn, Pinckney, J., and Smith, N., 2000, "Estuaries of the South Atlantic Coast of North America: their geographical signatures," *Estuaries*, 23, p. 793-819.
- Dyer, K.R., 1997, *Estuaries*, 2<sup>nd</sup> Ed., 195 p.
- Ensign, S.H., Halls, J.N., and Mallin, M.A., 2004, "Application of digital bathymetry data in an analysis of flushing times of two large estuaries," *Computers and Geosciences*, 30: 501-511.
- Geyer, R.W., Trowbridge, J.H., and Bowen, M.M., 2000, "The dynamics of a partially mixed estuary," *Journal of Physical Oceanography*, Vol. 30, p. 2035-2048.
- Hackney, C.T., Posey, M., Leonard, L.L., Alphin, T. and Avery, G.B., 2002, Monitoring Effects of Potential Increased Tidal Range in the Cape Fear River Ecosystem due to Deepening Wilmington Harbor, North Carolina," Department of Biological Sciences, University of North Carolina at Wilmington, 220 p.
- Hansen, D.V. and Rattray, M., 1965, "Gravitational circulation in straits and estuaries," *Journal of Marine Research*, 23, 104-122.
- Hetland, R.D and Geyer, W.R., 2004, "An idealized study of the structure of long, partially mixed estuaries," *Journal of Physical Oceanography*, Vol. 34, p. 2677-2691.
- Hornberger, G.M., Raffensperger, J.P., Wiber, P.L., and Eshleman, K.N., 1998, *Elements of Physical Hydrology*, 302 p.
- Jay, D.A., 1991, "Internal asymmetry and anharmonicity in estuarine flows," *Tidal Hydrodynamics*, edited by B.B. Parker, p. 403-418.

- Lamberti, P. and Pilati, S., 1996, "Flood propagation models for real-time forecasting," *Journal of Hydrology*, Vol. 175, p. 239-265.
- Lin, J., Xie, L., Peitrafesa, L., Shen, J., Mallin, M., and Durako, M., 2006, "Dissolved oxygen stratification in two micro-tidal partially mixed estuaries," *Estuarine, Coastal, and Shelf Science*, 70, p. 423-437.
- Lower Cape Fear River Program (LCFRP), 2004,  
(<http://www.uncwil.edu/cmsr/aquaticceology/LCFRP/>).
- Luettich Jr. R.A., Carr, S.D., Reynolds-Fleming, J.V., Fulcher, C.W., and McNinch, J.E., 2002, "Semi-diurnal seiching in a shallow, micro-tidal lagoonal estuary," *Continental Shelf Research*, 22, p. 1669-1681.
- MacCready, P., 2004, "Toward a unified theory of tidally-averaged estuarine salinity structure," *Estuaries*, 27, (4), p. 561-570.
- Mallin, M.A., 2000, "Impacts of industrial animal production on rivers and estuaries," *American Scientist*, 88, p. 26-37.
- Mallin, M.A., Burkholder, J.M., Cahoon, L.B., and Posey, M.H., 2000, "The North and South Carolina coasts," *Marine Pollution Bulletin*, 41, Nos. 1-6, p. 56-75.
- Mallin, M.A., McIver, M.R, Wells, H.A., Williams, M.S., Lankford, T, E., and Merritt, J. F., 2003, "Environmental Assessment of the Lower Cape Fear River System, 2002-2003," CMS Report Number 03-03, Center for Marine Sciences, University of North Carolina at Wilmington,  
(<http://www.uncwil.edu/cmsr/aquaticceology/lcfrp/>)
- McAdory Jr., R.T., 2000, "Cape Fear-Northeast Cape Fear River, North Carolina Numerical Model Study," US Army Corps of Engineers Engineer Research Development Center, Coastal and Hydraulics Laboratory, 95 p.
- McNinch, J.E., 2002, "Letter Report: Mean Current Flow across the Mouth of the Cape Fear River Tidal Inlet and the New Channel Region, 2002,"  
([http://www.frf.usace.army.mil/capefear/reports/mcninch%20adcp%20wil\\_harbor%20report%202002/mcninch%20adcp%20wil\\_harbor%20report%202002.stm](http://www.frf.usace.army.mil/capefear/reports/mcninch%20adcp%20wil_harbor%20report%202002/mcninch%20adcp%20wil_harbor%20report%202002.stm)).
- Monismith, S., Burau, J.R., and Stacey, M., 1996, "Stratification dynamics and gravitational circulation in northern San Francisco Bay," in *San Francisco Bay: The Ecosystem*, edited by J.T. Hollibaugh, p. 123-153.
- Monismith, S.G., Kimmerer, W., Burau, J.R., and Stacey, M.T., 2002, "Structure and Flow-induced Variability of the Subtidal Salinity Field in Northern San Francisco Bay," *Journal of Physical Oceanography*, 32, p. 3003-3019.



- Nepf, H.M. and Geyer, W.R., 1996, "Intratidal variations in stratification and mixing in the Hudson estuary," *Journal of Geophysical Research*, Vol. 101, No. C5, p. 12,079-12,086.
- North Carolina Division of Water Quality (NC DWQ), 1996, *Cape Fear River Basinwide Water Quality Management Plan*. North Carolina Department of Environment, Health, and Natural Resources, Division of Water Quality, Raleigh, NC.
- Orlando, S.P., Wendt, P.H., Klei, C.J., Pattillo, M.E., Dennis, K.C., and Ward, G.H., 1994, "Salinity Characteristics of South Atlantic Estuaries," National Oceanic and Atmospheric Administration, Ocean Resource Conservation and Assessment, Silver Springs, Maryland.
- Pawlowicz, R., B. Beardsley, and S. Lentz, 2002, "Classical Tidal Harmonic Analysis Including Error Estimates in MATLAB using T\_TIDE", *Computers and Geosciences*, (28), p. 929-937.
- Pritchard, D.W., 1956, "The dynamic structure of a coastal plain estuary," *Journal of Marine Research*, 15: 33-42.
- Reynolds-Fleming, J.V. and Luettich, R.A., 2004, "Wind-driven lateral variability in a partially mixed estuary," *Estuarine, Coastal, and Shelf Science*, 60(3), p. 395-407.
- Rutschmann, P. and Hager, W., 1996, "Diffusion of floodwaves," *Journal of Hydrology*, Vol. 178, p. 19-32.
- Simpson, J.H., Brown, J., Matthews, J., and Allen, G., 1990, "Tidal Straining, Density Currents, and Stirring in Control of Estuarine Stratification," *Estuaries*, Vol. 13, No. 2, p. 125-132.
- Sivapalan, M., Bates, B.C., and Larsen, J.E., 1997, "A generalized, non-linear, diffusion wave equation: theoretical development and application," *Journal of Hydrology*, Vol. 192, p. 1-16.
- Stacey, M.T., Burau J.R., and Monismith, S.G., 2001, "Creation of Residual flows in a partially stratified estuary," *Journal of Geophysical Research*, Vol. 106, No. C8, p. 17013-17037.
- Tetra Tech, Inc., 2001, "3-Dimensional EFDC Water Quality Model of the Lower Cape Fear River and its Estuary," prepared for City of Wilmington and New Hanover County, p. 1.1-3.34.
- United States Army Corps of Engineers (USACOE), 2004a, "Everett Jordan Dam and Lake Project Cape Fear River Basin, NC," (<http://epec.saw.usace.army.mil/bejpert.txt>)

United States Army Corps of Engineers (USACOE), 2004b, "Coastal Monitoring of the Wilmington Harbor Navigation Project," (<http://www.frf.usace.army.mil/capefear/>)

Welch, J.M. and Parker, B.B., 1979, "Circulation and Hydrodynamics of the Lower Cape Fear River, North Carolina," NOAA Technical Report NOS 80, 108 p.

---

Constituent	Amplitude near Southport	Amplitude near Southport	Phase Difference between Southport and Navassa (degrees)	Phase Difference between Southport and Navassa (degrees)
	NOAA (1979)	Least Squares Analysis of Elevation Data at S2.0	NOAA (1979)	Least Squares Analysis of Elevation Data at S2.0
M <sub>2</sub>	0.614	0.601 ± 0.006	67	63 ± 1.62
N <sub>2</sub>	0.132	0.164 ± 0.007	66	68 ± 6.09
S <sub>2</sub>	0.105	0.110 ± 0.006	80	74 ± 10.3
K <sub>1</sub>	0.081	0.067 ± 0.008	38	43 ± 14.8
O <sub>1</sub>	0.058	0.064 ± 0.008	56	36 ± 15.8
M <sub>4</sub>	0.001	0.004 ± 0.003	188	121 ± 60.3
M <sub>6</sub>	0.013	0.013 ± 0.002	224	209 ± 21.2

---

Table 2.1: Comparison of phase lags between Southport and Navassa. Values represent findings of Welch and Parker (1979) and our harmonic least squares analysis of the 1993 elevation data.

Vertical Location	Maximum Spring-Tide Velocity Mid Depth ( $\text{m s}^{-1}$ )	Maximum Spring-Tide Velocity Near-Bottom ( $\text{m s}^{-1}$ )
Lower Estuary	1.3	1.1
Mid Estuary	0.91	0.71
Upper Estuary	0.67	0.54

Table 2.2: Maximum spring-tide velocities at lower, middle, and upper sections of the estuary.

a)

Tidal Cycle	Mid-Depth Excursion Lower Estuary (km)	Mid-Depth Excursion Mid Estuary (km)	Mid-Depth Excursion Upper Estuary (km)	Mid-Depth Estuary-wide Excursion (km)
Spring Flood	13.1	12.1	7.7	11.0
Spring Ebb	21.4	10.1	11.3	14.3
Neap Flood	10.7	8.8	8.6	9.4
Neap Ebb	16.1	7.0	8.3	10.5

b)

Tidal Cycle	Near-Bottom Excursion Lower Estuary (km)	Near-Bottom Excursion Mid Estuary (km)	Near-Bottom Excursion Upper Estuary (km)	Near-Bottom Estuary-wide Excursion (km)
Spring Flood	10.4	9.4	6.6	8.7
Spring Ebb	15.0	4.7	6.8	8.8
Neap Flood	8.3	6.1	7.6	7.3
Neap Ebb	13.0	1.5	3.5	6.0

Table 2.3: Excursion distances at (a) mid-depth and (b) near-bottom for the lower, middle, and upper reaches of the estuary. Calculations were based on velocity data from stations S1.2, S3.9 and S6.9, respectively. Estuary-wide excursions (last column) are based on an average excursion distances at the three sections of the estuary.

Sampling Year	Mean Discharge Cape Fear River ----- Range of Total Peak Discharge during sampling (m <sup>3</sup> sec <sup>-1</sup> )	Linear Regression based on Computed Distance Upstream Slack after Flood Tide (HFM)		Linear Regression based On Computed Distance Upstream Slack after Flood Tide (CHFM)		Exponential Regression based on Computed Distance Upstream Slack after Flood Tide (CHFM)	
		Equation	R <sup>2</sup> value	Equation	R <sup>2</sup> value	Equation	R <sup>2</sup> value
1999	164 (31-1894)	Y=-0.039x+53.5	0.901	Y=-0.016x+51.2	0.947	Y=52.6 e <sup>-0.0004x</sup>	0.963
2000	125 (42-985)	Y=-0.043x+53.4	0.810	Y=-0.022x+52.7	0.861	Y=53.5e <sup>-0.0005x</sup>	0.880
2001	79 (37-1066)	Y=-0.059x+57.2	0.929	Y=-0.027x+55.4	0.921	Y=56.4e <sup>-0.0007x</sup>	0.961
2002	96 (38-469)	Y=-0.026x+54.3	0.663	Y=-0.019x+54.6	0.664	Y=54.6e <sup>-0.0004x</sup>	0.674
2003	254 (160-1249)	Y=-0.037x+54.8	0.727	Y=-0.021x+54.5	0.905	Y=56.8e <sup>-0.0006x</sup>	0.915
1999-2003	144 (31-1894)	Y=-0.039x+54.6	0.820	Y=-0.020x+53.4	0.889	Y=54.5e <sup>-0.0005x</sup>	0.921

Table 2.4: Regression equations for the salinity intrusion position versus discharge. Relationships were determined based on hydrologic floods on the Cape Fear River (HFM) and on the Cape Fear River, Black River, and Northeast Cape Fear River (CHFM). Discharge values in the second column reflect mean discharge on the Cape Fear River (gauged at Lock and Dam 1) and total (3 rivers) discharge corresponding to the CHFM for individual years.

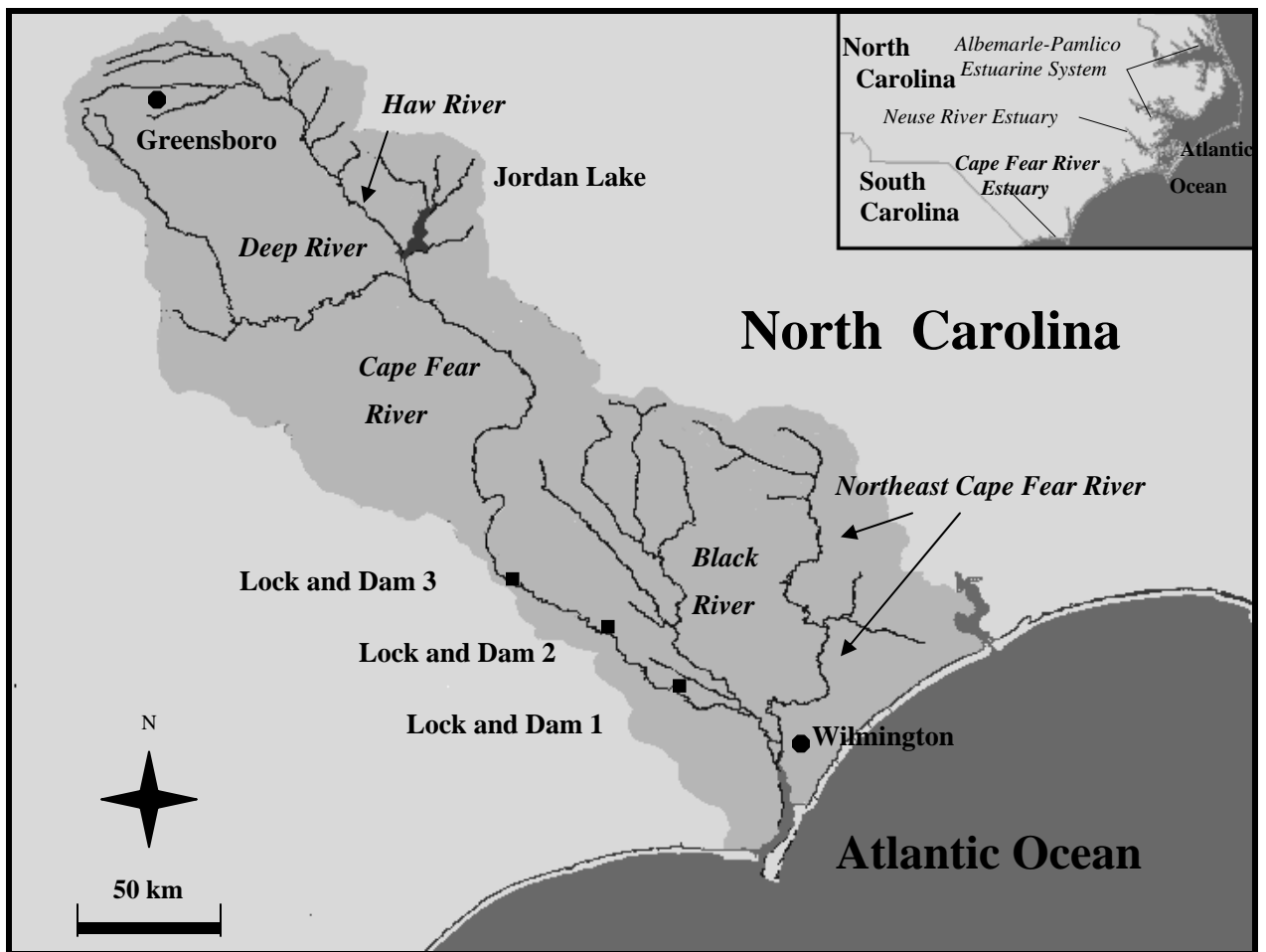


Fig. 2.1. Cape Fear River Watershed

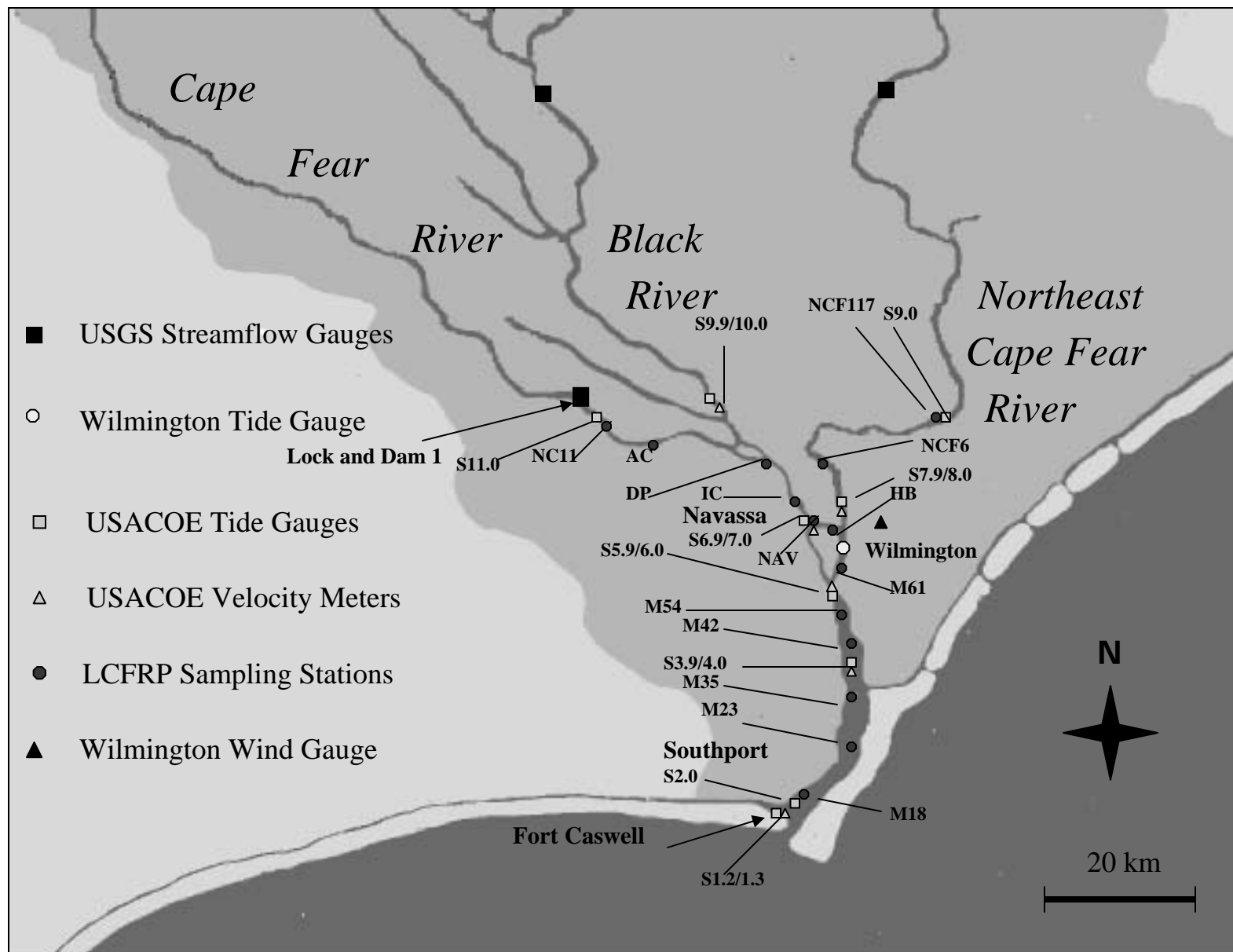
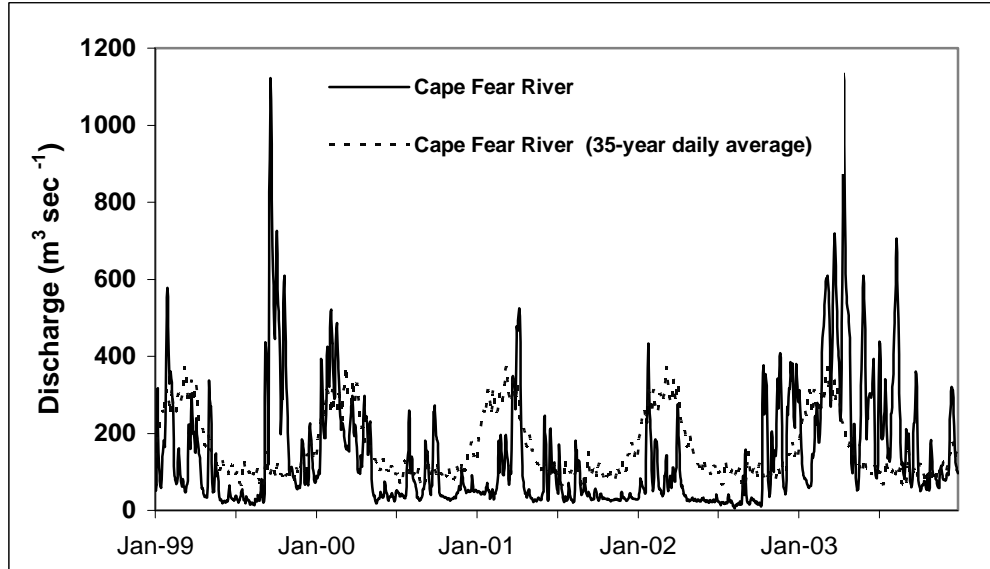


Fig. 2.2. Cape Fear River Estuary (CFRE) study area including locations of observational stations



3a)



3b)

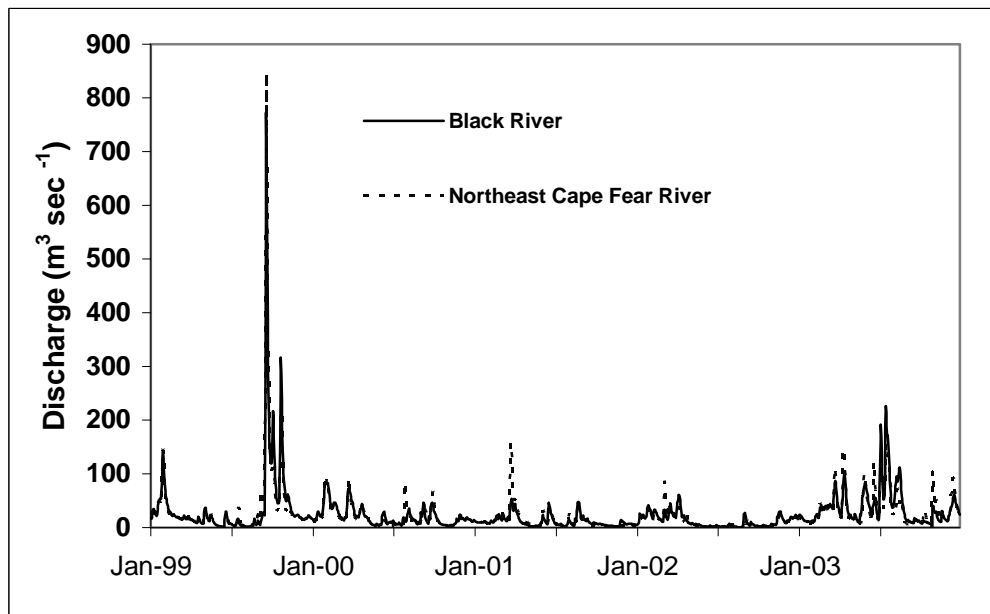
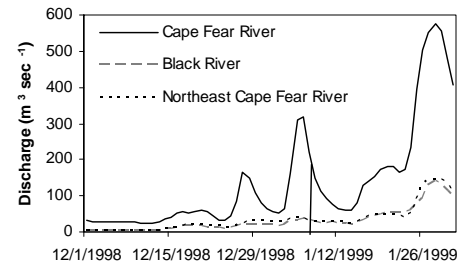
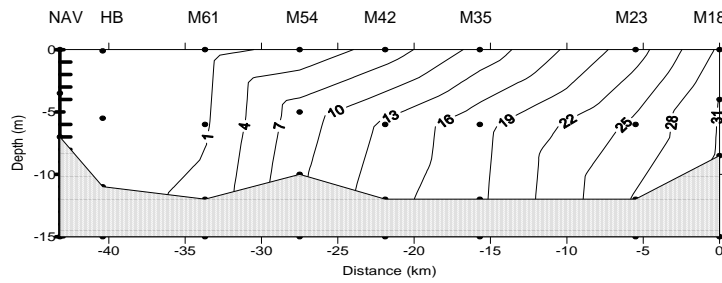


Fig. 2.3. Freshwater input in the CFRE: a) Mean daily discharge (1999-2003) on the Cape Fear River and the 35-year average of mean daily discharge and b) Mean daily discharge (1999-2003) on the Black and Northeast Cape Fear Rivers

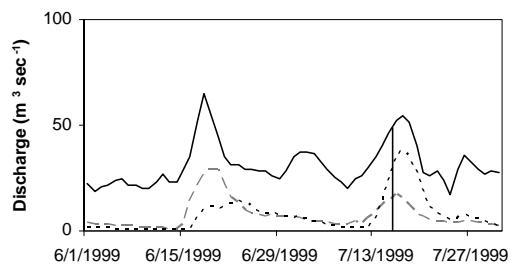
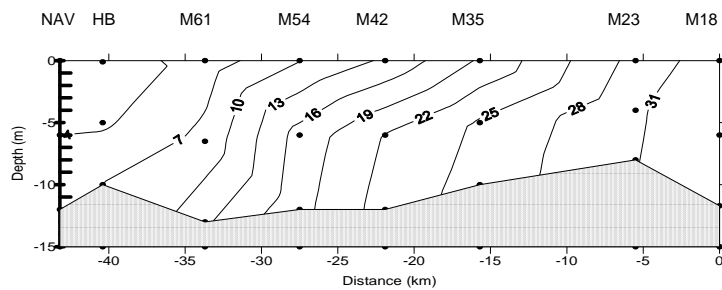
January 7, 1999

Salinity



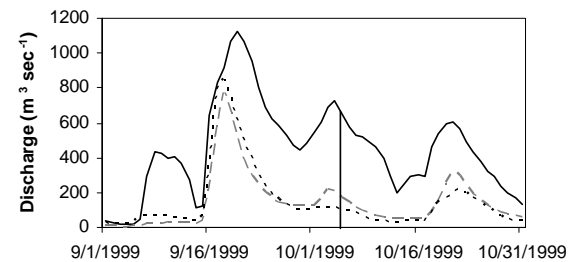
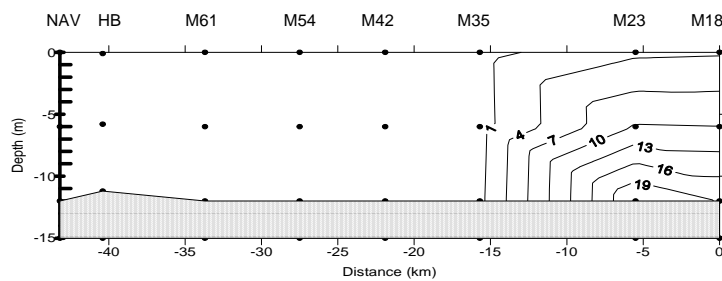
July 15, 1999

Salinity



October 5, 1999

Salinity



October 12, 2000

Salinity

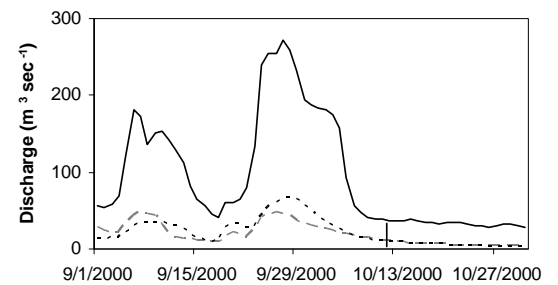
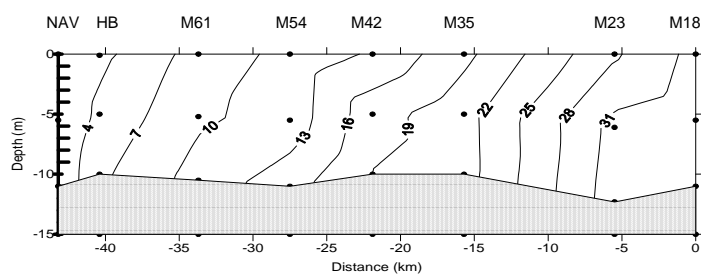


Fig. 2.4 Vertical salinity sections for the CFRE.

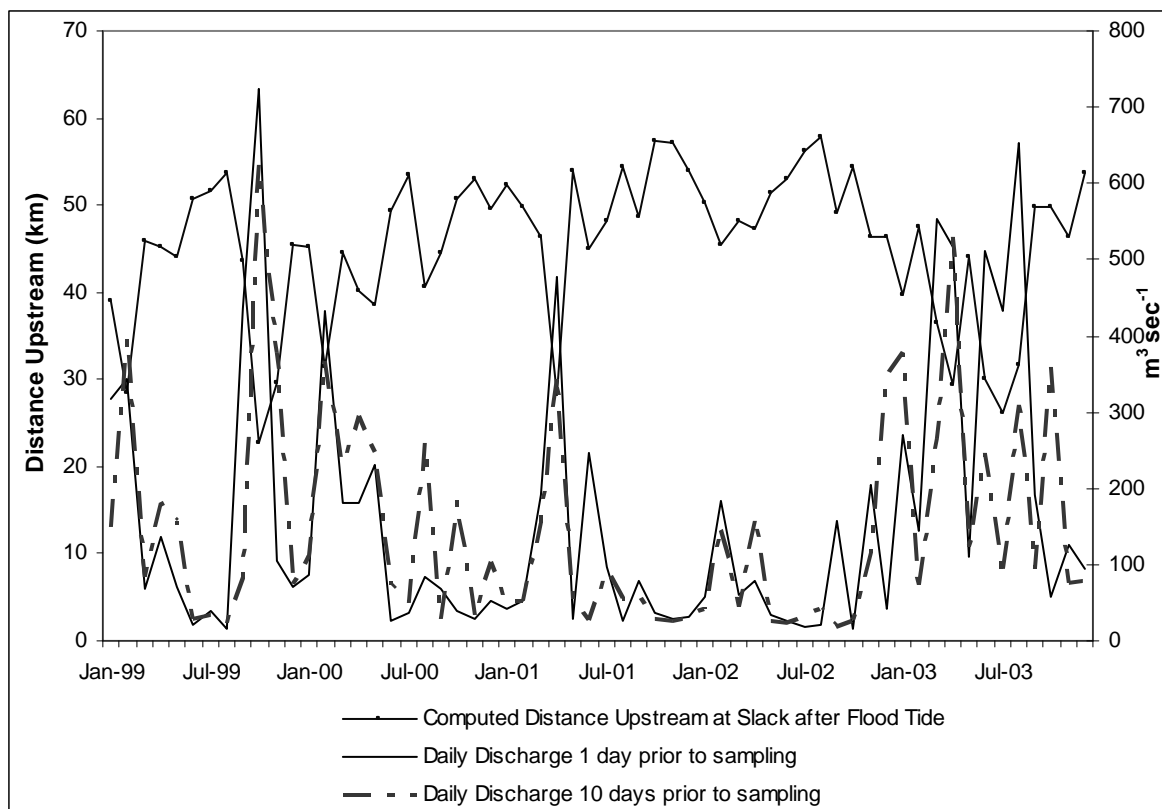


Fig. 2.5. Relationship between the observed salinity intrusion location and mean daily discharge.

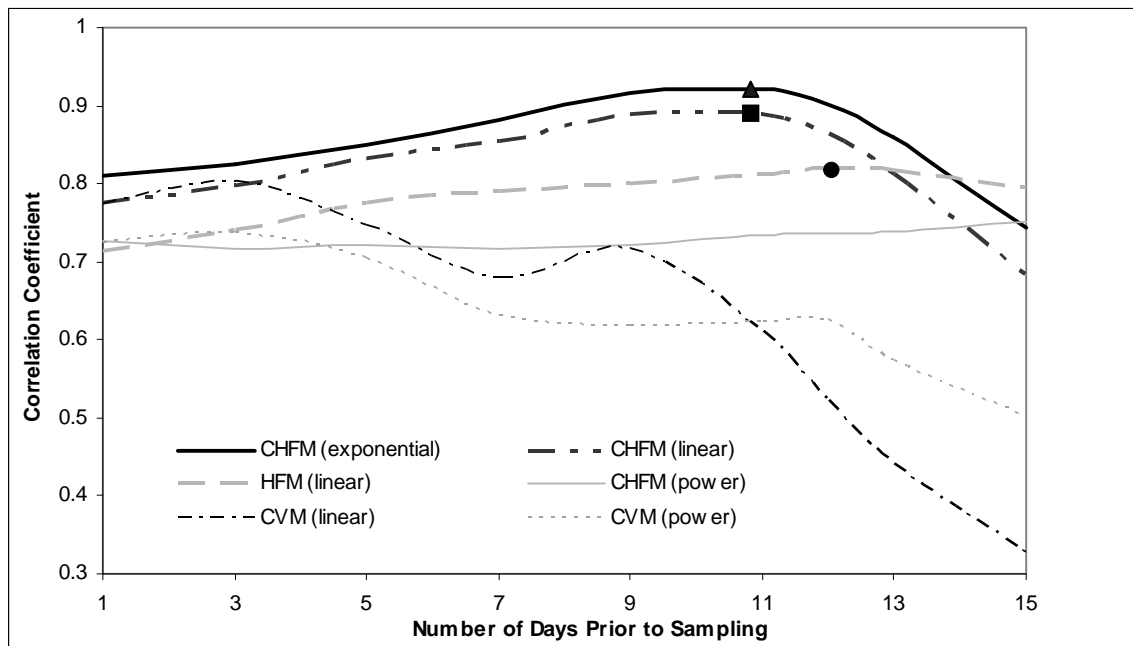


Fig. 2.6. Correlation coefficients for iterations of the Complete Hydrologic Flood Method (CHFM), the Hydrologic Flood Method (HFM), and Complete Value Method (CVM).

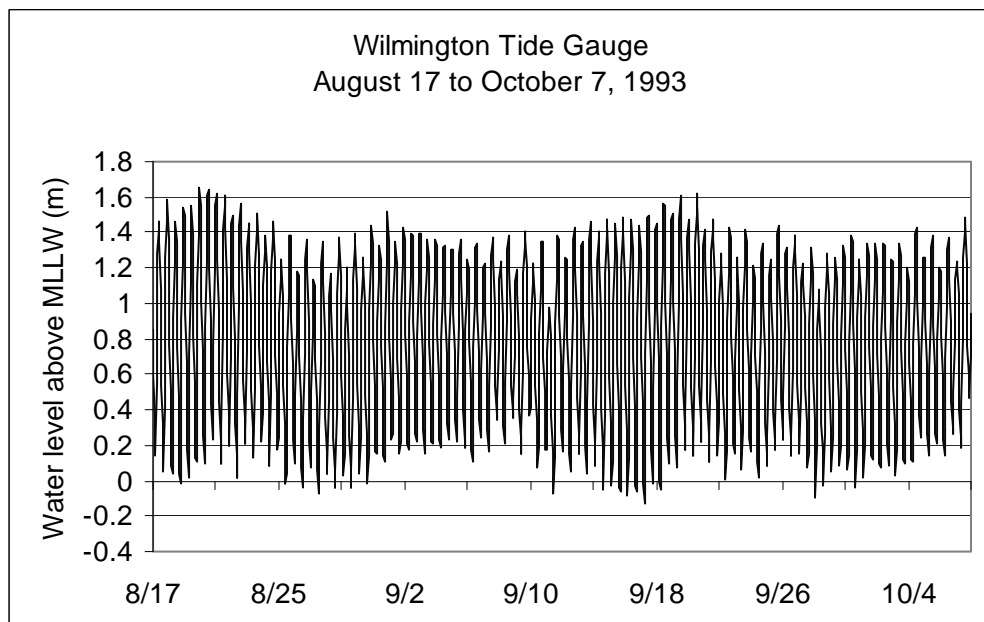


Fig. 2.7. Water-level record at Wilmington Tide Gauge.

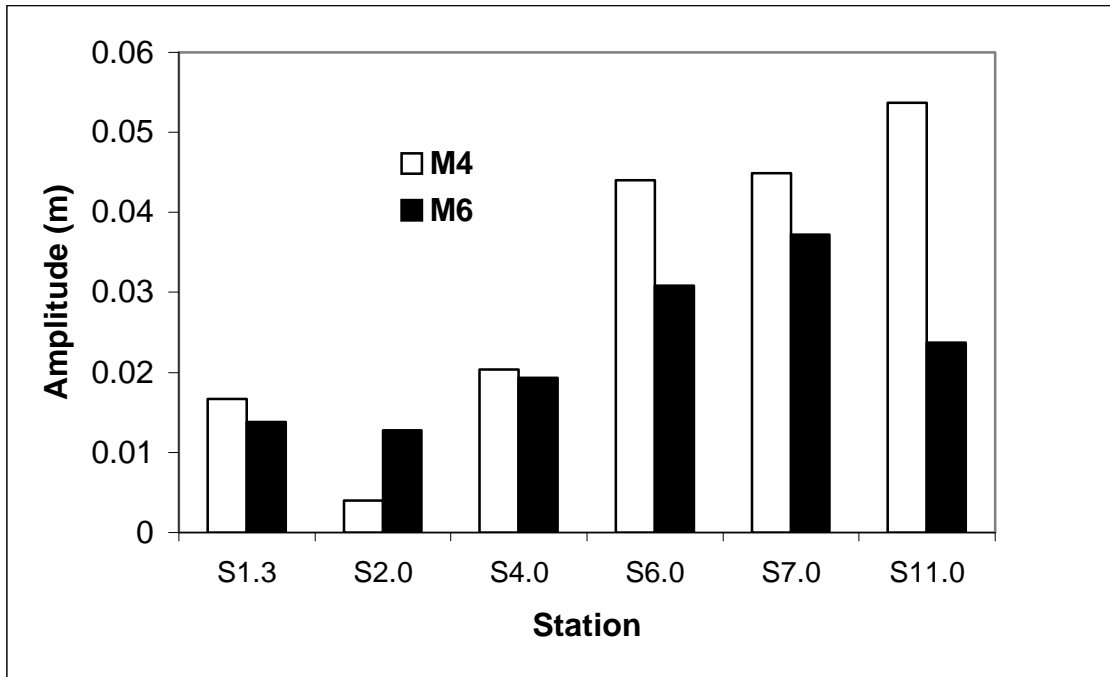
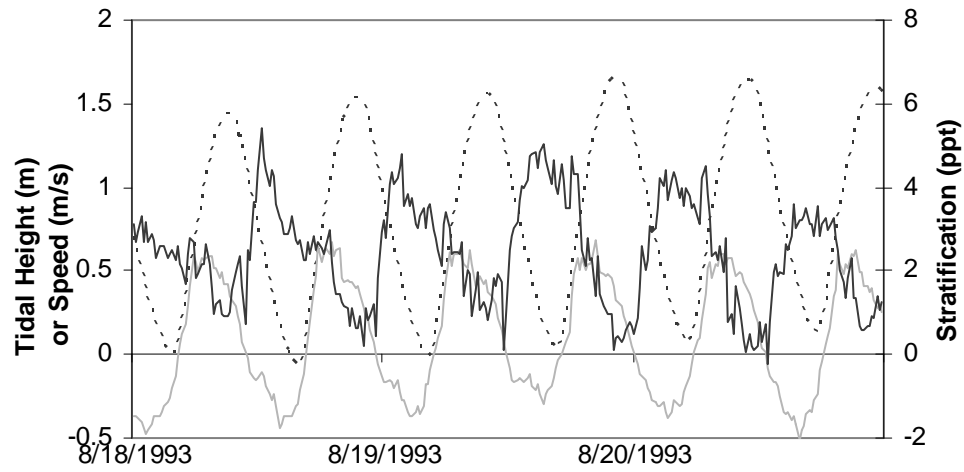


Fig. 2.8. Growth of the  $M_4$  and  $M_6$  tidal constituents.

a)



b)

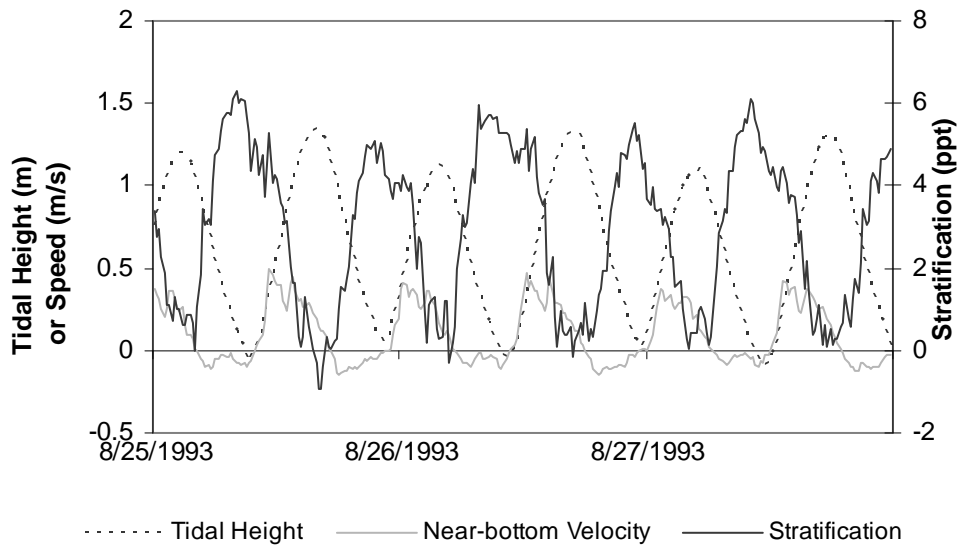
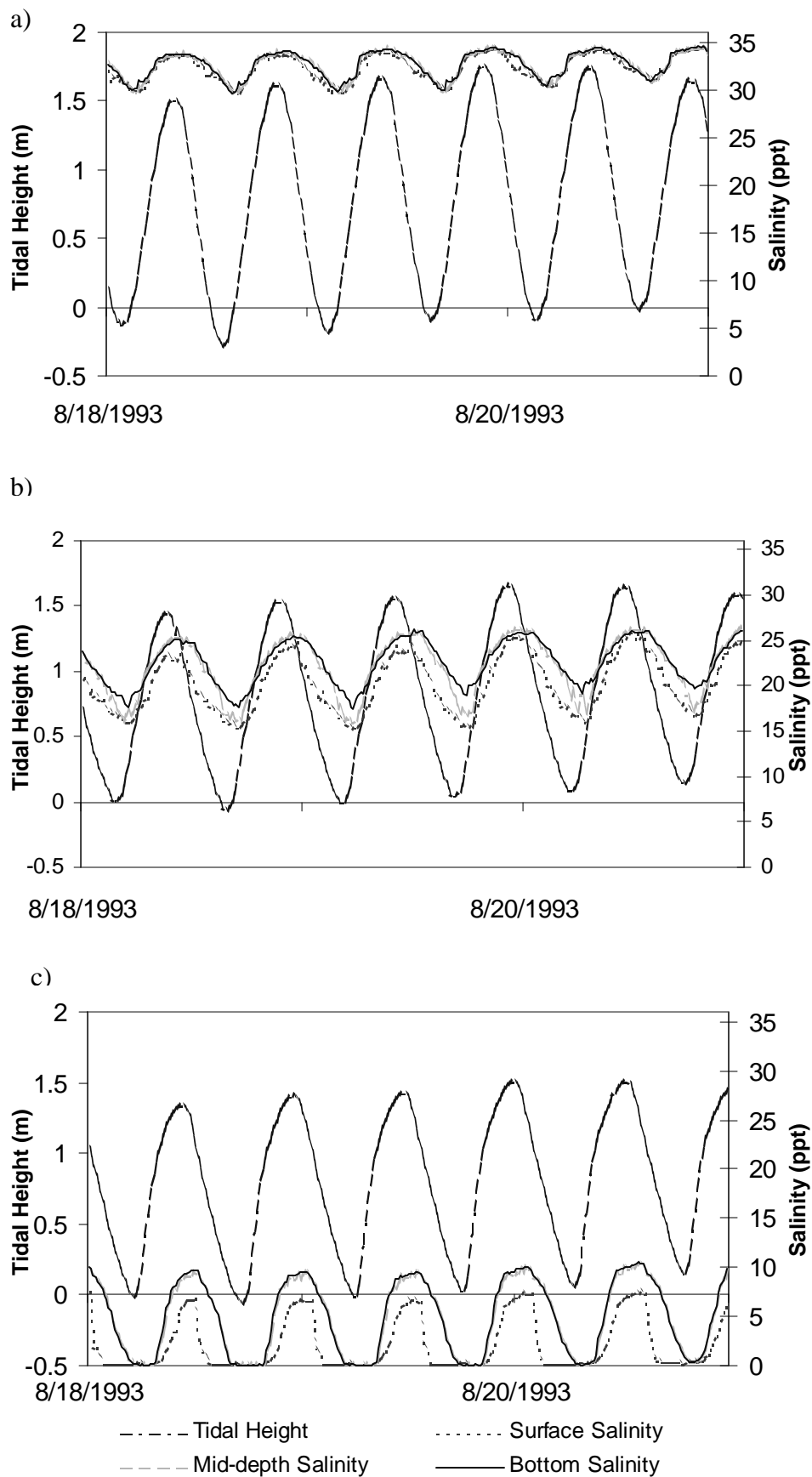


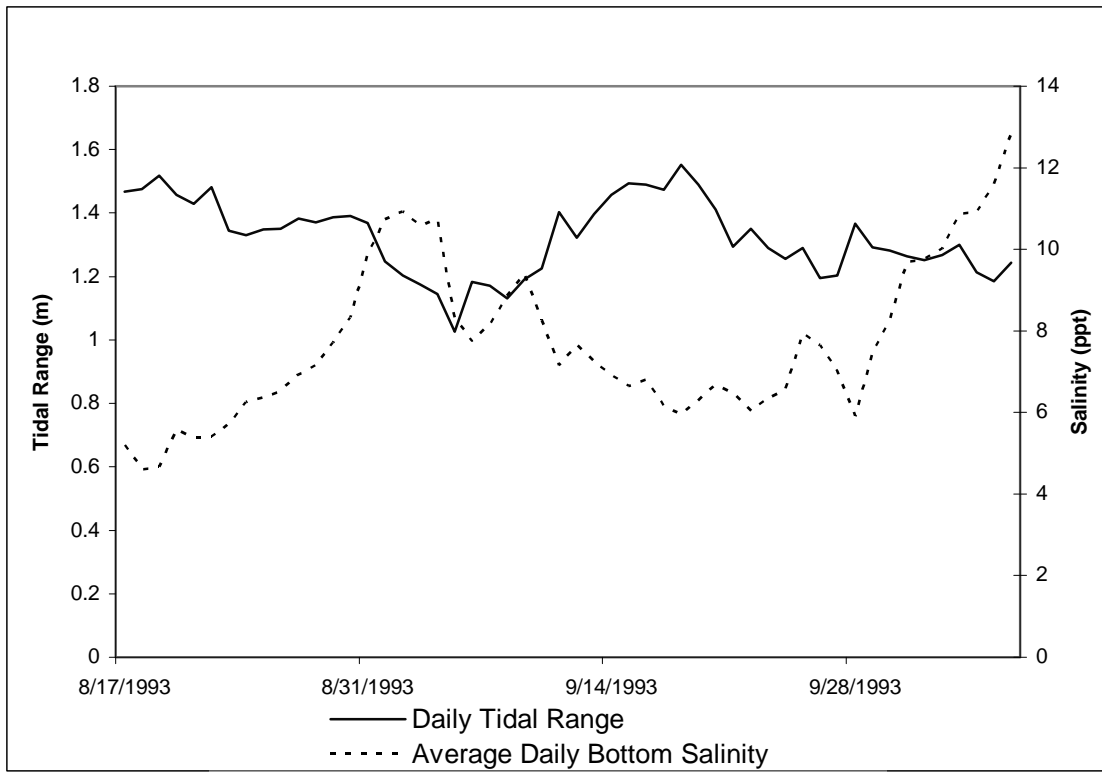
Fig. 2.9. Relationship between tidal height, near-bottom speed, and stratification at mid-estuary (S3.9 and S4.0) during a) spring tide and b) neap tide.



2.10. Tidal heights and near- surface, mid-depth, and bottom salinities for a) lower, b) middle, and c) upper estuary during a spring tidal cycle.



a)



b)

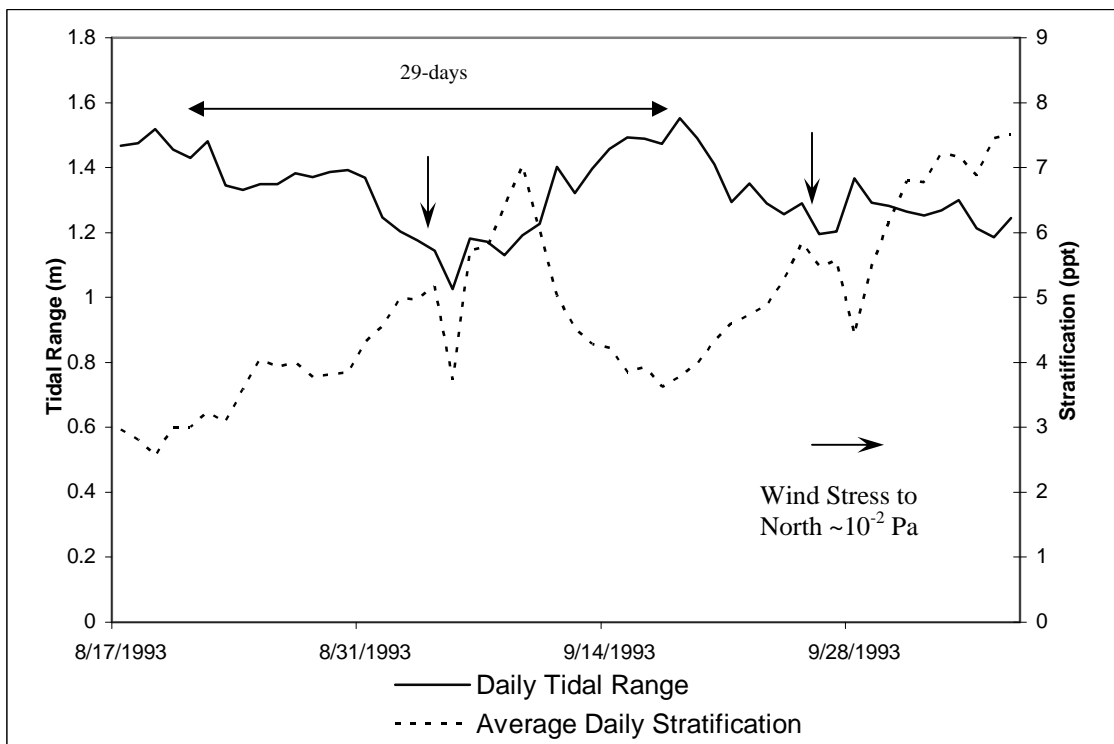
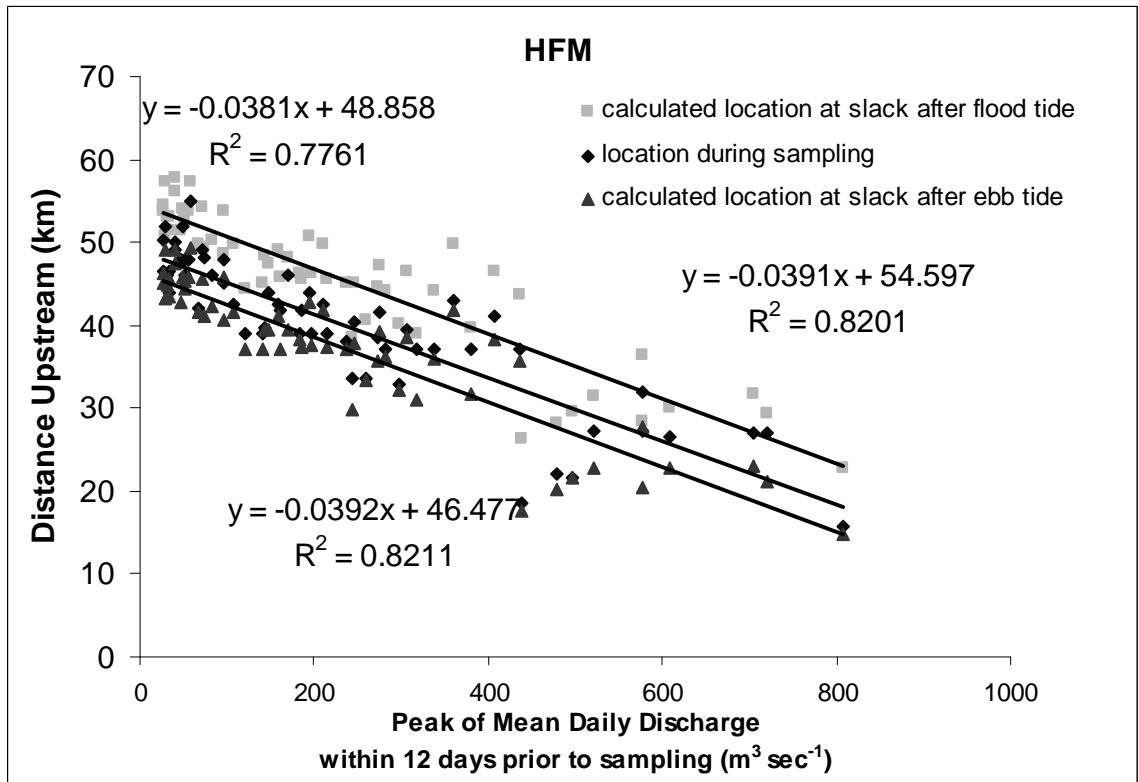
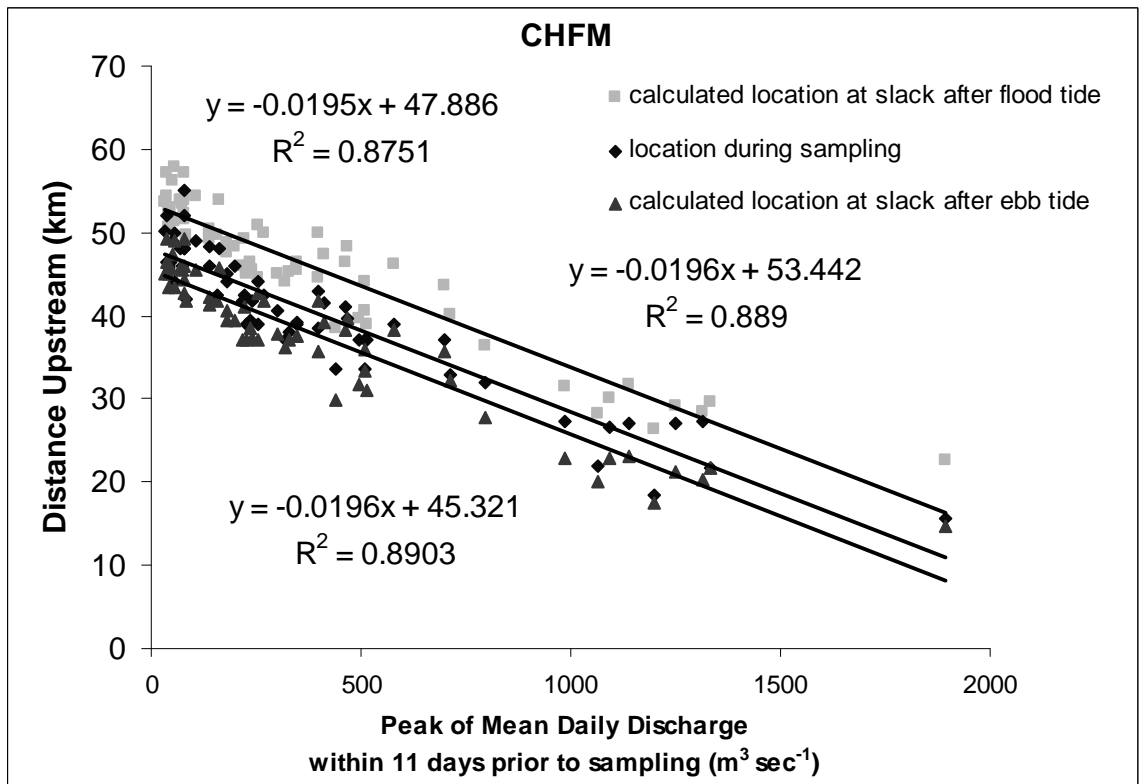


Fig. 2.11. Relationship between a) tidal range and bottom salinity and b) tidal range and stratification for a well-stratified section of the upper estuary (S6.9 and S7.0)

12a)



12b)



12c)

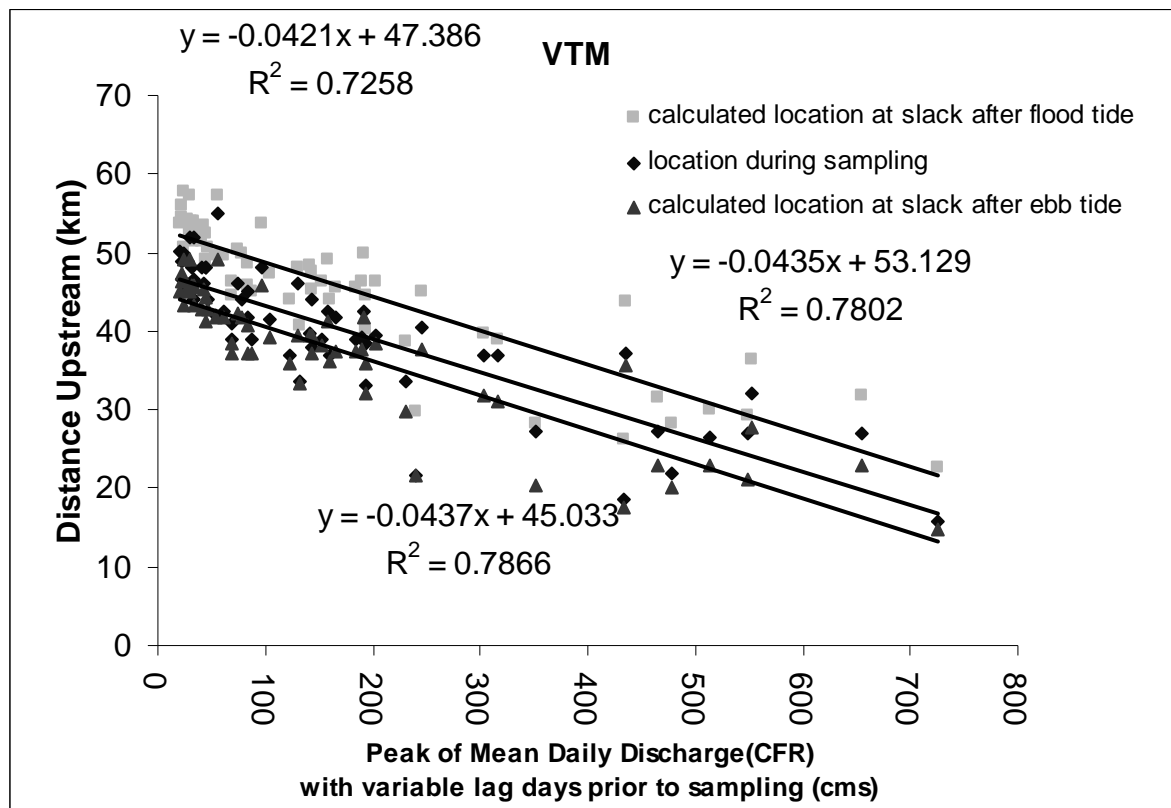
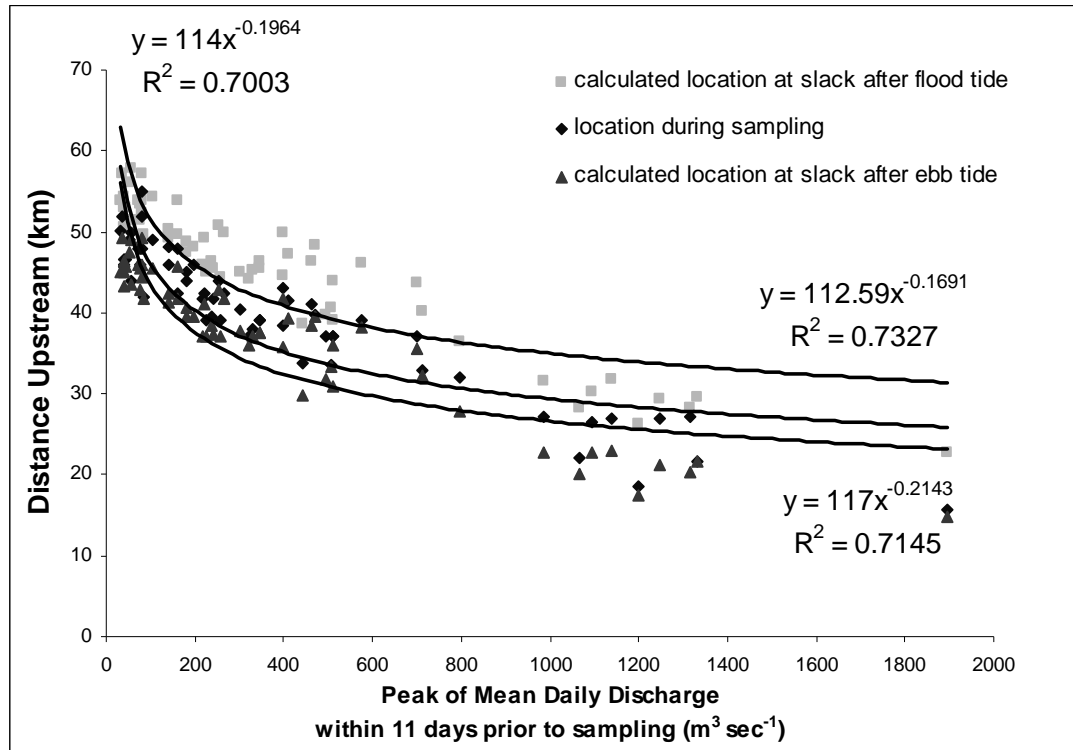


Fig. 2.12. Linear regression analysis for 1999 to 2000 based on the a) Hydrologic Flood Method (HFM), b) Complete Hydrologic Flood Method (CHFM) and c) Variable Travel-time Method (VTM).

13a)



13b)

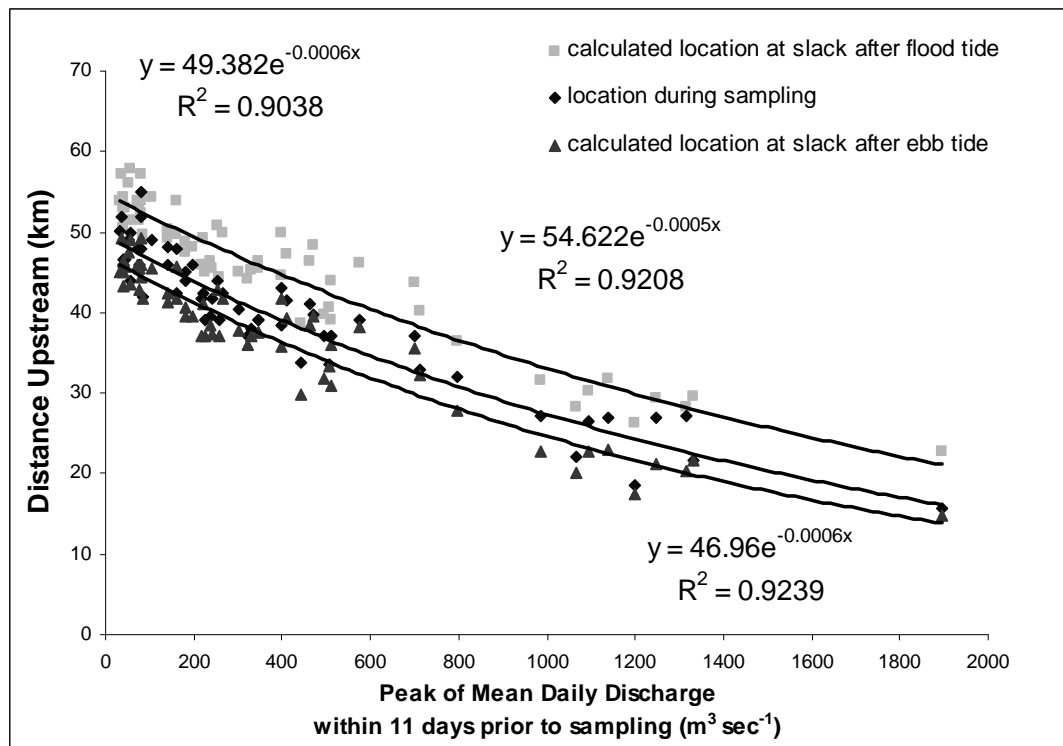


Fig. 2.13. Comparison of a) power-law and b) exponential regression analysis for CHFM.

## CHAPTER 3

### TIDAL INFLUENCES ON CIRCULATION AND SALINITY STRUCTURE IN THE CAPE FEAR RIVER ESTUARY

#### **Abstract**

In partially mixed estuaries, temporal changes in mixing, stratification, and residual circulation can significantly influence transport characteristics. In this study, we investigate tidal influences on circulation and the salinity structure of the Cape Fear River Estuary (CFRE), NC, a partially mixed estuary along the southeast coast of the United States. Through analysis of field data collected during two different tidal conditions (high tidal range versus low) when river inflow was low, we discuss observed differences in circulation and the structure by comparing differences in shear characteristics, gradient and horizontal Richardson numbers, calculated turbulent salt fluxes, and coefficients of vertical eddy diffusivity ( $K_z$ ) based on theoretical parameterizations and salt budget analysis. During each sampling period salinity and velocity data were collected over a semi-diurnal tidal cycle in a 2.8 km long transect along the estuary axis; water level was recorded in the vicinity of the transect near the middle section of the estuary.

Analyses indicate the CFRE estuary exhibits characteristics of a classic two-layer estuarine system in which density driven-circulation enhances inflow near the bottom while fresher, less dense water flows out near the surface and that the horizontal and vertical salinity structures are noticeably impacted by tidal-range differences and intra-tidal (flood-ebb) variations. That is, 1) during the low tidal-range conditions, near-surface to near-bottom

stratification persisted throughout the flood-ebb cycle, a well-defined pycnocline existed, and near-bottom salinities were relatively high, and 2) during high tidal-range conditions, stratification and the strength of the pycnocline were influenced by ebb-flood variability, and near-bottom salinities were reduced.

Findings indicate the vertical and horizontal salt transport characteristics are critically linked to differences in turbulent mixing characteristics and to the ability of stratification within the water column to be maintained, i.e. the absence or presence of a well-defined pycnocline. Specifically, 1) theoretical  $K_z$  values calculated based on chosen values of  $C_d$  (= 0.001-0.003) are in reasonably close agreement with values computed from the salt budget analysis 2) during the low tidal range flood tide,  $K_z$  values remained relatively low except near maximum flood tide below the pycnocline, whereas during the higher tidal range period, higher values of  $K_z$  extended into the upper water column, 3) during the higher tidal range ebb tide, turbulent mixing of fresh and salty water and relatively weak stratification contributed to lower observed near-bottom salinities. The analysis suggests variability in turbulent mixing characteristics on intra-tidal and tidal range timescales is responsible for the observed differences in salinity characteristics.

## **Introduction**

Physical mechanisms that determine transport of constituents can strongly influence the water quality and ecologic health of an estuarine system. Temporal and spatial changes in mixing, stratification, and residual circulation can impact the spatial distribution of dissolved oxygen, pollutants, and nutrients. In a partially mixed estuary, periodic fluctuations associated with tidal currents can contribute to variations in turbulence and consequent

changes in the stability of the water column. Asymmetries associated with tidal straining, for example, in which less dense water closer to the surface moves faster than denser water below, can result in increased stratification (and greater stability) during the ebb tide and the reverse effect during the flood. Evidence of the significance of such intra-tidal differences on circulation and mixing is relatively well-documented including findings in areas such as the Liverpool Bay region of the Irish Sea, Northern San Francisco Bay, and the Hudson River Estuary (Simpson et al., 1990; Monismith et al., 1996; Nepf and Geyer, 1996). Additional research observations have provided evidence that mixing and circulation are closely linked to periodic fluctuations in the strength of turbulence, as residual circulation may increase during periods when mixing is weaker (e.g during slack or neap tide) (Jay and Smith, 1990; Rippeth et al., 2001; Stacey et al., 2001; Stacey and Ralston, 2005). At the same time, freshwater inflow can further impact the density distribution of an estuary, including the horizontal salinity gradient (a basis for determining density-driven circulation), the boundary between fresh and salt water (salinity intrusion) that determines the spatial extent of estuarine habitat, and the degree to which buoyancy inputs can act to inhibit turbulence.

In partially mixed estuaries the strength of river inflow and tidal currents can significantly influence hydrodynamic characteristics depending on the time period of observation. In this paper, we examine tidal-cycle variations in salinity and circulation in the Cape Fear River Estuary (CFRE), NC, a partially mixed estuary along the southeast coast of the United States (Fig. 3.1). The focus of our research is on intra-tidal (flood vs. ebb) and tidal-range differences found to be two of the dominant periodic timescales that impact circulation (Becker, et al., in review). Using data collected during a field experiment designed to capture hydrodynamic and salinity variations for two different tidal-range

periods (i.e. conditions representing low versus higher ranges during periods when river inflow is low and relatively constant), we discuss observed differences in mixing, stratification, circulation, and transport characteristics and mechanisms that may affect these differences.

## **Background**

### *Study Area and Hydrodynamic Environment*

The CFRE (Fig. 3.1) is a funnel-shaped, partially mixed to well mixed (near the mouth) estuary in which river inflow and tidal currents can strongly influence hydrodynamic conditions (Becker et al., in review; Welch and Parker, 1979). The estuary is approximately 1800 m wide at the mouth and narrows to a width of about 180 m near Wilmington. A navigation channel is maintained from close to the mouth of the estuary near the Atlantic Ocean to near Navassa, a distance of approximately 50 km. Depths in the main channel are maintained to a minimum depth of 11.6 m and width of approximately 150 m (McAdory, 2000). Outside of the main channel, tidal marshes occupy parts of the estuary, while shoals and spoil areas typically reach depths of ~ 0.3 to ~ 5 meters.

The Cape Fear River accounts for approximately 60% of freshwater inflow into the CFRE. Flow from two smaller coastal plain rivers, the Northeast Cape Fear River and the Black River, also contribute to the amount of freshwater entering the estuary, particularly during moderate to high flow conditions. River flow from the Cape Fear River is highly variable with low-flow discharge ( $<100 \text{ m}^3 \text{ sec}^{-1}$ ) generally characteristic of summer conditions and greater freshwater inflow ( $\sim 300\text{-}600 \text{ m}^3 \text{ s}^{-1}$ ) more typical of spring and winter



conditions. Very high discharge events of greater than  $1100 \text{ m}^3 \text{ s}^{-1}$  have been observed with a recurrence interval of about 4 years based on a 32-year peak flow record.

Previous analyses of observational data suggest that the circulation and salinity distribution in the CFRE may be significantly impacted by intra-tidal variations associated with tidal straining, tidal-range differences associated with a 29-day periodicity, and sub-tidal changes in freshwater input which determine the extent of the salinity intrusion into the estuary. The salinity intrusion (defined as the location of the 1-psu salinity contour) was found to migrate up to 30 km between very low and very high flow conditions (Becker et al., in review).

In the present study we focus on the intra-tidal influence on salinity structure and circulation during conditions of low freshwater inflow ( $< 75 \text{ m}^3 \text{ sec}^{-1}$ ) when the salinity intrusion is expected to be in its base-flow (low-flow) position. First we describe a field study used to obtain data needed to characterize the velocity and salinity structure (e.g. changes in stratification with time) during low and higher tidal-range sampling periods. Next, we provide a synopsis of the velocity and salinity structure and observed differences between the two sampling periods. We follow with a discussion of mechanisms that may contribute to these changes through examination of variability in shear, dimensionless ratios (gradient and horizontal Richardson numbers), computed turbulent salt fluxes, and turbulent mixing coefficients based on theoretical (Munk and Anderson, 1948) formulations and salt budget analysis. Finally, we provide a descriptive discussion of the influence of stratification on the vertical and horizontal salinity structures.

*Related Research: Parameterization of Mixing, Stratification, and Circulation*

The relationship between stratification and circulation in estuaries has been a focus of both historical and recent research. Understanding the critical relationship between turbulent mixing and stratification is a key component to accurately depicting the strength of estuarine circulation and the associated transport. Classical models for prismatic (rectangular) channels (e.g. Hansen and Rattray, 1965) were based on tidally averaged conditions and led to stratification-circulation diagrams that depict the relationship between estuarine circulation and the vertical salinity structure. Based on velocity and salinity measurements, estuaries could be classified into different types including, for example, diffusion-dominated (analogous to well-mixed) estuaries with little or no up-estuary bottom flow on one end of the spectrum to more strongly stratified (analogous to salt wedge) estuaries in which gravitational circulation becomes significant and the system more closely resembles a two-layer representation. Further advances in estuarine research have led to extensions of the theory to include the influence of variations in bathymetry, tidal amplitude, or bed friction (Oey, 1984; Prandle, 1985) as well as to comparisons of alternate classification schemes (Fischer, 1972).

The classification methods described above rely on parameterization of tidally averaged conditions and do not take into account vertical variations in mixing and stratification that may influence circulation (Stacey et al., 2001; Hetland and Geyer, 2004). More recent research in stratification-circulation relationships, consequently, has addressed the effects of changes in mixing and stratification throughout the water column including variability on tidal and spring-neap timescales. Intra-tidal variations (e.g. changes in the strength of stratification due to tidal straining or asymmetry in shear generated during the

flood or ebb tide) have been found to be important factors in characterizing circulation (Simpson, et al., 1990; Jay, 1991; Nepf and Geyer, 1996; Monismith et al., 1996).

Observations and lab experiments provide evidence that circulation is closely linked to periodic fluctuations in the strength of turbulence, as residual circulation may increase during periods when mixing is weaker (Stacey et al., 2001; Linden and Simpson, 1988; Stacey and Ralston, 2005). As a result, researchers have focused on incorporating the effects of vertical density stratification on mixing including the use of dimensionless numbers (e.g. horizontal Richardson number) that describe the relative strength of stabilizing effects of buoyancy inputs to destabilizing influences of mixing (Monismith et al., 1996; Stacey et al., 2001; Simpson et al., 2005).

The horizontal Richardson number ( $Ri_x$ ) derivation is based on the assumption that changes in stratification are influenced by a balance between advection and mixing (Stacey et al, 2001; Stacey and Ralston, 2005). The horizontal Richardson number ( $Ri_x$ ) may be defined as:

$$Ri_x = \frac{N_x^2 H^2}{u_*^2} \quad (1)$$

where  $N_x^2 = \frac{-g}{\rho_0} \frac{\partial \rho}{\partial x}$ ,  $g$  = gravitational acceleration,  $\rho$  = density,  $\rho_0$  = constant reference density,  $x$  = along-channel distance,  $H$  = depth of the water column and  $u_*$  = friction velocity.

The dimensionless number,  $Ri_x$ , represents a ratio of stratifying effects of horizontal advection to destratifying frictional influences. For values greater than the critical value (of order 1), stratification would be expected to exist. For values less than approximately 1, tidal mixing would be strong enough to break down stratification, and a well mixed water column would be anticipated (Stacey et al., 2001).

The friction velocity ( $u_*$ ), representative of turbulent fluctuations in velocity, may be represented by a quadratic friction law:

$$u_*^2 = C_d U^2 \quad (2)$$

(Nepf and Geyer, 1996; Dyer, 1997; Stacey and Ralston, 2005) where  $U$  = average along-channel velocity in the bottom boundary layer and  $C_d$  = drag coefficient. Research indicates that for tidal velocities that are relatively large (e.g.  $\sim 0.50 \text{ m s}^{-1}$ ), the above parameterization of  $u_*$  agrees closely with observations and that its accuracy increases at greater velocities (Stacey and Ralston, 2005).

The gradient Richardson number ( $Ri_g$ ) may be defined as:

$$Ri_g = \frac{N^2}{(\partial u / \partial z)^2} \quad (3)$$

where  $N^2 = \frac{-g}{\rho_0} \frac{\partial \rho}{\partial z}$  = (vertical buoyancy frequency)<sup>2</sup>,  $g$  = gravitational acceleration,  $\rho$  = density,  $\rho_0$  = constant reference density,  $u$  = along channel velocity, and  $z$  = depth.

This dimensionless quantity reflects the strength of stabilizing influences of stratification relative to destabilizing effects of vertical velocity shear. Positive gradient Richardson numbers indicate stability in stratification, whereas negative values for  $Ri_g$  indicate an unstable density structure exists. For uniform flow, a gradient Richardson number equal to 0.25 generally marks the transition from laminar to turbulent conditions and may be regarded as a threshold value for mixing (Dyer, 1997; Miles, 1961).

Simpson et al. (2005) observed that turbulent production is linked to this critical  $Ri_g$ ; that is, significant production and increased mixing coefficients were found to occur during

periods when the  $Ri_g$  was low (or below the critical value). Nepf and Geyer (1996) defined a higher threshold value ( $Ri_g < 0.40$ ) to indicate areas of expected mixing (based on observations of Richardson numbers in the mixed layer, i.e. below the depth of maximum velocity during the flood tide). Stacey and Ralston (2005) found asymmetry in the structure of turbulence during flood versus ebb tides. During the ebb tide  $Ri_g$  approached 0.25 near the top of the boundary layer. During the flood tide, values within the boundary layer varied (including negative values and values greater than 25) whereas at or above the boundary layer (where shear was small) values were generally relatively large (greater than or equal to 2.5).

### **Methods: Experimental Design**

In order to characterize the salinity and velocity structure in the central CFRE during low versus higher tidal-range conditions, a field study was conducted in the summer of 2005, and it included the collection of tidal height, velocity, and salinity data. Velocity and salinity data were collected throughout the tidal cycle on July 12, 2005 and July 26, 2005, representing low and higher tidal ranges, respectively, using a vessel-mounted ADCP (for velocities) and CTD sampling instruments (for salinities).

#### *Setting and Physical Conditions*

The field-study area consisted of an approximately 2.8 km along-channel section near mid-estuary (Fig. 3.1). The section coincides with a location approximately mid-way between the estuarine mouth and the salinity intrusion position for low to average river-inflow conditions (Becker et al., in review).

The hydrograph of mean daily discharge from June 29 to August 7 is given in Fig. 3.2. Peaks in river discharge within a 12-day window prior to sampling, (Becker et al., in review) reach only  $73 \text{ m}^3 \text{ sec}^{-1}$  prior to the July 12 sampling day and  $67 \text{ m}^3 \text{ sec}^{-1}$  prior to the July 26 date, consistent with low-flow conditions in each case.

Winds during the two sampling dates were generally light. Winds during the July 12 sampling period (~ 8 a.m. to 10 p.m.), based on hourly measurements at Wilmington, were generally from the south or southwest with an average wind speed of  $2.9 \text{ m s}^{-1}$  and recorded wind speeds not exceeding  $6.2 \text{ m s}^{-1}$ . On July 26, the wind direction was generally from the north or northwest during the daytime sampling (~ 8 a.m. to 6 p.m.) and generally calm or variable in the evening. The average recorded wind speed was  $2.1 \text{ m s}^{-1}$  with recorded speeds not exceeding  $3.6 \text{ m s}^{-1}$ .

#### *Data Collection: Water Level, Velocity, and Salinity Measurements*

A water-level gauge was installed at a location near mid-estuary (S4.0, Fig. 3.1). Water-level values were recorded every 30-minutes from June 29 through August 7. Velocities were measured using a vessel-mounted, 1200 kHz Acoustic Doppler Current Profiler (R.D. Instruments Workhorse ADCP) from the vicinity of Channel Marker 42 to the vicinity of Channel Marker 46 (along-channel, downstream-to-upstream transects spanning a distance of approximately 2.8 km). Velocities were measured from near-surface to near-bottom in 1-m increments. Values were recorded every 3 seconds and later averaged to represent 5-min. intervals. Sampling continued throughout the tidal cycle each day in order to obtain data representing flood, ebb, and slack tides.

Salinities in the main channel were measured throughout the water column at Markers 42, 44, and 46 (Fig. 3.1). The salinity data were collected by lowering recording instruments (Hydrolab and YSI CTD's) from near-surface to near-bottom in 1-m increments from sampling vessels. One vessel was generally stationed at M44 throughout each measurement period (with the exception of after-sunset/evening sampling). Measurements at other stations were conducted in conjunction with velocity measurements. Salinity sampling was conducted in collaboration with the NC State Division of Water Quality Intensive Survey Unit.

The spatial resolution of the data-collection study (i.e. salinity sampling at locations ~ 700 to ~1400 meters apart over the total range of ~ 2.8 km) was designed to provide a reasonable representation of the along-channel salinity field while being able to complete a transect quickly enough so that each part of the tidal cycle would be well represented. The along-estuary salinity gradient in this part of the CFRE, based on analysis of vertical salinity sections, typically varies from about 0.6 to 1.2  $\text{psu km}^{-1}$  depending on river inflow. Values as low as ~ 0.4  $\text{psu km}^{-1}$  and as high as ~ 1.8  $\text{psu km}^{-1}$  in the middle to lower estuary have been observed (Becker et al., in review).

In order to estimate the appropriate vertical resolution for obtaining salinity data, vertical profiles from a United States Army Corps of Engineers field study (Benson and Parmen, 1995) were reviewed. Analysis of these salinity data suggested vertical salinity gradients in the proposed study area are typically from 0.3 to 0.7  $\text{psu m}^{-1}$ .

## Results

### *Tidal Elevations and Velocity Transects*

Measured tidal elevations at Wilmington and S4.0 during the summer 2005 study period indicate a 29-day modulation of the predominantly semi-diurnal tidal signal (Fig 3.3). Tidal ranges during the two field study periods were approximately 1.0 m on July 12 and 1.4 m on July 26. Sampling began at approximately low tide and ended at velocity slack for each sampling day. Transect- and depth-averaged along-channel velocities and tidal heights at S4.0 are given in Fig. 3.4. The maximum transect-averaged velocities reached  $0.63 \text{ m sec}^{-1}$  during the flood tide and  $0.62 \text{ m sec}^{-1}$  during the ebb tide on July 12 and  $0.86 \text{ m sec}^{-1}$  during the flood tide and  $0.78 \text{ m sec}^{-1}$  during the ebb tide on July 26.

Transect-averaged vertical profiles of along-channel velocities are shown in Fig. 3.5. Tidally averaged velocities are given in Fig. 3.6. “Tidal velocities,” defined as along-channel velocities minus tidally averaged velocities, are given in Fig. 3.7.

A total of thirteen velocity transects (numbered “0” to “12”, Fig. 3.5) were measured on July 12, and a total of nineteen transects (numbered “0” to “18”) were recorded on July 26. Time represents the number of hours into sampling (where  $t = 0$  represents the sampling time at the midpoint of Transect 0).

The first transect (Transect 0) on each sampling day (Fig. 3.5) represented a period close to low tidal elevation when the tide was still ebbing. Transect 1 on each day illustrates the development of the flood tide near the bottom of the water column. Transect 4 profiles show the velocity structure near maximum flood tide conditions, during which the velocity maximum occurs at approximately 4 m below the surface on each sampling day. Transect 8 on July 12 and Transect 11 on July 26 show the beginning of the ebb tide with stronger



velocities apparent near the top of the water column. Final transects of each day, Transects 12 (July 12) and 18 (July 26), display the velocity profiles near slack tide, a time when the velocity structure resembles that of a two-layer system in which outflow occurs near the surface and inflow is observed near the bottom. Tidally averaged velocity profiles (Fig. 3.6) reveal a similar structure for both July 12 and July 26, when residual velocities reach  $\sim -0.2 \text{ m sec}^{-1}$  about 2 m below the surface and  $\sim 0.1 \text{ m sec}^{-1}$  near the bottom. Depth-averaged residual velocities, measured from  $\sim 2 \text{ m}$  below the surface to near bottom, were  $-0.05 \text{ m sec}^{-1}$  on July 12 and  $-0.02 \text{ m sec}^{-1}$  on July 26. These depth-averaged outflows approximately correspond to the expected freshwater velocities of approximately  $-0.02 \text{ m sec}^{-1}$  during low-flow conditions (based on discharge divided by the estuarine cross sectional area in the transect vicinity).

#### *Salinity and Density Distributions*

The density structure during each study period was primarily influenced by salinity, as water temperatures were relatively constant (typically less than 1 degree C variation). Densities at M44 on each sampling day ranged from  $\sim 1007 \text{ kg m}^{-3}$  to  $\sim 1015 \text{ kg m}^{-3}$ .

Salinity stratification, measured as the near-surface to near-bottom salinity difference at M44, and tidal height are shown in Fig. 3.8. In each case, minimum stratification occurred near slack after flood tide. During low tidal-range conditions, stratification ranged from about 7 psu to 9 psu and showed relatively little variability with ebb and flood cycles. During the higher tidal-range period, in contrast, stratification ranged from less than 5 psu to about 10 psu, with increases generally observed during the ebb tide and decreases during the flood. Similar patterns were observed at M42 and M46.

Depth-averaged buoyancy frequencies, defined by  $N$  (Eq. 3), and depth-averaged, transect-averaged, along-channel velocities are shown in Fig. 3.9. During low tidal-range conditions, buoyancy frequencies remain at a relatively constant value of  $\sim 0.07\text{-}0.08 \text{ s}^{-1}$  (with the exception of a dip in values to  $\sim 0.06 \text{ s}^{-1}$  between  $\sim 11:30$  am and  $1:30$  pm, when observed wind stress toward the north reached a maximum of  $\sim 3.4 \times 10^{-2} \text{ Pa}$  at  $12:53$  pm). During higher tidal-range conditions, the buoyancy frequencies ranged from about  $0.05 \text{ s}^{-1}$  to  $0.08 \text{ s}^{-1}$ , with lower values generally occurring during the flood tide.

Salinity profiles at M44 and vertical salinity sections from M42 to M46 for different parts of the tidal cycle are shown in Figs. 3.10 and 3.11, respectively. On July 12, near-bottom salinity increased from  $\sim 18$  psu near slack tide to  $\sim 21$  psu near the end of the flood tide and then fell during the ebb tide from  $\sim 21$  psu to  $\sim 19$  psu near slack after ebb (Fig. 3.10a). On July 26 (Fig. 3.10b), in contrast, near bottom salinity increased from  $\sim 16$  psu during slack to  $\sim 21$  psu near the end of the flood tide and then fell back to  $\sim 16$  psu near slack after ebb. Near-bottom salinities at the end of the flood tide reached similar values ( $\sim 21$  psu) for both low and higher tidal-range conditions (with a greater slack to max-flood range on July 26). By the end of the ebb on July 12, salinities remained higher than at the start of the tidal cycle (and higher than on July 26); whereas, at the end of the ebb on July 26, near-bottom salinities were close to their values at the beginning of the cycle (Fig. 3.10c).

Buoyancy frequency squared ( $N^2$ ) and salinity contours throughout the water column at M44 are shown together in Fig. 3.12. Transect-averaged shear magnitude and salinity contours at M44 are shown in Fig. 3.13. Transect-averaged  $\text{Log}_{10}(4Ri_g)$  together with contours (solid lines) of shear magnitude are shown in Fig. 3.14.

Times of maximum flood (“F<sub>max</sub>”) and maximum ebb (“E<sub>max</sub>”) velocities are labeled in each figure. Depth-averaged, tidally averaged horizontal salinity gradients, calculated from salinity measurements at M42 and M46, were 0.4 psu km<sup>-1</sup> on July 12 and 0.6 psu km<sup>-1</sup> on July 26.

*Salt Balance and Mixing Coefficients:*

Coefficients of vertical eddy diffusivity for salt ( $K_z$ ) throughout the water column were calculated from commonly used theoretical relationships (Dyer, 1997; Nepf and Geyer, 1996; Munk and Anderson, 1948):

$$K_z = K_o (1 + 3.33 Ri_g)^{-3/2} \quad (4)$$

where  $K_o$  = diffusivity coefficient in the absence of stratification. In the bottom boundary layer,  $K_o$  may be represented by  $K_o = \kappa u_* z$ , where  $\kappa$  = von Karman constant = 0.4,  $u_*$  = friction velocity, and  $z$  = depth. For chosen  $C_d$  values (0.001 and 0.003),  $u_*$  was calculated according to Eq. (2). In order to determine  $U$ , the height of the bottom boundary layer (BBL) during the flood tide corresponded to the height of the maximum along-channel velocity during the flood tide (Stacey and Ralston, 2005). During the ebb tide, the average height of maximum shear and maximum stratification was used.

Calculated values of  $\text{Log}_{10}(K_z)$  based on Eq. (4) with  $C_d=0.001$  are shown in Fig. 3.15. Values of  $\text{Log}_{10}(K_z)$  less than -5 ignored (not assigned a number), as these values tended to coincide with areas of very low shear (i.e. around the velocity maximum at or above the height of the BBL).

Theoretical values of  $K_z$  were compared to those computed using a simple salt balance equation:

$$\frac{\partial s}{\partial t} = -u \frac{\partial s}{\partial x} + \frac{\partial}{\partial z} \left( K_z \frac{\partial s}{\partial z} \right) \quad (5)$$

where  $\left( K_z \frac{\partial s}{\partial z} \right) = -w' s'$ ,

$s$  = salinity,  $t$  = time,  $u(z, t)$  = along-channel velocity,  $x$  = along-channel distance,  $z$  = depth,

$K_z$  = coefficient of vertical eddy diffusivity of salt, and  $w's'$  = vertical turbulent salt flux.

Coefficients of vertical eddy diffusivity ( $K_z$ ) of salt were calculated by integrating Eq. (5)

stepwise from near-bottom to each depth based on the collected salinity and transect-

averaged velocity data. Changes in salinity with respect to time  $\left( \frac{\partial s}{\partial t} \right)$  and horizontal

salinity gradients  $\left( \frac{\partial s}{\partial x} \right)$  were calculated using grid calculus operations in Surfer (surface

mapping program). In order to evaluate Eq. (5), values for the change in salinity with respect

to time were chosen near mid-estuary, and values for the horizontal salinity gradient were set

to the average between M42 and M46 (as those at individual locations tended to be noisy).

The change in salinity with respect to depth was calculated from salinity data at M44.

Terms in Eq. (5), averaged from near-bottom to 5 m below surface and calculated  $K_z$  values are given in Fig. 3.16. Calculated vertical turbulent salt fluxes ( $w's'$ , Eq. 5) together with salinity contours are given in Fig. 3.17. Values of  $\text{Log}_{10}(K_z)$ , in which negative values of  $K_z$  were ignored, together with contours of calculated vertical turbulent salt fluxes ( $w's'$ ), are given in Fig. 3.18.

Theoretical  $K_z$  values (Fig. 3.15) in areas of weak stratification within the BBL are in reasonably close agreement with calculated values from the salt budget equation (Fig. 3.18). On July 12, the theoretical  $K_z$  values ( $C_d = 0.001$ ) near maximum flood tide below the pycnocline reach  $\sim 1 \times 10^{-2}$  to  $3 \times 10^{-2} \text{ m}^2 \text{ sec}^{-1}$  (and  $\sim 2 \times 10^{-2} \text{ m}^2 \text{ sec}^{-1}$  based on the salt budget computations). On July 26, values near maximum flood tide in the bottom part of the water column reach  $\sim 1 \times 10^{-2}$  to  $5 \times 10^{-2} \text{ m}^2 \text{ sec}^{-1}$  ( $\sim 1 \times 10^{-2} \text{ m}^2 \text{ sec}^{-1}$  to  $\sim 9 \times 10^{-2} \text{ m}^2 \text{ sec}^{-1}$  based on the salt budget). Near-surface values during the flood tide are  $\sim 2 \times 10^{-3}$  to  $\sim 1 \times 10^{-2} \text{ m}^2 \text{ sec}^{-1}$  (and  $\sim 3 \times 10^{-3}$  up to  $\sim 8 \times 10^{-3} \text{ m}^2 \text{ sec}^{-1}$  based on the salt budget).

During the ebb tide on July 12,  $K_z$  values generally remained low in the bottom part of the water column, with typical values of  $\sim 3 \times 10^{-4} \text{ m}^2 \text{ sec}^{-1}$  (and  $\sim 1 \times 10^{-4}$  to  $\sim 9 \times 10^{-4} \text{ m}^2 \text{ sec}^{-1}$  based on the salt budget). On July 26,  $K_z$  values in the bottom layer were greater than during the low tidal range period, with values of  $\sim 3 \times 10^{-3} \text{ m}^2 \text{ sec}^{-1}$  to  $\sim 2 \times 10^{-2} \text{ m}^2 \text{ sec}^{-1}$  (and  $\sim 3 \times 10^{-3}$  to  $\sim 2 \times 10^{-2} \text{ m}^2 \text{ sec}^{-1}$  within the water column based on the salt budget).

We note that an increase in the drag coefficient ( $C_d = 0.003$ ) leads to similar patterns within the boundary layer, with  $K_z$  values as high as  $6 \times 10^{-2} \text{ m}^2 \text{ sec}^{-1}$  near maximum flood on July 12 and  $9 \times 10^{-2} \text{ m}^2 \text{ sec}^{-1}$  on July 26. Ebb tide values were  $\sim 6 \times 10^{-4} \text{ m}^2 \text{ sec}^{-1}$  on July 12 and reached  $\sim 2 \times 10^{-2} \text{ m}^2 \text{ sec}^{-1}$  in the lower part of the water column on July 26.

## Discussion

Observed velocity profiles (Fig 3.5), tidally-averaged velocities (Fig 3.6), together with earlier research (Becker et al., in review) provide evidence that the CFRE estuary exhibits characteristics of a classic two-layer estuarine system in which density-driven circulation

enhances inflow near the bottom and fresher and less dense water flows out near the surface. Buoyancy-frequency profiles (Fig. 3.12) show the presence of a relatively well defined pycnocline separating saltier bottom water from fresher, less dense surface water during July 12 ebb and flood conditions and during July 26 ebb conditions. The notably weaker stratification during the July 26 flood is consistent with earlier results (Becker et al., in review) that tidal asymmetry is a significant factor influencing the circulation and salinity structure in the CFRE.

At the same time, salinity profiles and vertical sections are consistent with previous findings in the CFRE (Becker et al., in review) that near-bottom salinities are lower during periods of increased tidal range. More specifically, we note that salinity profiles at M44 (Fig. 3.10) show near-bottom salinities on July 12 around slack tide (at the beginning of sampling) are greater than those on July 26 around slack tide ( $\sim 18$  vs.  $\sim 16$  psu).

Results from these two sampling periods suggest the following differences in the horizontal and vertical salinity structures. 1) During lower tidal-range periods the stratification changes minimally through the tidal cycle and near-bottom salinities are relatively high. 2) During higher tidal-range periods the stratification varies significantly over the tidal cycle and near-bottom salinities are lower.

We expect that the presence or absence of strong stratification and the vertical or horizontal transport of salt are critically linked. We discuss this link more closely in the sections that follow. First, we describe observed differences in the vertical shear structures, gradient Richardson numbers ( $Ri_g$ ), and horizontal Richardson numbers ( $Ri_x$ ) for the two tidal range periods. Next, we discuss processes that influence the salinity structure including terms in the salt balance equation, calculated turbulent salt fluxes, and vertical eddy diffusivity ( $K_z$ )

values based on the salt-balance analysis. Finally, we provide a descriptive characterization of the relationship between stratification and the horizontal and vertical transport of salt for the two tidal range periods.

Earlier research characterizing the behavior of residual flow (including scale analyses and laboratory experiments) suggests residual circulation should increase during periods of reduced turbulence, e.g. during slack tide and low tidal ranges (Stacey et al., 2001, Linden and Simpson, 1988). One may expect, therefore, that increases in residual circulation during lower tidal ranges may allow for greater up-estuary advection of salt. Previous research in the CFRE estuary indicated estuarine-wide flood-tide excursions exceeded ebb-tide excursions near the bottom during lower tidal ranges but were about equal during the higher tidal-range conditions. Around mid-estuary, however, near-bottom flood tide excursions exceeded ebb tide excursions during both high and low tidal ranges (Becker et al., in review).

Examination of results of the mid-estuarine velocity data in the CFRE does not show a clear trend of increased residual circulation during the low tidal-range sampling period, as along-channel velocities near slack tide are similar in magnitude near the bottom ( $\sim 0.29 \text{ m sec}^{-1}$  vs.  $0.33 \text{ m sec}^{-1}$  at  $\sim 12 \text{ m}$  depth and  $0.45 \text{ m sec}^{-1}$  vs.  $0.37 \text{ m sec}^{-1}$  at  $\sim 13 \text{ m}$  depth for low and higher tidal range conditions, respectively, Fig. 3.5). Further, the analysis indicates tidally averaged along-channel velocities (Fig. 3.6) are greater during higher tidal-range conditions ( $\sim 0.15 \text{ m sec}^{-1}$  at  $\sim 12 \text{ m}$  depth) than for lower tidal-range conditions ( $\sim 0.08 \text{ m sec}^{-1}$  at  $\sim 12 \text{ m}$  depth). Rather, we expect that differences in turbulent mixing during the two tidal range periods contribute to differences in observed near-bottom salinities and examine these differences in the following sections.

### *Shear Structure*

Analysis of the vertical shear of the horizontal velocity together with salinity contours at M44 (Fig. 3.13) show similar patterns are notable during the low and higher tidal-range sampling periods. Three regions of increased shear magnitude (during the flood-slack-ebb cycles) are found at: 1) near-bottom (and above) during the strengthening flood; 2) near-surface during the developing (strengthening) ebb; and 3) near mid-column and below during the entire latter half of the ebb cycle. Greatest shear magnitudes ( $\sim 0.11 \text{ s}^{-1}$ ) occur during the ebb for both sampling periods. During the flood tide, lowest shear values (close to 0) tend to occur at the depth of maximum velocity (suggested by Stacey and Ralston, 2005 to represent the top of the bottom boundary layer). During the ebb tide, low shear values appear to be more closely tied to the stratification structure.

The magnitude of shear during the ebb tide generally exceeds that of the flood tide for both tidal-range conditions. During the ebb, higher tidal-range period, transect-averaged values of velocity shear indicate largest values occur closer to the bottom, whereas during the lower tidal-range period maximum shear values appear higher in the water column. Further analysis, discussed below, indicates these observed differences (in particular, increased bottom shear during the high tidal range period) are critical in explaining differences in salinity characteristics between the two tidal range periods.

### *Gradient Richardson Number*

Gradient Richardson numbers (Eq. 3) were calculated using transect-averaged along-channel velocity and salinity measurements near the mid-transect location (at M44). As calculated values span a large range, the magnitude of  $Ri_g$  is represented in Fig. 3.14 as  $\text{Log}_{10}(4Ri_g)$ , a



convenient scale for comparison to the critical value of 0.25 (Stacey and Ralston, 2005; Simpson et al., 2005). We note that inclusion of cross-channel velocities in these calculations did not significantly affect trends, as cross-channel velocities were typically small relative to along-channel velocities (typically an order of magnitude less and never exceeding  $0.07 \text{ m s}^{-1}$ , the value reached near flood-tide maximum during the low tidal-range period).

In general, the magnitude of  $Ri_g$ , which was generally positive for both tidal-range sampling periods, appeared closely tied to the shear structure (Figs. 3.14). Calculated values were close to and below the critical value of 0.25 (dashed line) during certain periods of increased shear (e.g. in the lower water column during the flood tide). In general, higher  $Ri_g$  coincided with areas of minimal shear, for example near the velocity maximum during the flood tide on July 26 and about 3-5 m below the surface during the ebb tide (July 26).

On July 26,  $Ri_g$  values during the weakening ebb tide were relatively low (and close to the critical value) in the lower part of the water column (e.g. below  $\sim 8.5 \text{ m}$  depth where shear was high). On July 12, in contrast, higher values of  $Ri_g$  on the weakening ebb were observed (relative to those observed on July 26). This provides evidence that increased turbulent mixing during the high tidal range period allows for greater freshening of near-bottom waters toward the end of the ebb tide.

#### *Horizontal Richardson Number*

Horizontal Richardson numbers ( $Ri_x$ ) for both tidal-range conditions, calculated according to Eq. (2) and Eq. (3) for chosen  $C_d$  values (0.001 and 0.003), are given in Table 3.1. We have compared calculated  $Ri_x$  for periods close to maximum flood and maximum ebb tides in

order to investigate general, tidal-range related differences and because we expect the  $u_*$  formulation of Eq. (2) to be more accurate at higher velocities (Stacey and Ralston, 2005). In addition, as discussed by Lacy et al. (2003), we expect lateral effects may become important in determining changes in stratification toward the end of the flood tide.

Comparisons of  $Ri_x$  that have been averaged throughout the boundary layer indicate lowest values occur during the higher tidal-range flood tide, when stratification decreased (Figs. 3.8, 3.12). Greatest  $Ri_x$  values were observed during the ebbs ( $Ri_x = 5.0, 3.4$  for  $C_d = 0.001$ ). For  $C_d = 0.001$ ,  $Ri_x$  exceeds the critical value of one during each sampling period (low tidal-range flood, ebb; higher tidal-range, ebb) except during the higher tidal-range flood, when the calculated value dropped to 0.60. When  $Ri_x$  values remained above the critical value of one, the analysis suggests stratification was relatively high (Fig. 3.8). We note, however, that although stratification was lowest during the high tidal-range flood tide, it remained above 5 psu during both sampling periods.

### *Salt Balance and Mixing Coefficients*

The salt budget equation assumes that changes in salinity with time ( $\frac{\partial s}{\partial t}$ ) represent a balance between advection (first term on right hand side, Eq. 5) and turbulent diffusion (second term on right hand side). Salinity generally increases with time during the flood tide, when ( $\frac{\partial s}{\partial t}$ ) is positive, and decreases during the ebb (Fig. 3.16). The advective terms are generally positive during the flood tide, when advection acts to increase salinity, and negative during the ebb tide. For both the low and higher tidal range periods, turbulent diffusion terms generally act in opposition to advection during the flood tide (e.g. to diminish salinities with time in the lower water column during the flood tide). During the ebb tide, we

expect terms omitted in the simplified salt budget equation (e.g. cross-channel transport or vertical velocities) may become significant. In particular, we note that during parts of the ebb tide, calculated turbulent vertical salt fluxes ( $w's'$ ) were negative, and changes in salinity may not be explained by a simplified balance between advection and diffusive processes.

In order to compare differences between the two tidal range periods, we examine vertical turbulent salt fluxes (Fig. 3.17). During the low tidal-range flood, relatively large values ( $\sim 1 \times 10^{-3}$  to  $2 \times 10^{-3}$  m psu sec<sup>-1</sup>) occur when the pycnocline is close to the surface (Fig. 3.12) and along-channel velocities are relatively high (e.g. near maximum flood). Areas of relatively high vertical turbulent salt flux are generally constrained to the upper parts of the water column. During the higher tidal range flood, in contrast, greater values of vertical turbulent salt fluxes ( $\sim 1 \times 10^{-3}$  to  $3 \times 10^{-3}$  m psu sec<sup>-1</sup>) extend throughout much of the water column. During the high tidal range period, relatively high values also occur during the ebb tide, when the interaction between turbulent bottom friction, internal shear, and stratification may become significant, for example in explaining the weaker stratification and lower observed near-bottom salinities near the end of the ebb tide (Fig. 3.12).

Examination of estimated  $K_z$  values calculated from the salt budget equation (Fig. 3.18) indicates that on July 12,  $K_z$  values were generally relatively low ( $\sim 2 \times 10^{-4}$  to  $\sim 2 \times 10^{-3}$  m<sup>2</sup> sec<sup>-1</sup>) except near maximum flood tide below the pycnocline (when  $K_z$  values reach  $\sim 2 \times 10^{-2}$  m<sup>2</sup> sec<sup>-1</sup> in the lower portion of the water column). These higher values of  $K_z$  in the lower part of the water column (as opposed to higher values of turbulent salt flux in the upper water column described above) result from more well mixed conditions closer to the bed (i.e. bottom generated shear and associated turbulence would be expected to contribute to well mixed conditions in the lower water column). On July 26, relatively high (generally positive)

values of  $K_z$  are found during much of the flood tide (e.g.  $\sim 1 \times 10^{-2} \text{ m}^2 \text{ sec}^{-1}$  to  $\sim 9 \times 10^{-2} \text{ m}^2 \text{ sec}^{-1}$  near the bottom part of the water column), and increased values of  $K_z$  (relative to the lower tidal range period) extend into the upper water column (e.g.  $\sim 3 \times 10^{-3}$  up to  $\sim 8 \times 10^{-3} \text{ m}^2 \text{ sec}^{-1}$ ). The analysis is consistent with observations (Fig. 3.12) that relatively salty water may reach upper parts of the water column during the higher tidal range flood tide (as a result of increases in turbulent mixing) but that relatively salty water is constrained to the lower water column during the lower tidal ranges (as a result of weaker mixing). The observed differences may be a result of differences in bed-generated shear and resulting turbulence during the two tidal-range periods.

During the ebb tide,  $K_z$  values remain relatively low on July 12 ( $\sim 1 \times 10^{-4}$  to  $\sim 9 \times 10^{-4} \text{ m}^2 \text{ sec}^{-1}$ ) with some negative values appearing as processes represented by terms omitted in the salt budget equation may have been important. On July 26, greater  $K_z$  values ( $\sim 3 \times 10^{-3}$  to  $\sim 2 \times 10^{-2} \text{ m}^2 \text{ sec}^{-1}$ ) relative to low tidal range observations following the ebb-tide velocity maximum provide evidence that mixing of fresh and salty water contribute to a reduction in near-bottom salinities observed during the high tidal-range period (Fig. 3.12). We note that these increased  $K_z$  values during the high tidal range ebb tide are consistent with patterns observed using the theoretical (Munk and Anderson, 1948) formulations (Fig. 3.15).

Negative values of  $K_z$  from the salt budget analysis occur near maximum ebb tide during both high and low tidal range periods. We hypothesize the influence of cross-channel transport, vertical velocities, or internal waves may be significant during this part of the tidal cycle.

### *Salinity and Stratification Structure: A Descriptive Characterization*

Observations of salinity and stratification profiles and vertical salinity sections provide evidence that the horizontal and vertical movement of salt is strongly influenced by the strength of stratification. Although the greatest stratification occurs during the ebb tide for both sampling periods, particularly weak stratification during the higher tidal-range flood is notable (Fig. 3.12), and evidence of its influence on the salinity structure through mixing and transport is found in the observations. For example, we may define “near-bottom water” as the salinity of near-bottom water near M44 during Transect 1 sampling (i.e. close to slack-tide, when the tide is just starting to flood) and consider variability in salinity during low and higher tidal-range conditions. These salinity contours, highlighted by the 19-psu salinity contour during the low tidal-range period and 17-psu contour during the higher range period, respectively, appear constrained to the middle to lower portion of the water column during times when stratification is maintained (i.e. when a well-defined pycnocline is present, Figs. 3.11, 3.12). More specifically, during low tidal-range conditions (flood and ebb), the 19 psu salinity contour is restricted to sections near mid-water column and below. During higher tidal-range conditions, in contrast, the “near bottom water” (or 17-psu salinity contour) is able to reach near-surface sections of the water column during the flood tide (when stratification within the water column is weak), but remains more restricted to lower sections during the ebb.

As the flood develops, the degree to which the water column can mix vertically appears strongly related to the periodic presence or lack of stratification: during the flood tide on July 12 we describe the water column as “constrained mixed,” as evidence suggests salt is transported vertically but appears to be “capped” by mid-column stratification. During

the flood tide on July 26, observations suggest the stratification “cap” is broken down by the time the flood tide weakens (“partially constrained mixed,” Fig. 3.12).

During the ebb tide, our analysis indicates the strength of stratification continues to influence salinity characteristics. That is, weaker stratification during the ebb, higher tidal-range period (in particular toward the end of the ebb tide, Fig. 3.12) can allow for greater freshening of near-bottom waters and thereby accounts for lower observed near-bottom salinities, relative to observations during the low tidal-range period. We expect more detailed study of variability in the interaction of stratification, baroclinic circulation, and bed-generated friction (Jay, 1991) are intriguing topics for future research.

## **Conclusions**

Our analyses of data collected during two low-river-flow sampling periods, representing low and higher tidal ranges in the CFRE, suggest the horizontal and vertical salinity structure is significantly impacted by tidal range differences and intra-tidal (flood-ebb) variations. The analysis suggests salinity characteristics are critically linked to the ability of stratification within the water column to be maintained. For the low tidal-range period, near-surface to near-bottom stratification was relatively strong throughout the flood-ebb cycle, a well defined pycnocline persisted, and near-bottom salinities were relatively high. During the higher tidal-range period the stratification varied with flood-ebb cycles (e.g. diminished near-surface to near-bottom stratification and a weaker pycnocline were observed during the flood tide) and near-bottom salinities were relatively low.

More specifically, our findings may be summarized as follows:

1. Observations of the velocity and density structure provide evidence that the CFRE estuary exhibits characteristics of a classic two-layer estuarine system in which density driven-circulation enhances saltier inflow near the bottom and fresher, less dense water flows out near the surface (e.g. during periods of low turbulence, such as the slack tide). Residual velocities reach approximately  $0.08 \text{ m sec}^{-1}$  and  $1.5 \text{ m sec}^{-1}$  near the bottom and approximately  $-0.20 \text{ m sec}^{-1}$  and  $-0.18$  near the surface for low and high tidal range periods, respectively.
2. Analysis of the field data indicates salinity and circulation characteristics are critically linked to ebb-flood and tidal-range variability. During the low tidal-range period prolonged near-surface to near-bottom stratification ( $\sim 7$  to  $9 \text{ psu}$ ) existed. During the higher tidal-range period, near-surface to near-bottom salinity stratification increased during the ebb tide and decreased during the flood (with near-surface to near bottom ranges from less than  $5 \text{ psu}$  to  $\sim 10 \text{ psu}$  observed throughout the tidal cycle). Observations suggest saltier near-bottom water may be constrained to a bottom boundary layer capped by the well defined pycnocline during low tidal ranges, but is able to reach near-surface levels during higher tidal-range conditions.
3. Increases and decreases in stratification on intra-tidal and tidal range timescales (during maximum flood and ebb for high and low tidal range periods) were consistent with expected patterns based on computed values of the horizontal Richardson number ( $Ri_x$ ) if one assumes a reasonable value of  $C_d$  ( $= 0.001$ - $0.003$ ) in a quadratic relationship to convert the mean velocity to the friction velocity. For  $C_d = 0.001$ , greatest  $Ri_x$  values occurred during the ebb ( $Ri_x = 5.0$  and  $3.4$

during low and high tidal ranges, respectively). Lower values occurred during the flood ( $Ri_x = 1.1$  and  $0.60$ ).

4. Estimates of turbulent vertical salt fluxes and coefficients of vertical eddy diffusivity ( $K_z$ ) from analysis of a simple salt budget balance provide evidence that turbulent mixing of fresh and salty water contribute to lower near-bottom salinities observed during the higher tidal range ebb tide (relative to observations during the low tidal range ebb). Weaker stratification toward the end of the higher tidal range ebb tide can allow for greater freshening of near-bottom waters.
5. Vertical eddy diffusivity ( $K_z$ ) values estimated from the salt budget analysis indicate that during the low tidal range flood tide,  $K_z$  values reach  $\sim 2 \times 10^{-2} \text{ m}^2 \text{ sec}^{-1}$  in the lower portion of the water column below the pycnocline near maximum flood tide but otherwise generally remain relatively low ( $\sim 2 \times 10^{-4}$  to  $\sim 2 \times 10^{-3} \text{ m}^2 \text{ sec}^{-1}$ ). During the higher tidal range period, greater values of  $K_z$  are found during much of the flood tide ( $\sim 1 \times 10^{-2} \text{ m}^2 \text{ sec}^{-1}$  to  $\sim 9 \times 10^{-2} \text{ m}^2 \text{ sec}^{-1}$  near the bottom part of the water column), and increased values of  $K_z$  (relative to the lower tidal range period) extend into the upper water column (e.g.  $\sim 3 \times 10^{-3}$  up to  $\sim 8 \times 10^{-3} \text{ m}^2 \text{ sec}^{-1}$ ). During the ebb tide,  $K_z$  values remain relatively low on July 12 ( $\sim 1 \times 10^{-4}$  to  $\sim 9 \times 10^{-4} \text{ m}^2 \text{ sec}^{-1}$ ). On July 26, greater  $K_z$  (positive) values ( $\sim 3 \times 10^{-3}$  to  $\sim 2 \times 10^{-2} \text{ m}^2 \text{ sec}^{-1}$ ) relative to low tidal range observations were observed following the ebb-tide velocity maximum.
6. Theoretical  $K_z$  values (Munk and Anderson, 1948), calculated based on chosen values of  $C_d$  ( $= 0.001$ - $0.003$ ), are in reasonably close agreement with values computed from the salt budget analysis (within the bottom boundary layer, in areas



of relatively weak stratification). The analysis is consistent with findings that turbulent mixing of fresh and salty water contributes to the lower observed near-bottom salinities during the higher tidal range ebb tide ( $K_z \sim 3 \times 10^{-3}$  to  $\sim 2 \times 10^{-2} \text{ m}^2 \text{ sec}^{-1}$ , for  $C_d = 0.001$ ) and provides evidence of significant turbulent mixing ( $K_z \sim 2 \times 10^{-3}$  to  $\sim 1 \times 10^{-2} \text{ m}^2 \text{ sec}^{-1}$ ) in the upper water column during the flood tide.

## Literature Cited

- Becker, M.L., Luettich, R.A. Jr., and Mallin, M.A, in review, "Hydrodynamic behavior of the Cape Fear River and estuarine system: an observational synthesis," *Estuaries and Coasts*.
- Benson, H.A. and Parmen, J.W. 1995, "Field Data Collection Report, Cape Fear River, Wilmington, North Carolina," United States Army Corps of Engineers Waterways Experiment Station, 193 p.
- Dyer, K.R., 1997, *Estuaries*, 2<sup>nd</sup> Ed., 195 p.
- Fischer, H.B., 1972, "Mass transport mechanisms in partially stratified estuaries," *Journal of Fluid Mechanics*, 53, p. 672-687.
- Hansen, D.V. and Rattray, M., 1965, "Gravitational Circulation in Straits and Estuaries," *Journal of Marine Research*, 23, 104-122.
- Hansen, D.V. and Rattray, M., 1966, "New Dimensions in Estuary Classification," *Limnology and Oceanography*, Vol. 11, No. 3 (July 1966), p. 319-326.
- Hetland, R.D and Geyer, W.R., 2004, "An Idealized Study of the Structure of Long, Partially Mixed Estuaries," *Journal of Physical Oceanography*, Vol. 34, p. 2677-2691.
- Jay, D.A., 1991, "Internal Asymmetry and Anharmonicity in Estuarine Flows," *Tidal Hydrodynamics*, edited by B.B. Parker, p. 403-418.
- Jay, D.A. and Smith, J.D., 1990, "Residual circulation in shallow estuaries, 2, Weakly stratified and partially mixed estuaries," *Journal of Geophysical Research*, 95, p. 733-748.
- Lacy, J.R., Stacey, M.T., Burau, J.R., and Monismith, S.G., 2003, "Interaction of lateral baroclinic forcing and turbulence in an estuary," *Journal of Geophysical Research*, Vol. 108, No. C3, 3089, doi:10.1029/2002JC001392
- Linden, P.F. and Simpson, J.E., 1988, "Modulated mixing and frontogenesis in shallow seas and estuaries," *Continental Shelf Research*, 8(10), p. 1107-1127, 1988.
- McAdory Jr., R.T., 2000, "Cape Fear-Northeast Cape Fear River, North Carolina Numerical Model Study," US Army Corps of Engineers Engineer Research Development Center, Coastal and Hydraulics Laboratory, 95 p.
- Miles, J., 1961, "On the stability of heterogeneous shear flows," *Journal of Fluid Mechanics*, 10, p. 496-508.

- Monismith, S., Burau, J.R., and Stacey, M., 1996, "Stratification dynamics and gravitational circulation in northern San Francisco Bay," in *San Francisco Bay: The Ecosystem*, edited by J.T. Hollibaugh, p. 123-153.
- Munk, W. H., and Anderson, E.R., 1948, "Notes on a theory of the thermocline," *Journal of Marine Research*, 3, 276-295.
- Nepf, H.M. and Geyer, W.R., 1996, "Intratidal variations in stratification and mixing in the Hudson estuary," *Journal of Geophysical Research*, Vol. 101, No. C5, p. 12,079-12,086.
- Oey, L-Y, 1984, "On steady salinity distribution and circulation in partially mixed and well mixed estuaries," *Journal of Physical Oceanography*, 14, p. 629-645.
- Prandle, D., 1985, "On salinity regimes and vertical structure of residual flows in narrow tidal estuaries," *Estuarine, Coastal, and Shelf Science*, 20, p. 615-635.
- Rippeth, T.P., Fisher, N.R., and Simpson, J.H., 2001, "The cycle of turbulent dissipation in the presence of tidal straining," *Journal of Physical Oceanography*, 31, p. 2458-2471.
- Simpson, J.H., Brown, J., Matthews, J., and Allen, G., 1990, "Tidal Straining, Density Currents, and Stirring in Control of Estuarine Stratification," *Estuaries*, Vol. 13, No. 2, p. 125-132.
- Simpson, J.H., Williams, E., Brasseur, L.H., Brubaker, and J.M., 2005, "The Impact of tidal straining on the cycle of turbulence in a partially stratified estuary," *Continental Shelf Research*, 25, p. 51-65.
- Stacey, M.T., Burau J.R., and Monismith, S.G., 2001, "Creation of Residual flows in a partially stratified estuary," *Journal of Geophysical Research*, Vol. 106, No. C8, p. 17013-17037.
- Stacey, M.T. and Ralston, D.K., 2005, "The Scaling and Structure of the Estuarine Boundary Layer," *Journal of Physical Oceanography*, 35, p. 55-71.
- Welch, J.M. and Parker, B.B., 1979, "Circulation and Hydrodynamics of the Lower Cape Fear River, North Carolina," NOAA Technical Report NOS 80, 108 p.

Sampling Cycle	Horizontal Richardson Number ( $C_d = 0.001$ )	Horizontal Richardson Number ( $C_d = 0.003$ )
Low Tidal-range Flood (Transect 3, 4)	1.1	0.36
Low Tidal-range Ebb (Transect 10, 11)	5.0	1.7
High Tidal-range Flood (Transect 4, 5)	0.60	0.20
High Tidal Range Ebb (Transect 15, 16)	3.4	1.1

Table 3.1. Calculated horizontal Richardson numbers around maximum flood and maximum ebb tide for low and higher tidal-range conditions.

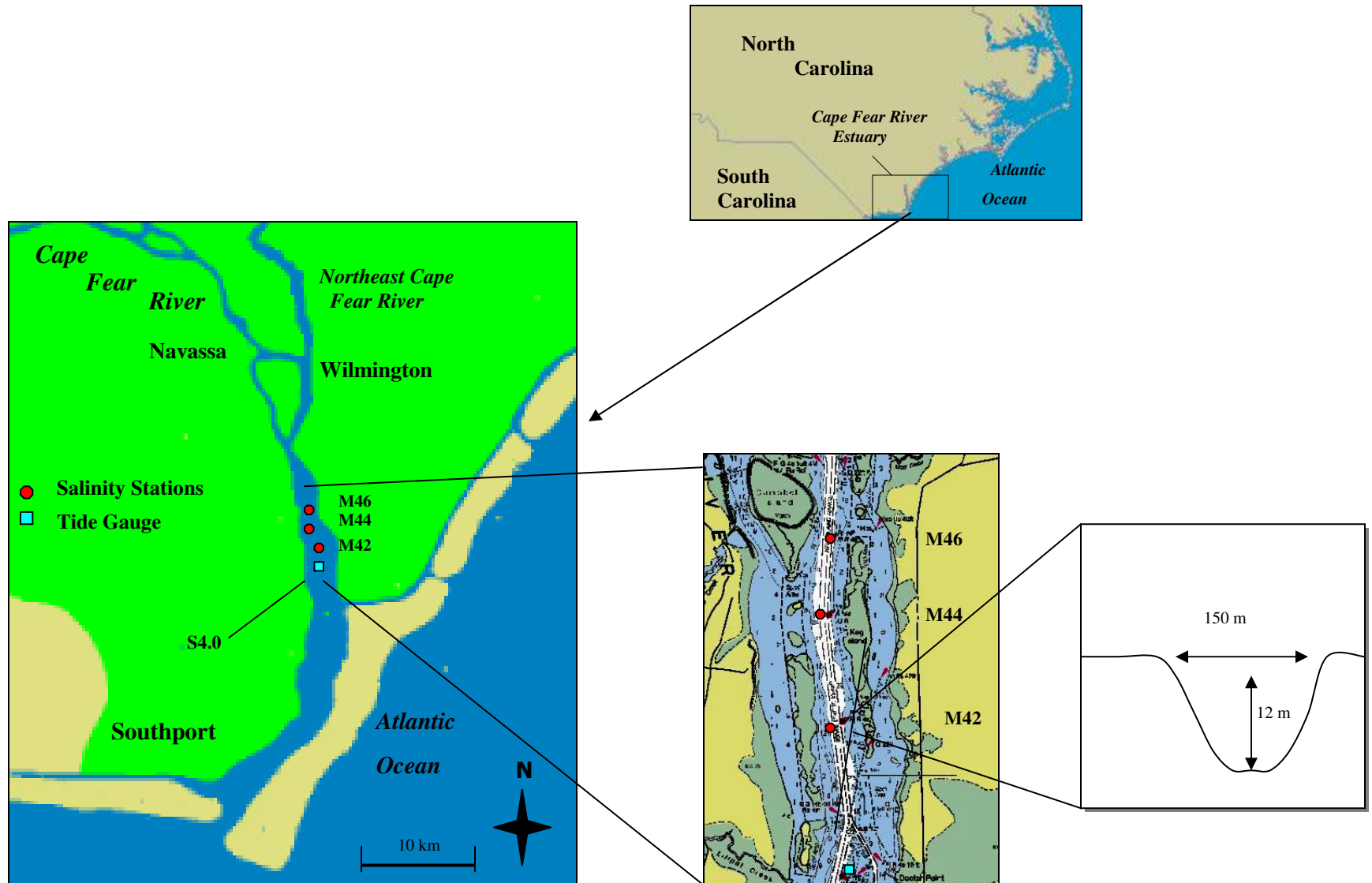


Fig. 3.1: Cape Fear River Estuary field study area including field survey stations and charted channel (modified after NOAA Chart No.11537).

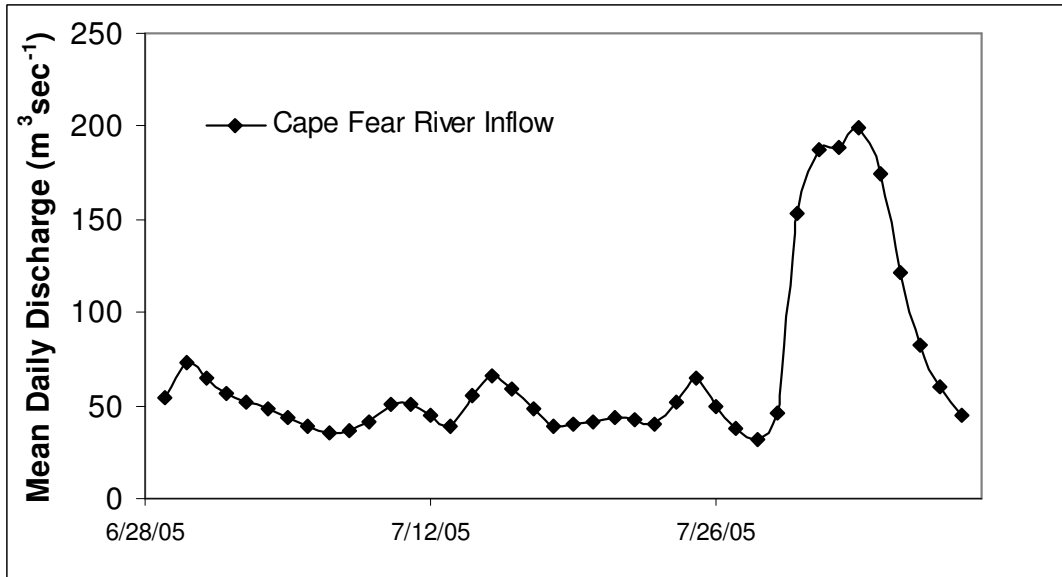


Fig. 3.2. Mean daily discharge from the Cape Fear River during the summer 2005 sampling period. Peaks in river flow within a 12-day window prior to the velocity and salinity sampling dates (July 12 and July 26) are  $73 \text{ m}^3 \text{ sec}^{-1}$  and  $67 \text{ m}^3 \text{ sec}^{-1}$ . Sampling represents low river inflow conditions.

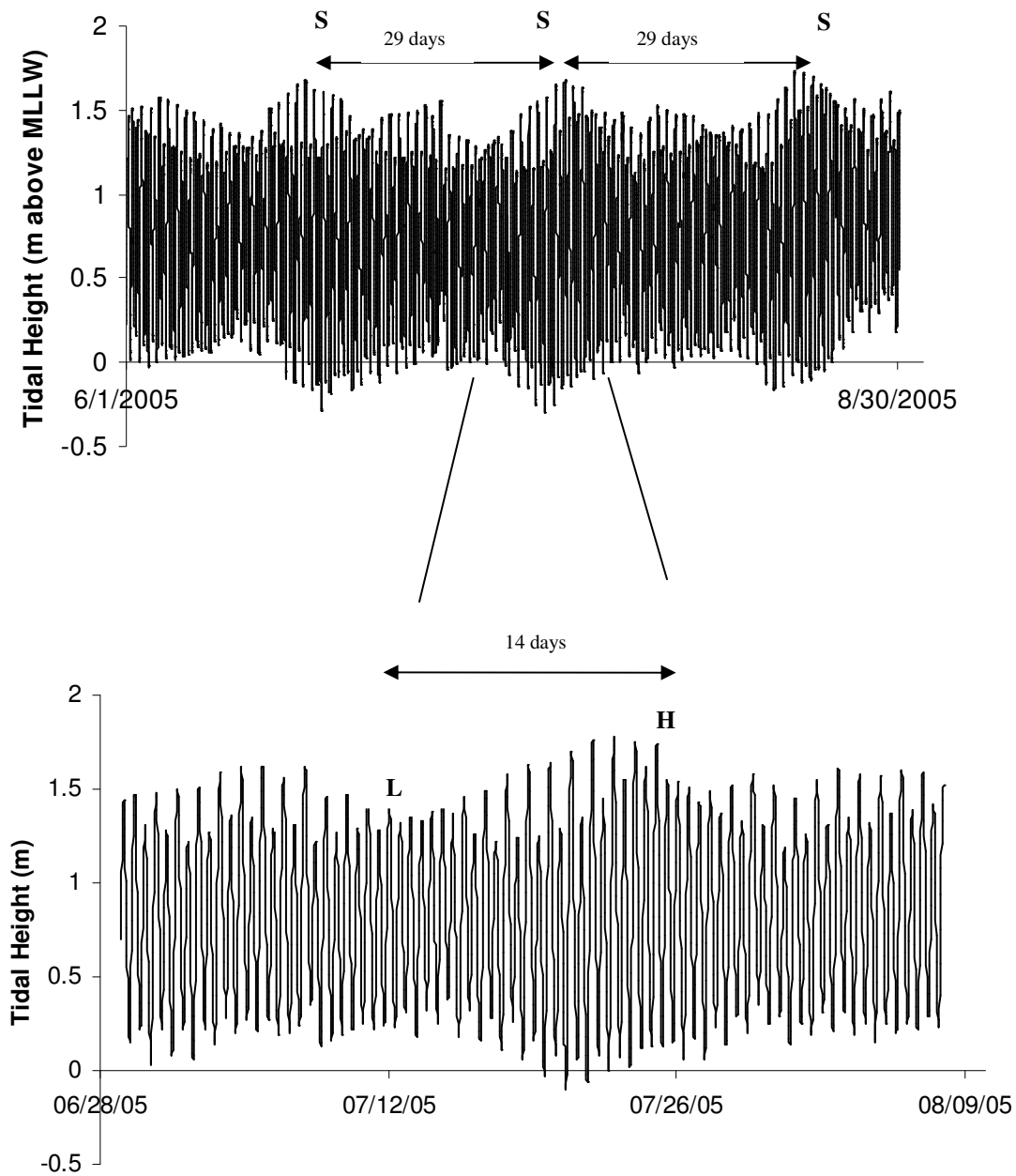
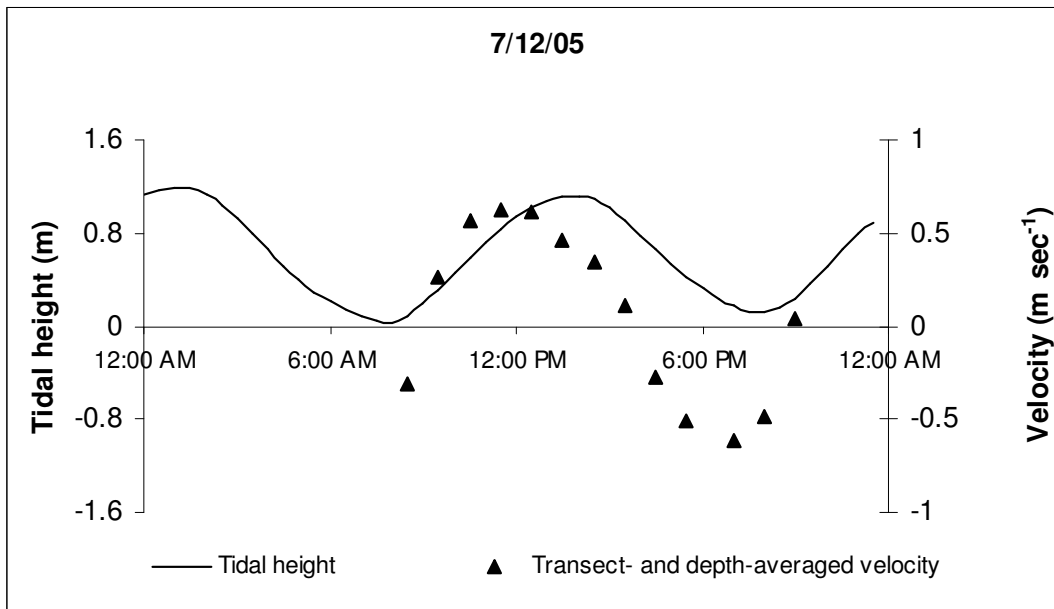


Fig. 3.3 Measured tidal heights at a) Wilmington tide gauge and b) field data station S4.0. "S" indicates times of particularly large spring tides. "L" (low) and "H" (high) indicate differences in tidal ranges for the July 12 and July 26 sampling periods.

a)



b)

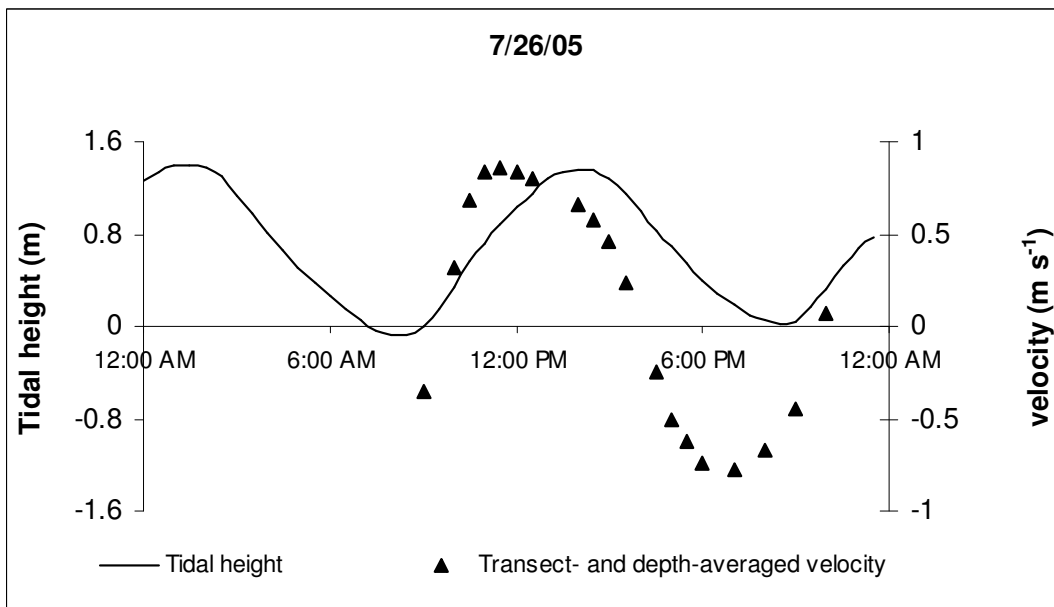
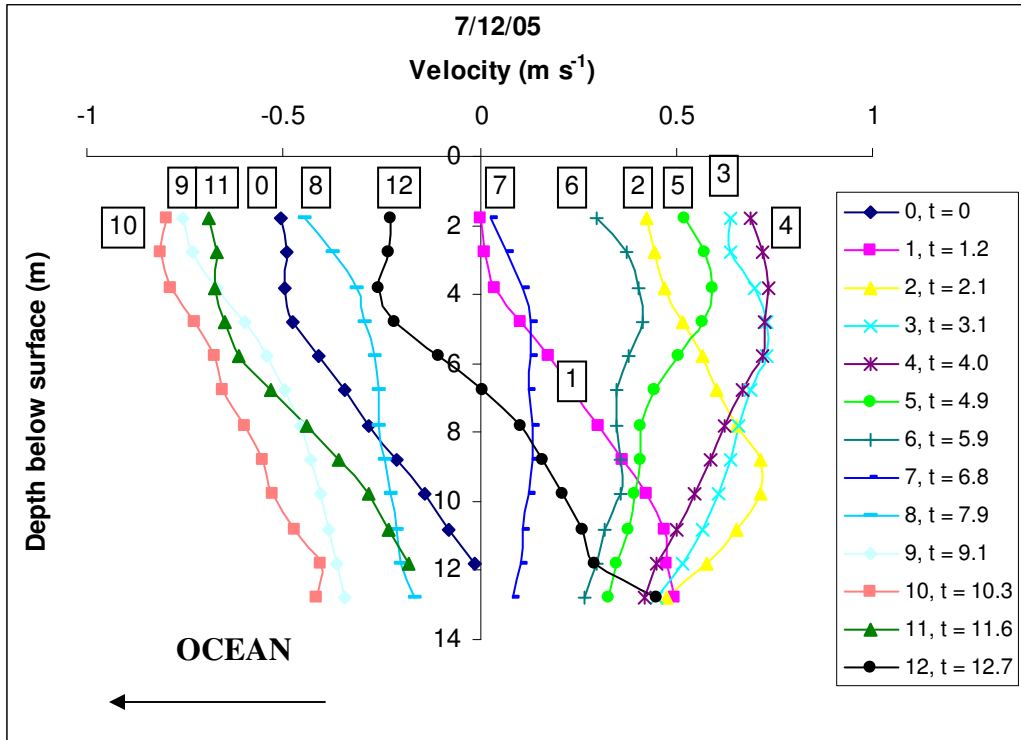


Fig. 3.4. Tidal height at S4.0 and depth-averaged along-channel velocity on a) July 12 and b) July 26, 2005.



a)



b)

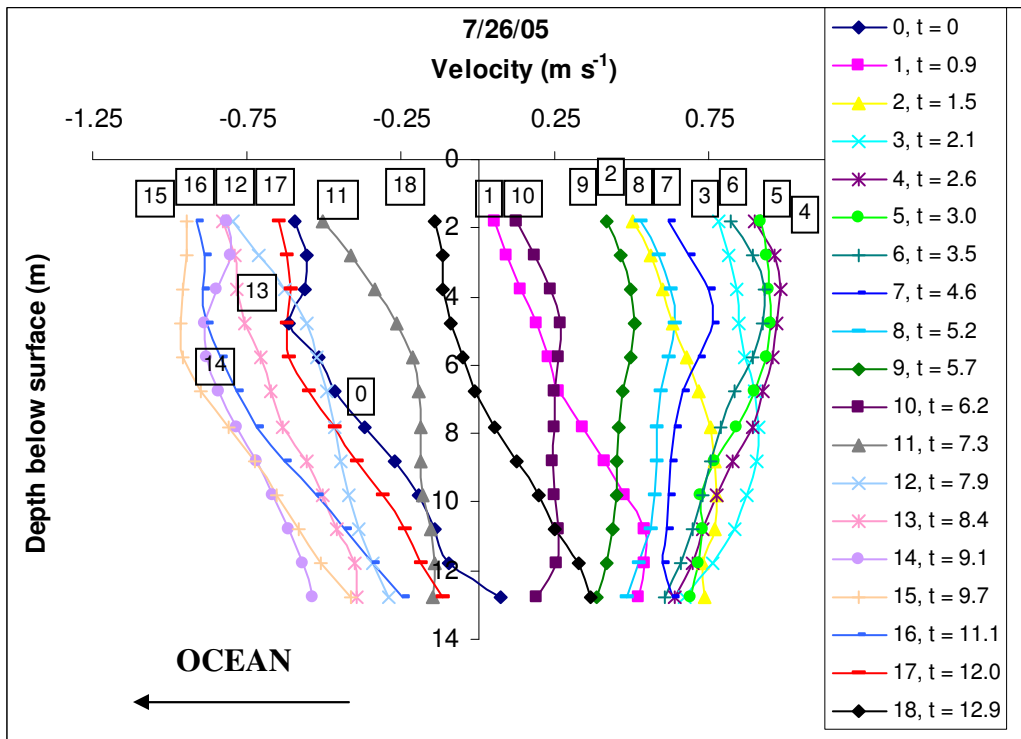


Fig. 3.5. Along-channel velocities on a) July 12 and b) July 26. Times ( $t$ ) represent the number of hours into sampling (where  $t = 0$  represents the sampling time at the midpoint of the first transect).

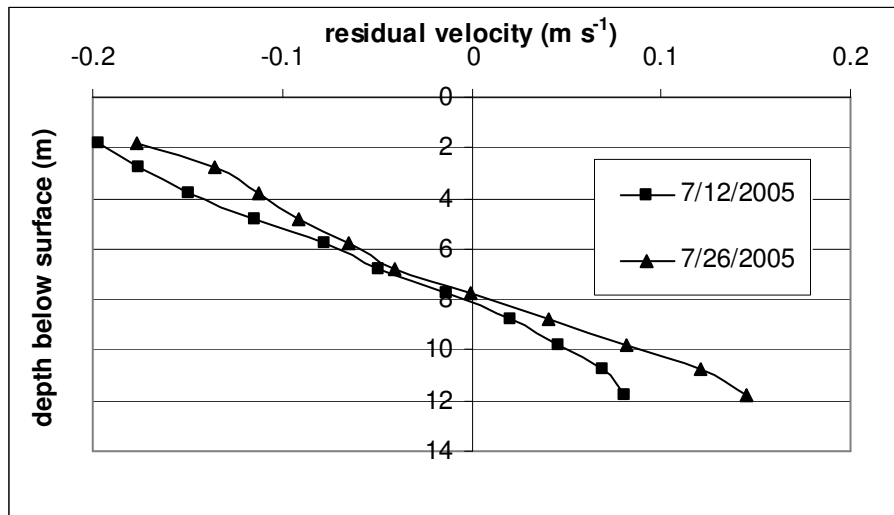
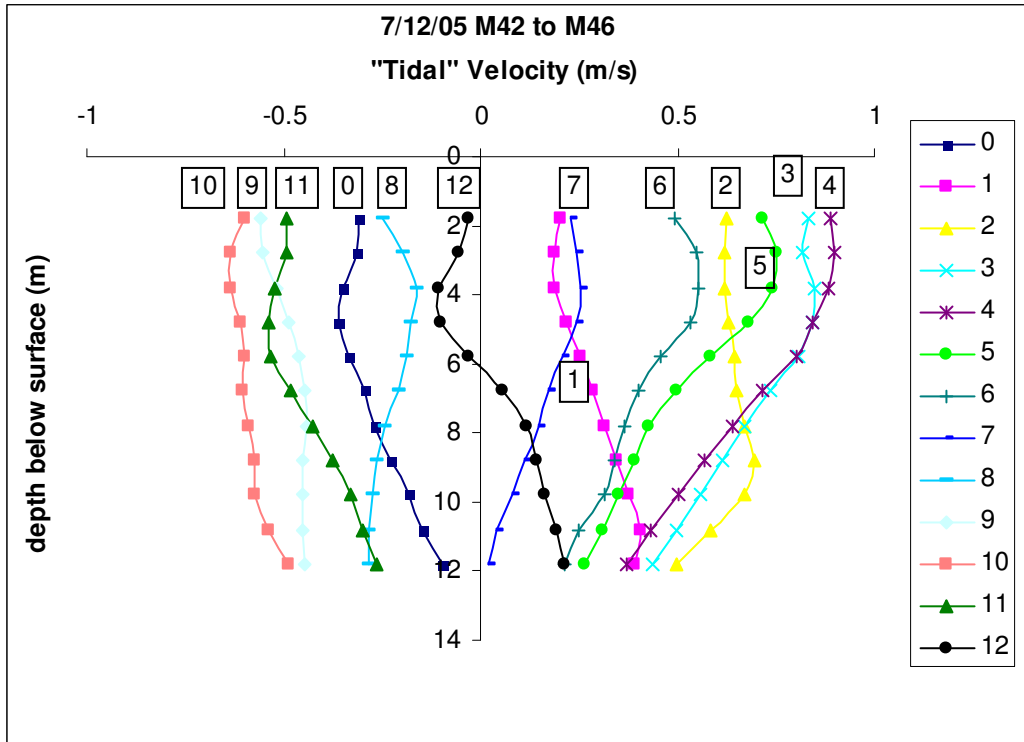


Fig. 3.6. Tidally averaged (residual) velocity on July 12 and July 26.

a)



b)

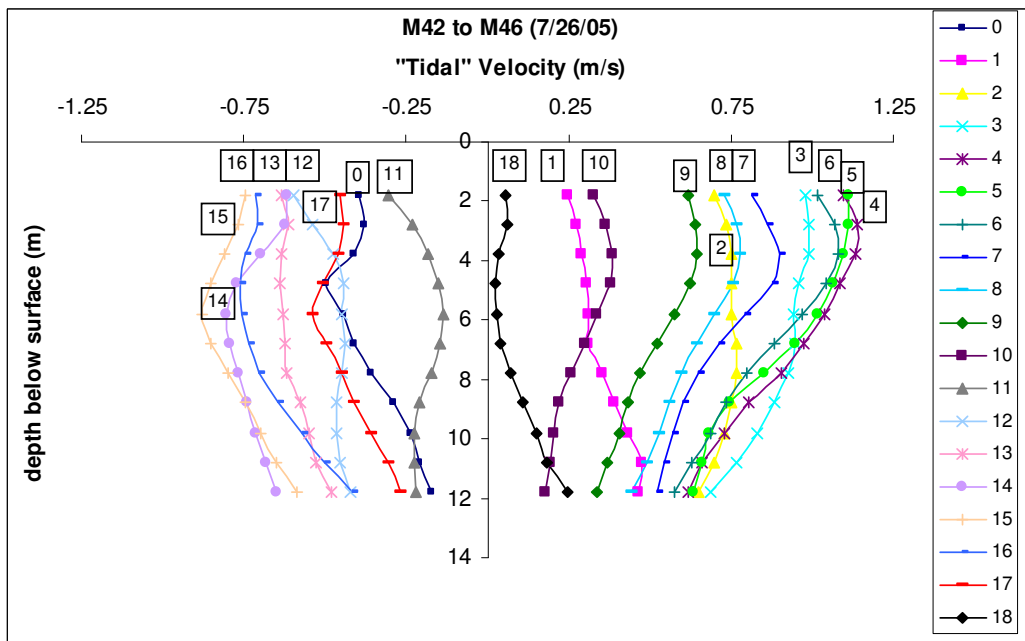
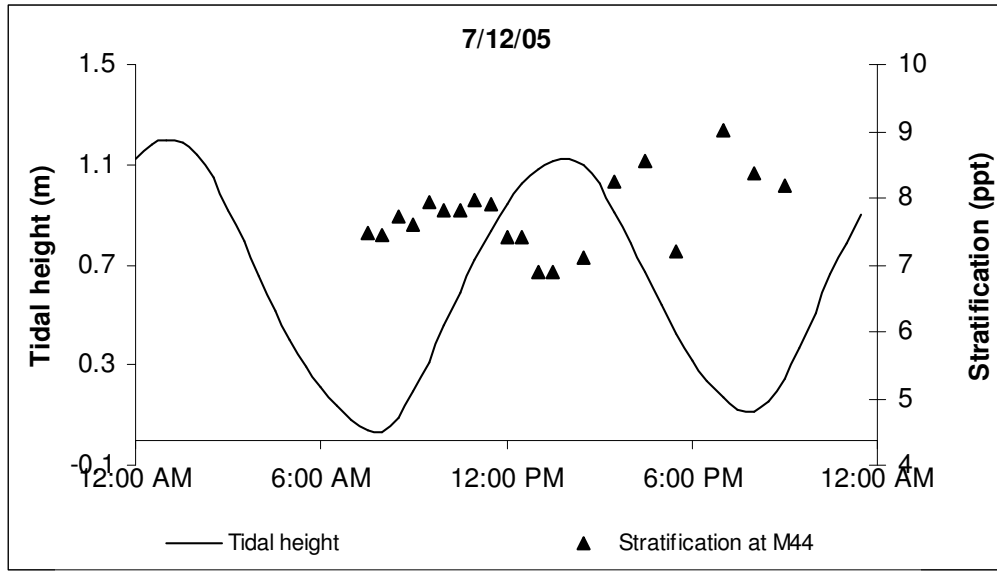


Fig. 3.7. Tidal velocity on a) July 12 and b) July 26.

a)



b)

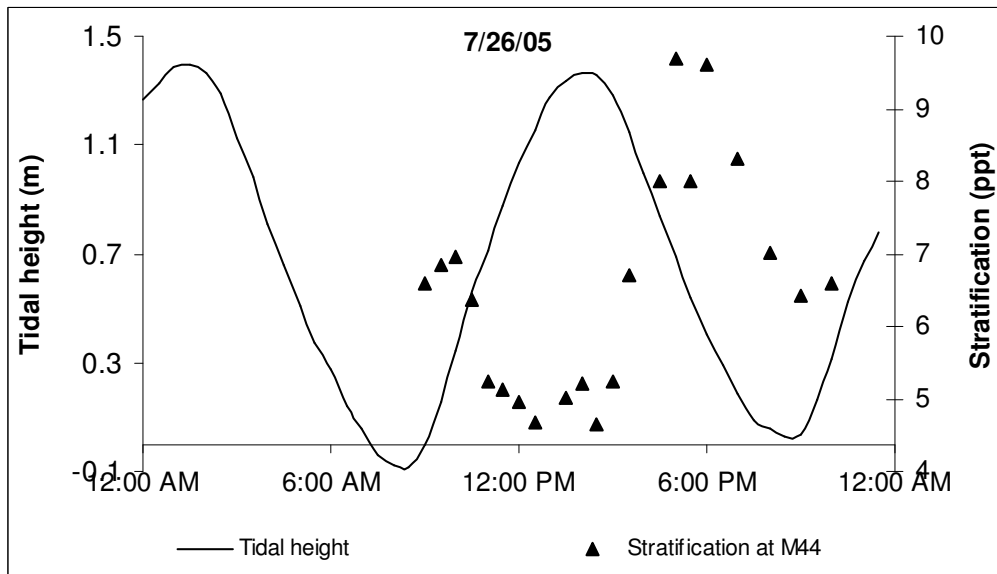
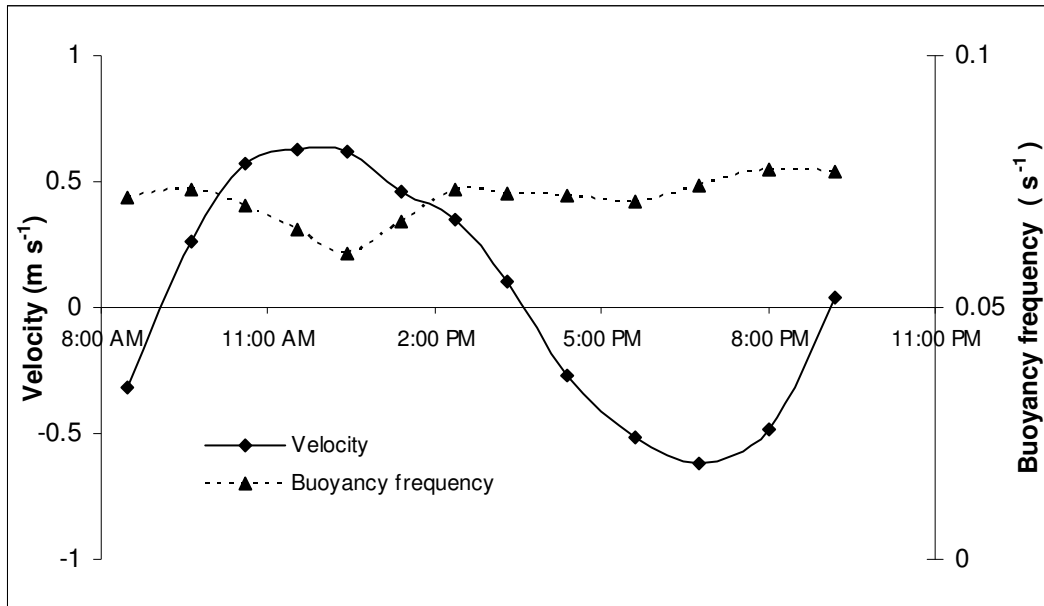


Fig. 3.8. Salinity stratification and tidal height at M44 on a) July 12 and b) July 26.

a)



b)

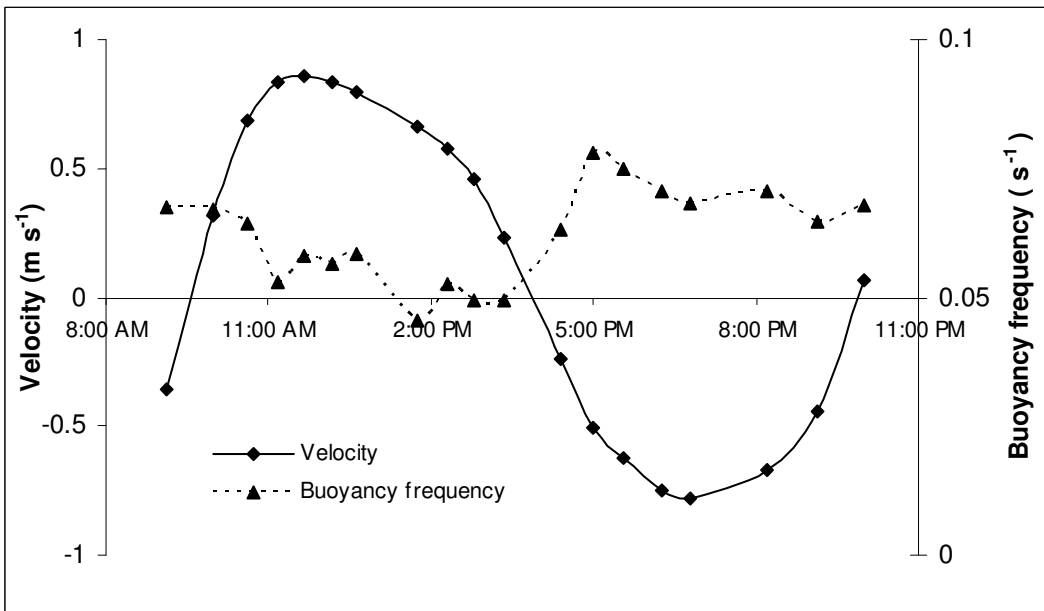
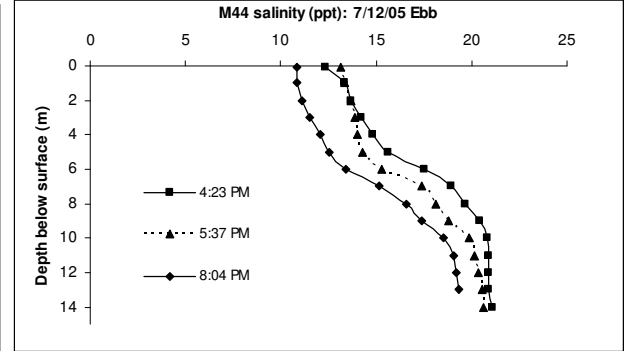
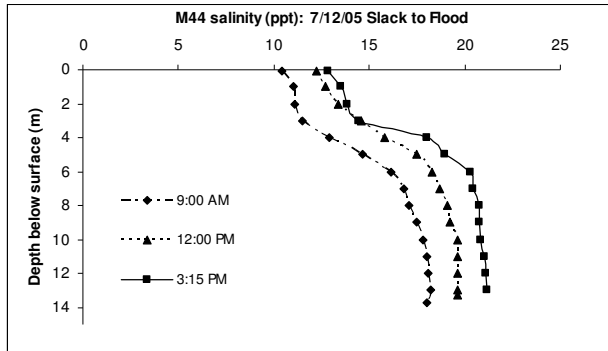
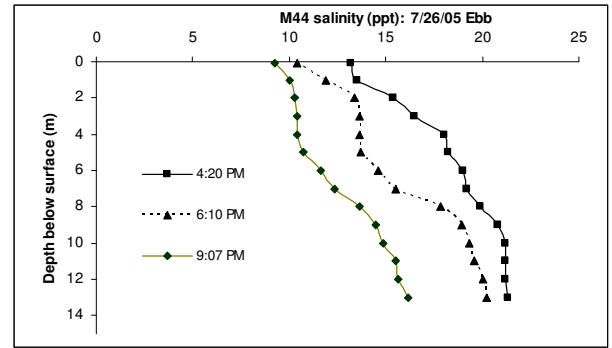
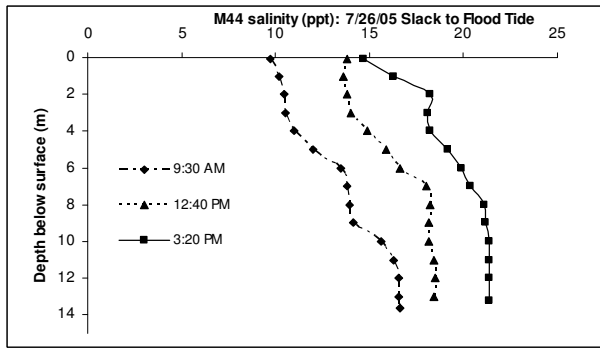


Fig. 3.9. Transect- and depth-averaged along-channel velocities and depth-averaged buoyancy frequencies at M44 on a) July 12 and b) July 26.

a)



b)



c)

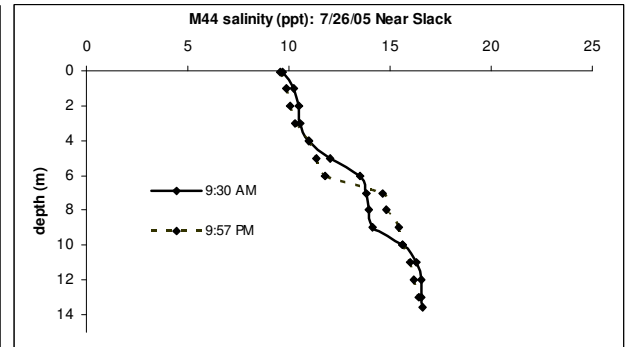
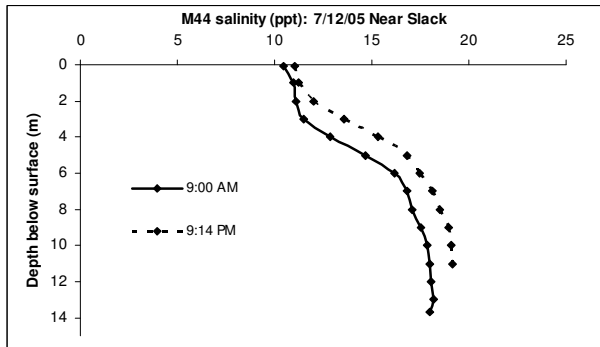


Fig. 3.10. Salinity profiles at M44 on a) July 12, b) July 26, and c) near slack tide on July 12 and July 26.

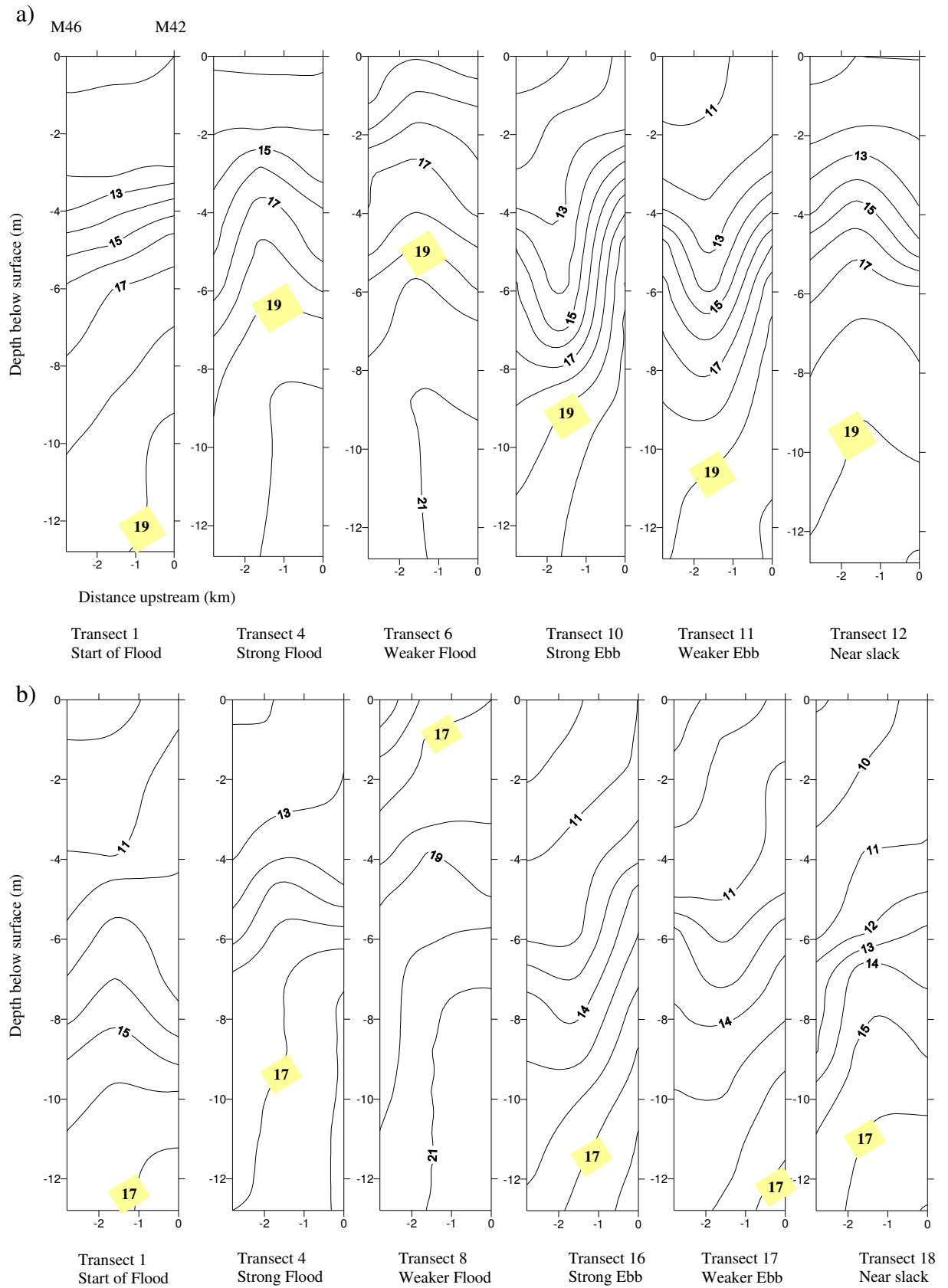


Fig. 3.11. Along-channel vertical salinity sections on a) July 12 and b) July 26. The 19-psu and 17-psu salinity contours are highlighted for July 12 and July 26, respectively.

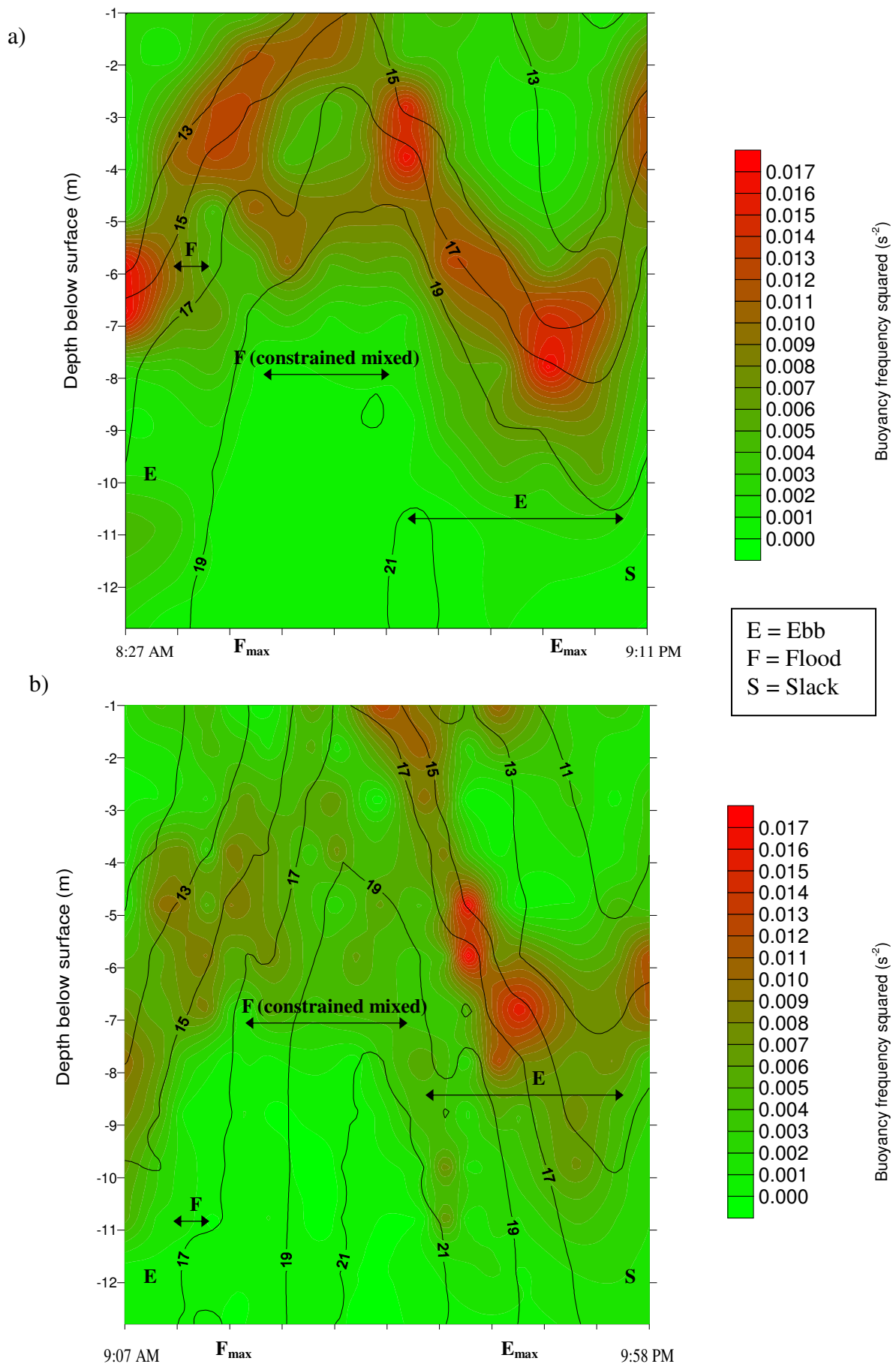


Fig. 3.12. Buoyancy frequency squared ( $N^2$ ) and salinity contours at M44 on a) July 12 and b) July 26.



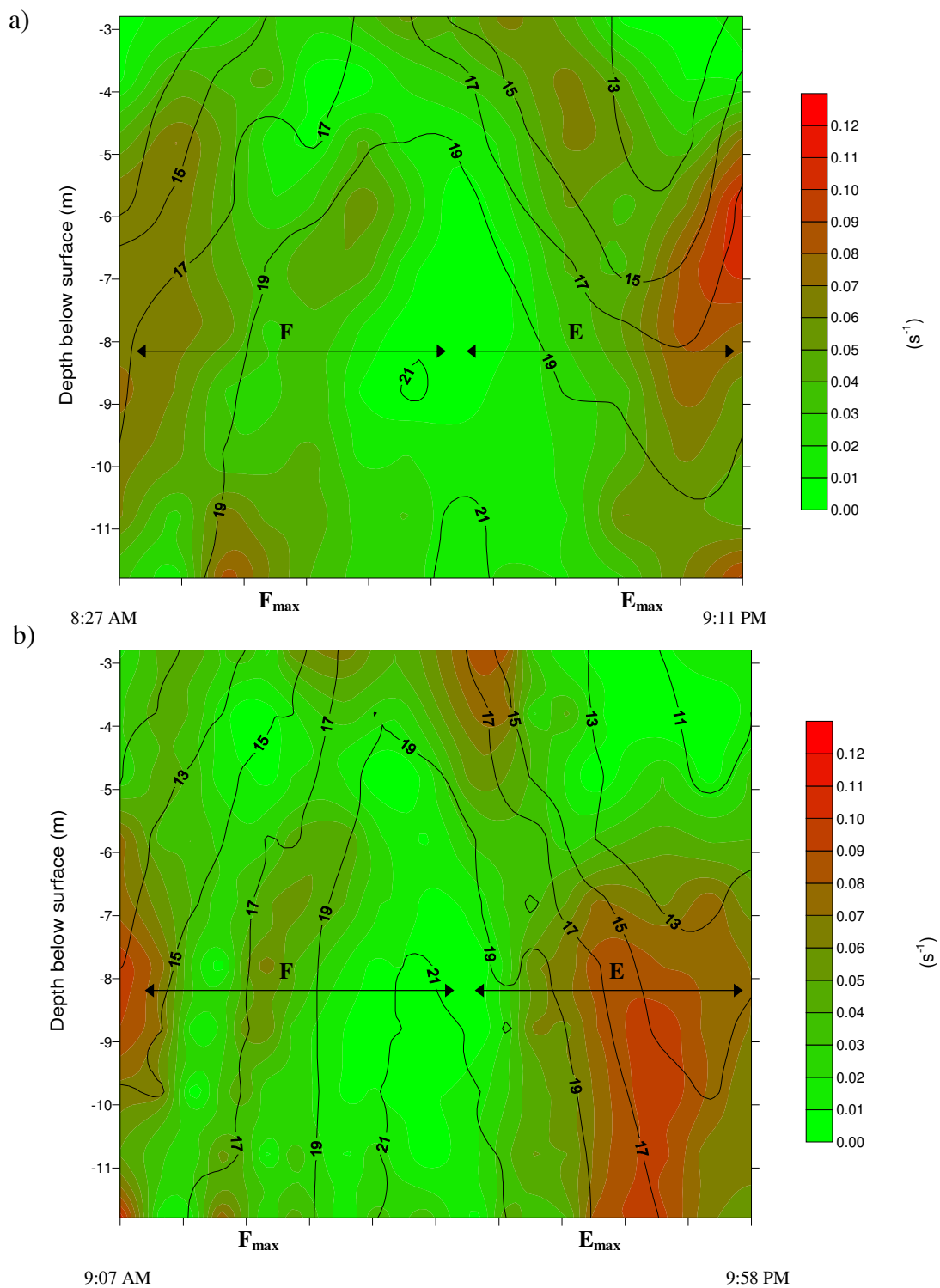


Fig. 3.13. Transect-averaged shear magnitude and salinity contours at M44 on a) July 12 and b) July 26.

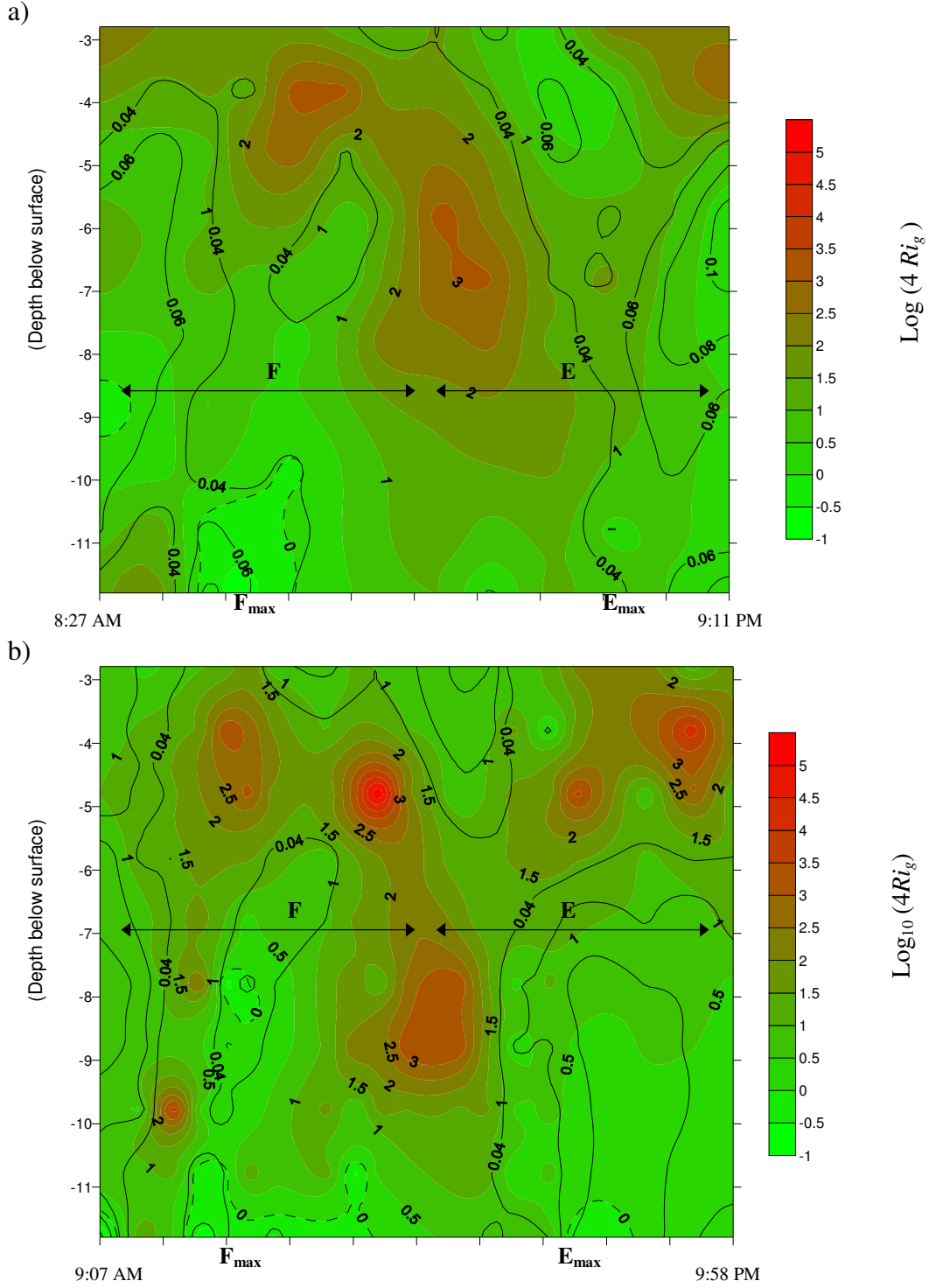
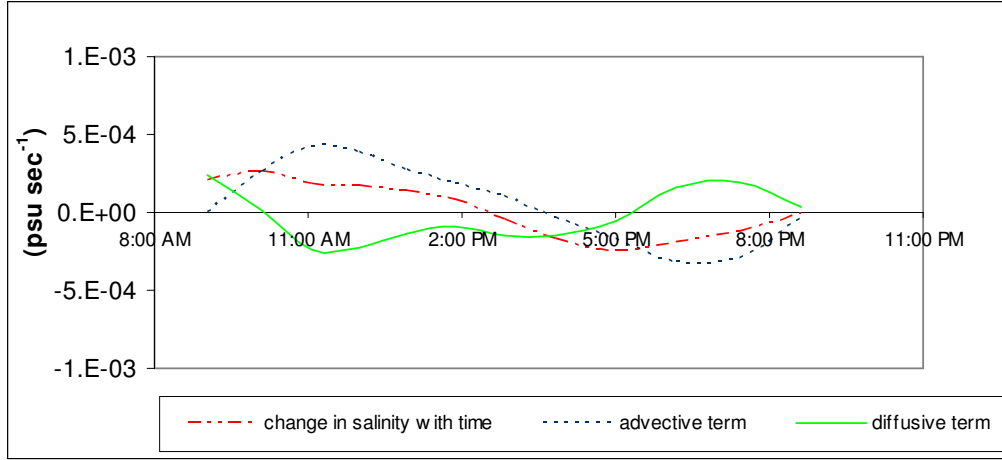


Fig. 3.14. Transect-averaged  $\text{Log}_{10}(4 Ri_g)$  together with contours of shear magnitude (solid lines) on a) July 12 and b) July 26. The dashed line indicates the location where  $\text{Log}_{10}(4 Ri_g) = 0$ .



a)



b)

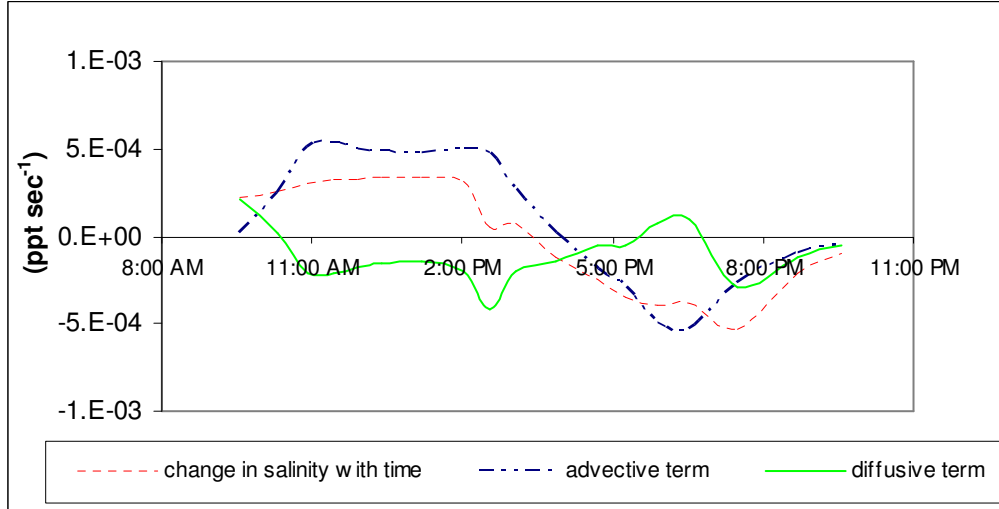


Fig. 3.16. Terms of simplified salt budget equation (Eq. 5) averaged from near-bottom to 5 m below surface on a) July 12 and b) July 26.

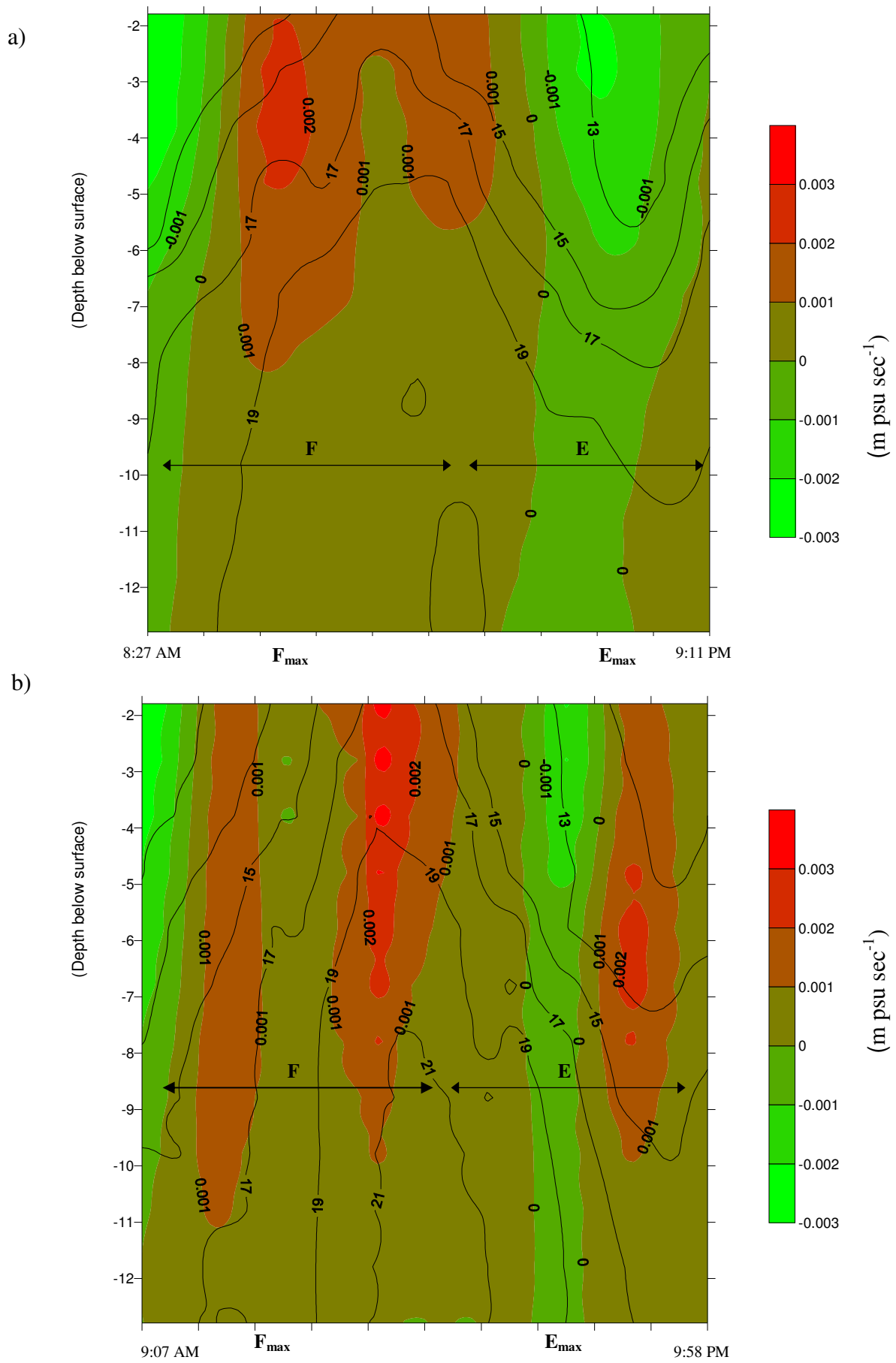


Fig. 3.17. Estimated vertical turbulent salt flux ( $w's'$ ) calculated from a simplified salt budget equation together with salinity contours at M44 on a) July 12 and b) July 26.



## **CHAPTER 4**

### **SYNTHESIS OF CONCLUSIONS**

The salinity structure and circulation of the CFRE depend on the relative strength of the principal forcing mechanisms including river discharge (which induces a barotropic pressure gradient and adds buoyancy inputs), density differences (which induce a baroclinic pressure gradient) and tidal currents (which can generate turbulence and can act to inhibit stratification). Freshwater input from the Cape Fear River (a major piedmont river) as well as the Black and Northeast Cape Fear Rivers (coastal plain rivers) influences the location of the boundary between fresh and salty water, referred to as the salinity intrusion. The salinity intrusion location varies from about 29 km upstream (referenced to M18 near the CFRE mouth) during high (non-hurricane) flow to about 53 km upstream during low river inflow, based on the computed extent at slack after flood tide. Calculated tidal excursion distances, in comparison, are on the order of 8 km near the bottom.

Our analyses indicate the salinity structure and circulation are impacted by sub-tidal scale variations in freshwater input which influence the location of the salinity intrusion, tidal-range differences that occur over an approximately 29-day period, and intra-tidal variations associated with tidal straining.

The observational data provide evidence that the CFRE estuary exhibits characteristics of a classic two-layer estuarine system in which density driven-circulation enhances inflow near the bottom and fresher, less dense water flows out near the surface (e.g.

during periods of low turbulence such as near slack tide). The analysis suggests salinity and up-estuarine transport characteristics are critically linked to the ability of stratification within the water column to be maintained.

More specific conclusions are as follows:

1. The location of the salinity intrusion varies as a result of river discharge and migrates approximately 30 km between drought and extreme-flow periods. Following sluggish river-flow periods the salinity intrusion (at slack after flood) is typically located upstream of Navassa, whereas after higher flow events the intrusion is closer to mid-estuary.
2. Approximately ninety percent of the variability of the salinity intrusion location can be attributed to peaks in flow from the three rivers during the 11 days prior to sampling in the estuary using an exponential relationship between the peak discharge and the location of the salinity intrusion. We hypothesize that the salinity intrusion location is dependent upon the relative size of the hydrologic “flood,” defined as a peak in river discharge associated with “quickflow” (e.g. the runoff contribution from storm events).
3. Classical estuarine theory predicts the salinity intrusion would vary with discharge to the power of  $(-1/3)$  in exchange-dominated systems and to the power of  $(-1)$  in diffusion-dominated systems (MacCready, 2004; Chatwin, 1976). In general, our data were not well fit by a power-law relationship, but rather by an exponential function. We hypothesize that in river-estuary systems in which hydrologic flood peaks are large relative to base flow (and in which variations in



width and bathymetry between the estuarine head and mouth may be significant), the hydrologic flood exponential decay model may be a more accurate method of predicting the estuarine salinity response than classical power-law relationships.

4. Tidally driven flow is dominated by the  $M_2$ ,  $N_2$ , and  $S_2$  constituents with significant  $M_4$  and  $M_6$  components in the upper estuary (upstream of S6.0). The combination of the dominant tidal constituents ( $M_2$ ,  $N_2$ , and  $S_2$ ) leads to an approximately 29-day periodicity in the elevation record (i.e. particularly large spring tides are observed about every 29 days).
5. Average daily bottom salinity and average daily stratification vary according to the 29-day modulation in the elevation record. The analysis suggests that during low tidal ranges, when turbulence is expected to weaken, greater stratification and increased up-estuary transport may be observed.
6. The analysis supports the paradigm that asymmetry (e.g. tidal straining and differences in mixing) during the flood and ebb tide is significant in explaining estuarine circulation. An increase in stratification during the ebb and a decrease during the flood are observable in the middle to upper estuary. The analysis suggests stratification, circulation, and up-estuarine transport are significantly impacted by intra-tidal variations.
7. Field data analysis suggests the strength of stratification within the water column significantly influences salinity characteristics. Observations indicate saltier near bottom water may be constrained to a bottom boundary layer capped by a well-defined density gradient (pycnocline) during low tidal ranges but is able to reach near-surface levels during higher tidal-range periods.

8. Estimates of turbulent vertical salt fluxes and coefficients of vertical eddy diffusivity ( $K_z$ ) from analysis of a simple salt budget balance provide evidence that turbulent mixing of fresh and salty water contribute to lower near-bottom salinities observed during the higher tidal range ebb tide (relative to observations during the low tidal range ebb). Weaker stratification toward the end of the higher tidal range ebb tide can allow for greater freshening of near-bottom waters.
9. Vertical eddy diffusivity ( $K_z$ ) values estimated from the salt budget analysis indicate that during the low tidal range flood tide,  $K_z$  values reach  $\sim 2 \times 10^{-2} \text{ m}^2 \text{ sec}^{-1}$  in the lower portion of the water column below the pycnocline near maximum flood tide but otherwise generally remain relatively low ( $\sim 2 \times 10^{-4}$  to  $\sim 2 \times 10^{-3} \text{ m}^2 \text{ sec}^{-1}$ ). During the higher tidal range period, greater values of  $K_z$  are found during much of the flood tide ( $\sim 1 \times 10^{-2} \text{ m}^2 \text{ sec}^{-1}$  to  $\sim 9 \times 10^{-2} \text{ m}^2 \text{ sec}^{-1}$  near the bottom part of the water column), and increased values of  $K_z$  (relative to the lower tidal range period) extend into the upper water column (e.g.  $\sim 3 \times 10^{-3}$  up to  $\sim 8 \times 10^{-3} \text{ m}^2 \text{ sec}^{-1}$ ). During the ebb tide,  $K_z$  values remain relatively low during the low tidal range period ( $\sim 1 \times 10^{-4}$  to  $\sim 9 \times 10^{-4} \text{ m}^2 \text{ sec}^{-1}$ ). During the higher tidal range period, greater  $K_z$  (positive) values ( $\sim 3 \times 10^{-3}$  to  $\sim 2 \times 10^{-2} \text{ m}^2 \text{ sec}^{-1}$ ) relative to low tidal range observations were observed following the ebb-tide velocity maximum.
10. Theoretical  $K_z$  values (Munk and Anderson, 1948), calculated based on chosen values of  $C_d$  ( $= 0.001$ - $0.003$ ), are in reasonably close agreement with values computed from the salt budget analysis (within the bottom boundary layer, in areas

of relatively weak stratification). The analysis is consistent with findings that turbulent mixing of fresh and salty water contributes to the lower observed near-bottom salinities during the higher tidal range ebb tide ( $K_z \sim 3 \times 10^{-3}$  to  $\sim 2 \times 10^{-2} \text{ m}^2 \text{ sec}^{-1}$ , for  $C_d = 0.001$ ) and provides evidence of significant turbulent mixing ( $K_z \sim 2 \times 10^{-3}$  to  $\sim 1 \times 10^{-2} \text{ m}^2 \text{ sec}^{-1}$ ) in the upper water column during the flood tide.